Brigham Young University
BYU ScholarsArchive

All Theses and Dissertations

2015-05-01

Synthesis and Characterization of Carbonized Poly (Divinylbenzene) Microspheres for Carbon/ Nanodiamond/Polymer-Based Core-Shell Materials and Applications of This Mixed-Mode Phase to High-Performance Liquid Chromatography

Chuan-Hsi Hung
Brigham Young University - Provo

Follow this and additional works at: https://scholarsarchive.byu.edu/etd

 Part of the Biochemistry Commons, and the Chemistry Commons

BYU ScholarsArchive Citation

Hung, Chuan-Hsi, "Synthesis and Characterization of Carbonized Poly (Divinylbenzene) Microspheres for Carbon/Nanodiamond/ Polymer-Based Core-Shell Materials and Applications of This Mixed-Mode Phase to High-Performance Liquid Chromatography" (2015). *All Theses and Dissertations*. 5497.
https://scholarsarchive.byu.edu/etd/5497

This Dissertation is brought to you for free and open access by BYU ScholarsArchive. It has been accepted for inclusion in All Theses and Dissertations by an authorized administrator of BYU ScholarsArchive. For more information, please contact scholarsarchive@byu.edu, ellen_amatangelo@byu.edu.

Synthesis and Characterization of Carbonized Poly(divinylbenzene) Microspheres for Carbon/Nanodiamond/Polymer-Based Core-Shell Materials and Applications of This Mixed-Mode Phase to High-Performance Liquid Chromatography

Chuan-Hsi Hung

A dissertation submitted to the faculty of
Brigham Young University
in partial fulfillment of the requirements for the degree of

Doctor of Philosophy

Matthew R. Linford, Chair
Daniel E. Austin
Robert C. Davis
David V. Dearden
Milton L. Lee

Department of Chemistry and Biochemistry

Brigham Young University

May 2015

Copyright © 2015 Chuan-Hsi Hung

All Rights Reserved

ABSTRACT

Synthesis and Characterization of Carbonized Poly(divinylbenzene) Microspheres for Carbon/Nanodiamond/Polymer-Based Core-Shell Materials and Applications of This Mixed-Mode Phase to High-Performance Liquid Chromatography

Chuan-Hsi Hung
Department of Chemistry and Biochemistry, BYU
Doctor of Philosophy

This work focuses on improving the quality of carbon-based core-shell materials for high performance liquid chromatography (HPLC) via the characterization of the core materials, and also the development of chromatographic methods (separations) for them. In the early part of this work, I applied organic synthesis to make uniform, spherical poly(divinylbenzene) (PDVB) microspheres, and then carbonized them to prepare carbon core materials for core-shell particle synthesis. Here, I studied in detail the surface and material properties of these particles with multiple instruments, which allowed me to describe the physical and chemical changes that took place during each treatment. The uniform, spherical carbon core materials greatly improved the efficiency of the previously developed carbon-based core-shell HPLC columns from ca. 70,000 plates per meter (N/m) to ca. 110,000 N/m for various alkyl benzenes. Later, I focused on generating application notes to showcase these mixed-mode HPLC columns. Here, liquid chromatography mass spectrometry (LC-MS) was used for the detection of analytes that lack chromophores for UV detection.

In this dissertation, Chapter 1 contains a historical background and theory of HPLC along with a review of the use of carbon-based core-shell materials for elevated pH and temperature applications. Chapter 2 describes the improvement of the efficiency of carbon-based materials for HPLC using carbonized PDVB microspheres as the carbon core material. Chapter 3 is a study on the characterization of carbonized PDVB microspheres with multiple instruments. Chapter 4 describes the separation of cannabinoids using three types of carbon-based mixed-mode HPLC columns. Chapter 5 consists of (i) guidelines for the retention mechanism of the core-shell particles that have been commercialized for chromatography by Diamond Analytics, a US Synthetic Company in Orem, Utah, and (ii) application notes for these columns. Finally, Chapter 6 discusses possible future work.

Keywords: poly(divinylbenzene), nanodiamond, chromatography, core-shell, mixed-mode, multi-instruments, cannabinoids

ACKNOWLEDGEMENTS

I give my greatest appreciation to my adviser, Dr. Matthew R. Linford, who has inspired and given me guidance during my Ph.D. studies at Brigham Young University (BYU). I admire his knowledge and expertise in chemistry, especially in analytical chemistry/surface science.

I also appreciate my committee members, Dr. Milton L. Lee, Dr. Robert C. Davis, Dr. David. V. Dearden, and Dr. Daniel E. Austin, who have given me useful feedback and suggestions that have supported my graduate work.

I also appreciate my co-workers in Linford's group: Dr. Landon A. Wiest, Dr. Nitesh Madaan, Dr. Supriya S. Kanyal, Bhupinder Singh, Anubhav Diwan, Hao Wang, and Cody Cushman for their suggestions and support during my graduate studies.

I appreciate Diamond Analytics for funding this project. I appreciate Andrew E. Dadson, Michael A. Vail, Andrew J. Miles, Dr. Janusz Zukowski and Dr. David S. Jensen for their support of this research.

I thank the Department of Chemistry and Biochemistry at Brigham Young University for their graduate program, which provides students the opportunity to develop themselves and improve their career opportunities.

I deeply appreciate my beautiful wife, Faith (Feng-Ying) Chiang, for supporting my graduate work and her sacrifice in taking care of our three beautiful daughters during this challenging time.

TABLE OF CONTENTS

ABSTRACT ii

ACKNOWLEDGEMENTS iii

LIST OF TABLES xi

LIST OF FIGURES xiii

Chapter 1: Introduction 1

1.1. A Brief History of HPLC 1

1.2. Theory of Chromatography 2

1.2.1. Plate Theory 2

1.2.2. Rate Theory and the van Deemter Equation 16

1.3. Manipulating Resolution in HPLC 19

1.3.1. pH and Temperature Effects on Resolution 20

1.3.2. Effects of Bonded Phases on Resolution 21

1.4. Silica-Based Packing Materials and Their Limitations 22

1.4.1. Development of Non-Silica Materials for HPLC 22

1.4.2. Approaches for Making Carbon-Based, Mixed-Mode HPLC Columns in the Linford Group at BYU 23

1.5. Conclusions 24

1.6. References 24

Chapter 2: Improved Efficiency of Reversed Phase Carbon/Nanodiamond/Polymer Core-Shell Particles for HPLC Using Carbonized, Poly(divinylbenzene) Microspheres as the Core Materials* 31

2.1. Abstract 31

2.2. Introduction 32

2.3. Materials and Methods 34

2.3.1. Reagents, Solvents, and Instrumentation 34

2.3.2. Synthesis of Poly(divinylbenzene) (PDVB) Microspheres 37

2.3.3. Air Oxidation, Carbonization, and Oxidation of PDVB 38

2.3.4. Layer-by-Layer (LbL) Deposition of an Aminopolymer and Nanodiamond on Carbon, and Cross-Linking and Functionalization with a C18 Ligand 39

2.3.5. Column Packing 40

2.3.6. Column Efficiency and Temperature Stability Tests 40

2.4. Results and Discussion 40

2.4.1. Carbon Core Particle Preparation from Poly(divinylbenzene) (PDVB) Microspheres 40

2.4.2. Oxidation of the Carbon Core for Improved Poly(allylamine) (PAAm) Deposition and Layer-by Laer (LbL) PAAm/Nanodiamond Growth 43

2.4.3. Improved Particle Size Distribution (PSD) by Sieving and Column Packing 46

2.4.4. Brunauer-Emmett-Teller (BET) Measurements on Particles 52

2.4.5. Reproducibility of Particle Functionalization and Packing 52

2.4.6. van Deemter Studies 52

2.4.7. Elevated Temperature Stability 58

2.4.8. Packing Longer Columns 58

2.4.9. Applications 62

2.5. Conclusions 62

2.6. References 65

Chapter 3: Multi-Instrument Characterization of Poly(divinylbenzene) Microspheres for Use in Liquid Chromatography: As Received, Air Oxidized, Carbonized, and Acid Treated* 69

3.1. Abstract 69

3.2. Introduction 70

3.3. Experimental 73

3.3.1. Reagents and Solvents 73

3.3.2. Instrumentation 74

3.3.3. Air Oxidation, Carbonization, and Acid-Oxidation of Poly(divinylbenzene) (PDVB) 76

3.4. Results and Discussion 77

3.4.1. SEM of PDVB Microspheres 77

3.4.2. BET 79

3.4.3. FTIR 82

3.4.4. XPS and Elemental Analysis 86

3.4.5. ToF-SIMS Including Chemometrics (PCA and Cluster Analysis) of the Data 89

3.4.6. XRD and Raman 95

3.4.7. TGA 98

3.5. Conclusions 100

3.6. References 101

Chapter 4: Separation of Cannabinoids on Three Different Mixed-Mode Columns Containing Carbon/Nanodiamond/Amine-Polymer Superficially Porous Particles* 107

4.1. Abstract 107

4.2. Introduction 108

4.3. Experimental 111

4.3.1. Reagents 111

4.3.2. Instrumentation 113

4.3.3. Method Development 114

4.4. Results and Discussion 114

4.4.1. Separation on a Reversed Phase (C18) Mixed-Mode Column under Acidic Conditions 114

4.4.2. Separation under Basic Conditions of Reversed Phase (C18) Mixed-Mode Column 117

4.4.3. Separation under Polar Organic Mobile Phase (POMP) of Reversed Phase (C18+) Mixed-Mode Column 119

4.4.4. Separation under Basic Conditions of Hydrophilic-Interaction Chromatography (HILIC) Mixed-Mode Column 122

4.4.5. Comparison of Shorter (4.6 x 33 mm) and Longer (4.6 x 100 mm) Reversed Phase (C18) Mixed-Mode Columns under Basic Conditions 122

4.4.6. Separation of a Real World (Bubble Hash) Extract 124

4.5. Conclusions 125

4.6. References 126

Chapter 5: Conclusions and Future Work 129

5.1. Conclusions 129

5.2. Future Work 130

5.3. References 132

Appendix 1: General Tutorial on Acid-Base Chemistry as a Basis for Understanding the Diamond Analytics Flare Mixed-Mode Column* 134

A1.1. Auto-Ionization of Water 134

A1.2. K_w 135

A1.3. pH and pOH 136

A1.4. Dissociation of Acids and Bases in Water 136

A1.5. K_a and K_b 137

A1.6. pK_a and pK_b 138

A1.7. Henderson-Hasselbach Equation 140

Appendix 2: Guidelines for Understanding the Retention Mechanism of the Diamond Analytics Flare Mixed-Mode Column* 142

A2.1. The Stationary Phase of the Diamond Analytics Flare Column 143

A2.2. Ionization Behavior of Major Classes of Analytes 144

A2.2.1. Neutral Analytes (No Permanently Charged or Ionizable Moiety) 145

A2.2.2. Permanently Charged Analytes 145

A2.2.3. Weak Acids and Bases with Protonation States that Depend on pH 146

Appendix 3: Flare C18 Mixed-Mode Column: Tricyclic Antidepressants (TCAs)* 149

A3.1. Introduction 149

A3.2. Experimental 150

A3.3. References 153

Appendix 4: Flare C18 Mixed-Mode Column: Alkaloids* 154

A4.1. Introduction 154

A4.2. Experimental 157

A4.3. References 158

Appendix 5: Regeneration of the Diamond Analytics Flare Mixed-Mode Column after Exposure to TFA* 159

A5.1. Introduction 159

A5.2. Experimental 161

A5.3. Results and Discussion 162

A5.4. References 165

Appendix 6: Flare C18 Mixed-Mode Column: Separation of Apo-Transferrin and Bovine Serum Albumin (BSA) by LC-MS* 166

A6.1. Introduction 166

A6.2. Experimental 170

A6.3. Conclusions 172

A6.4. References 173

Appendix 7: Flare C18 Mixed-Mode Column: Separation of Gingsenosides Re and Rd by LC-MS* 174

A7.1. Introduction 174

A7.2. Experimental 178

A7.3. References 180

Appendix 8: Sonication for Improved Particle Size Distribution of Core-Shell Particles* 181

A8.1. Abstract 181

LIST OF TABLES

Table 2.1 XPS data. The oxygen to carbon (O/C) and nitrogen to carbon (N/C) ratio for (A) carbon core, (B) nitric acid-treated carbon core, (C) carbon core coated with PAAm, and (D) nitric acid-treated carbon core coated with PAAm. 45

Table 2.2 Efficiencies obtained with a conventional HPLC system for decylbenzene on three columns prepared with commercial, 5 μm particles. Mobile phase: 40/60/0.1 H_2O/ACN/TEA (v/v/v), flow rate: 0.7 mL/min, 35 °C. 51

Table 2.3 BET data of particles giving surface areas and pore diameters. 53

Table 2.4 The *A*-, *B*-, *C*-terms, and plate heights (*H*) from the van Deemter equation for the columns: "in-house, not sieved," "in-house, sieved," and "commercial, sieved #1, #2, and #3." The reduced values of *A*, *B*, *C*, and *H* (divided by d_p) are also given. Efficiencies were obtained using a UHPLC system with triplicate injections at each linear velocity (0.02 – 0.14 cm/s, inclusive, at 0.02 cm/s increments). The analyte was decylbenzene with a mobile phase of 40/60/0.1 H_2O/ACN/TEA v/v/v, pH 11.3, at 35 °C 57

Table 2.5 *k* and N/m before and after heating cycles (all were 5 h) for decylbenzene at 120 °C and 140 °C. 59

Table 2.6 Retention factors (*k*), tailing factors, asymmetries (**A**sym$_{10\%}$), and efficiencies (N/m) of 2.1 x 50 mm columns obtained with a UHPLC system. 61

Table 3.1 BET surface area measurements of as-received PDVB, PDVB air oxidized at 250 °C, PDVB air oxidized at 250 °C and then carbonized at 900 °C, and PDVB air oxidized at 250 °C, carbonized at 900 °C, and then treated with nitric acid. The errors (standard deviations) on the as-received PDVB and also on the nitric acid treated particles correspond to three measurements performed on the same batch of particles. The measurements following air

oxidation and carbonization were performed on at least three different batches of particles. 81

Table 3.2 XPS of as-received PDVB microspheres, PDVB air oxidized at 250 °C, PDVB air oxidized at 250 °C and carbonized at 900 °C, and PDVB air oxidized at 250 °C, carbonized at 900 °C, and treated with nitric acid. 87

Table 3.3 Elemental analysis of as-received PDVB microspheres, PDVB air oxidized at 250 °C, PDVB air oxidized at 250 °C and carbonized at 900 °C, and PDVB air oxidized at 250 °C, carbonized at 900 °C, and treated with nitric acid. The first and second values in the ”Oxygen (at. %)” column are values for that element when hydrogen is either considered or not considered in the calculation, respectively. 88

LIST OF FIGURES

Figure 2.1 SEM images (taken with an FEI XL30 SFEG) of PDVB microspheres after (A) the first step in the particle synthesis (ca. 3.3 μm particle diameters), (B) the second step in the synthesis (ca. 4.0 μm diameters), (C) carbonization and filtration (ca. 2.8 μm diameters) – some particles of submicron dimensions are present in the lower right corner of this image, and (D) oxidation and carbonization of commercially obtained 5.0 μm PDVB particles (ca. 3.6 μm diameters). 42

Figure 2.2 XPS survey spectra of (A) carbon core particles, (B) nitric acid-treated carbon core particles, (C) carbon core particles coated with PAAm, and (D) nitric acid-treated carbon core particles coated with PAAm. The actual O/C ratios for (A) and (B) are 0.05 and 0.25, respectively (see Table 2.1). 44

Figure 2.3 SEM images (taken with an FEI XL30 SFEG) of (A) 5, (B) 15, and (C) 25 bilayers of PAAm/nanodiamond on in-house prepared carbonized PDVB particles, and SEM images (taken with an FEI Helio NanoLab 600) of (D) 5, (E) 15, and (F) 25, bilayers of PAAm/nanodiamond on commercially obtained, carbonized PDVB. Both kinds of particles were pretreated in nitric acid at 60 °C for 24 h. (G) Growth curve for the LbL process on the commercially obtained, carbonized particles (error bars are standard deviations of measurements on 30 - 40 particles), and (H) 95% confidence intervals (C.I.) of the data in (G). See Figure 2.4 for additional images. The starting diameter for the particles in (G) and (H) was ca. 3.2 μm, which suggests some heterogeneity in the carbonization process, c.f., Figure 2.1. 47

Figure 2.4 SEM images (taken with an FEI XL30 SFEG) of (A) 10, (B) 20, and (C) 30 bilayers of PAAm/nanodiamond on in-house prepared carbonized PDVB particles. SEM images

(taken with an FEI Helio NanoLab 600) of (D) 10, (E) 20, and (F) 28, bilayers of PAAm/nanodiamond on commercially obtained, carbonized PDVB particles. Both kinds of particles were treated in nitric acid at 60 °C for 24 h prior to PAAm/nanodiamond deposition. 48

Figure 2.5 Particle size distributions (PSD) of nitric acid-treated carbon-core particles after deposition of 30 bilayers of PAAm and nanodiamond: (A) particles from cores prepared in-house, (B) particles as in (A) after passage through a 40 μm sieve (d90/d10: 1.42), (C) particles from carbonized, commercial 5 μm PDVB starting material after passage through a sieve as in (B) (d90/d10: 1.36). 50

Figure 2.6 Reproducibility of three columns prepared from commercial, PDVB 5 μm particles with final particle size of 4 μm (see Figure 2.5C). The columns are designated as: "Commercial, Sieved, #1" (solid line), "Commercial, Sieved, #2" (dotted line), and "Commercial, Sieved, #3" (dashed line). From left to right analytes were ethyl, butyl, hexyl, octyl, and decylbenzene. Mobile phase: 40/60/0.1 H_2O/ACN/TEA (v/v/v), flow rate: 0.7 mL/min, 35 °C. 54

Figure 2.7 van Deemter plot for decylbenzene with *A*, *B*, and *C* terms of 4.97, 1.31, and 3.78. Column: Commercial, Sieved #1 (see Table 2.2 and Figure 2.6). Mobile phase and temperature: 40/60/0.1 H_2O/ACN/TEA (v/v/v), 35 °C. 56

Figure 2.8 Chromatograms of an alkybenzene test mixture (ethyl-, butyl-, hexyl-, octyl-, and decylbenzene) taken at 35 °C with 60/40/0.1 H_2O/ACN/TEA (pH 11.3) (v/v/v) at 0.7 mL/min before [(a) and (d)] and after [(b), (c), (e), and (f)] stability tests (5 h each) on the same column. The same mobile phase and conditions were used for the 120 °C purges. For the 140 °C purges, the mobile phase was 70/30/0.1 H_2O/ACN/TEA (pH 11.3) (v/v/v) at

0.7 mL/min. The mobile phase was made up twice – before and after the 140 °C experiments, which accounts for the small shifts in retention. 60

Figure 2.9 UHPLC separation of alkylbenzene analytes (1. ethyl- 2. butyl- 3. hexyl- 4. octyl- and 5. decyl-benzene) using a 2.1 x 50 mm column packed with the particles prepared in the same way as those for Figure 2.6. The mobile phase was 40/60 H_2O/ACN at 35˚C with a flow rate of 0.15 mL/min. The efficiency of the decylbenzene was 89,000 N/m with a tailing factor of 1.08. 63

Figure 2.10 Separation of eucalyptus, lavender, melaleuca, and peppermint essential oils under gradient elution. Linear gradient from 90/10 H_2O/ACN at 0 min to 0/100 H_2O/ACN at 30 min. The flow rate was 0.6 mL/min at 35 ˚C with UV detection at 210 nm. 64

Figure 3.1 SEM images of (a) commercially obtained, as-received, PDVB microspheres, (b) PDVB microspheres that were air oxidized at 250 °C, and (c) air oxidized (at 250 °C), carbonized (at 900 °C), acid treated PDVB microspheres. (d) Average particle diameters of PDVB particles before and after various treatments. The labels (a) – (c) correspond to the particles represented in the panels of this figure. Label (e) corresponds to measurements of air oxidized (at 250 °C), carbonized (at 900 °C) PDVB microspheres. Error bars, which are standard deviations, are given in the text. 78

Figure 3.2 SEM image of carbonized PDVB. 80

Figure 3.3 FTIR-ATR of PDVB after air oxidation at temperatures ranging from 25 – 250 °C. These spectra are not on the same scale. 83

Figure 3.4 FTIR-ATR spectra of PDVB after air oxidation at 250 °C followed by carbonization at 300 – 900 °C. These spectra were taken with a single bounce ATR accessory with a diamond crystal. The spectra in the inset were taken with a single bounce ATR accessory

that had a Ge crystal. Spectrum (a) is of the same 900 °C material used to obtain the '900°C' spectrum in the main figure. Spectrum (b) is of this '900°C' material after treatment with nitric acid. 85

Figure 3.5 Principle components analysis of selected peak areas from the negative ion spectra of PDVB microspheres before and after various treatments. (a) Plot of the scores on PC1 and PC2. (b) Loadings on PC1. (c) Loadings on PC2. 91

Figure 3.6 T^2 and Q residuals of scores plot of ToF-SIMS data..... 93

Figure 3.7 Cluster analysis of the same negative ion spectra used in the PCA analysis shown in Figure 3.5. 94

Figure 3.8 XRD data of (a) PDVB, (b) PDVB air oxidized at 250 °C, (c) PDVB air oxidized at 250 °C and carbonized at 900 °C, (d) PDVB air oxidized at 250 °C, carbonized at 900 °C, and treated with nitric acid, and (e) graphite. 96

Figure 3.9 Raman data of (a) PDVB, (b) PDVB air oxidized at 250 °C and carbonized at 900 °C, and (c) PDVB air oxidized at 250 °C, carbonized at 900 °C, and treated with nitric acid. 97

Figure 3.10 TGA of (a) PDVB, (b) PDVB air oxidized at 250 °C, (c) PDVB air oxidized at 250 °C, and carbonized at 900 °C, and (d) PDVB air oxidized at 250 °C, carbonized at 900 °C, and treated with nitric acid..... 99

Figure 4.1 Mixed-mode bonded phases (C18, C18+, and HILIC) tested in this study. 110

Figure 4.2 Chemical structures of cannabinoids tested in this study [1]..... 112

Figure 4.3 (A) Separation of CBD, THC, CBN, and THCA under acidic conditions with a reversed phase (C18) mixed-mode column (4.6 x 33 mm) at 65 °C with mobile phase: A: 40/60 (H_2O/MeOH) and B: 60/40 (MeOH/methyl tert-butyl ether). Two percent formic acid was

added into solvents A and B. Gradient elution conditions: 0 min 90 % A, 1.5 min 10 % A, 1.51 min 90 % A and 4.5 min end. The flow rate was 1.5 mL/min and the injection volume was 1 µL. The peak capacity (gradient time divided by the average peak width) for this separation was 26. (B) Separation of THCA, CBN, CBD, and THC under basic conditions using a reversed phase (C18) mixed-mode column (4.6 x 33 mm) at 45 °C with solvents A: 95/5 (H_2O/ACN) and B: MeOH with 0.4 % $N(CH_3)_4^+OH^-$ (25 % in MeOH). The isocratic elution condition was 40/60 (A/B), the flow rate was 1.0 mL/min, and the injection volume was 1 µL. Retention factors, k, and efficiencies, N/m, for THCA, CBN, CBD, and THC in this separation are 1.50 and 13,600, 1.64 and 16,800, 2.33 and 41,500, and 3.27 and 48,950, respectively. 115

Figure 4.4 The chromatogram showed the details for the separation of CBD, THC, and CBN in Figure 4.3A. 116

Figure 4.5 The chromatogram showed the details for the separation of CBN, CBD, and THC in Figure 4.3B. 118

Figure 4.6 (A) Separation of CBD, THC, CBN, and THCA using a reversed phase (C18+) mixed-mode column (4.6 x 33 mm) at 35 °C with a polar organic mobile phase: 20/80 (ACN/MeOH) with 0.4 % $N(CH_3)_4^+OH^-$ (conc. 25 % in MeOH). Flow rate was 1.0 mL/min and injection volume was 1 µL. Retention factors, k, and efficiencies, N/m, for CBD, THC, CBN, and THCA in this separation are 0.16 and 16,700, 0.37 and 22,600, 0.74 and 24,000, and 2.55 and 25,000, respectively. (B) Separation of CBD, THC, CBN, and THCA using a HILIC mixed-mode column (4.6 x 150 mm) at 35 °C with solvent A: 10/90 (H_2O/ACN) with 0.5 % ammonium hydroxide (28-30%, pH 10.4) and B: ACN. Isocratic condition was 40/60 (A/B). Flow rate was 1.5 mL/min and injection volume was 1 µL. Retention factors,

k, and efficiencies, N/m, for CBD, THC, CBN, and THCA in this separation are 0.31 and 8,200, 0.94 and 54,300, 3.72 and 25,800, and 12.75 and 48,000, respectively. 121

Figure 4.7 (A) Separation of CBDA, THCA, CBN, CBD and THC under basic condition using a reversed phase (C18) mixed-mode column (4.6 x 33 mm) at 30°C with solvents A: 95/2.5/2.5 (H_2O/MeOH/ACN) and B: 10/20/70 (H_2O/MeOH/ACN). 0.2 % $N(CH_3)_4^+OH^-$ (conc. 25 % in MeOH) was added to solvents A and B. Gradient elution conditions: 0 min 100 % A, 3 min 0 % A, 3.01 min 100 % A, and 8 min end. The flow rate was 1.0 mL/min, and the injection volume was 1 µL. The peak capacity (gradient time divided by the average peak width) for this separation was 55. (B) Separation of CBDA, THCA, CBN, CBD and THC under basic conditions using a longer reversed phase (C18) mixed-mode column (4.6 x 100 mm) at 35 °C with solvents A: 95/2.5/2.5 (H_2O/MeOH/ACN), and B: 10/20/70 (H_2O/MeOH/ACN). 0.2 % $N(CH_3)_4^+OH^-$ (conc. 25 % in MeOH) was added to solvent A and B. Gradient elution conditions: 0 min 100% A, 8min 0 % A, 8.01 min 100 % A, and 14 min end. The flow rate was 1.0 mL/min, and the injection volume was 1 µL. The peak capacity (gradient time divided by the average peak width) for this separation was 44. (C) Separation of bubble hash extract under basic conditions using a reversed phase (C18) mixed-mode column (4.6 x 50 mm) at 30 °C with solvents A: 95/2.5/2.5 (H_2O/MeOH/ACN) and B: 10/20/70 (H_2O/MeOH/ACN). 0.2 % $N(CH_3)_4^+OH^-$ (conc. 25 % in MeOH) was added to solvents A and B. Gradient elution conditions: 0 min 100 % A, 10 min 0 % A, 10.01 min 100 % A, and 16 min end. The flow rate was 1.0 mL/min, and the injection volume was 2 µL. The DAD detector was set at 230 nm. The peak capacity (gradient time divided by the average peak width) for this separation was 56..... 123

Figure A3.1 Structure of separated tricyclic antidepressants..... 151
Figure A3.2 Chromatogram of (1) doxepin, (2) nortriptyline, (3) imipramine, (4) amitriptyline, and (5) clomipramine separated at pH 12..... 152
Figure A4.1 Structure of separated alkaloids..... 155
Figure A4.2 Chromatogram of (1) prilocaine, (2) lidocaine, and (3) bupivacaine separated at pH 12..... 156
Figure A5.1 Retention times of hexylbenzene (top points) and butylbenzene (lower points) at different mobile phase pHs. 163
Figure A5.2 Chromatograms of ethyl-, butyl-, and hexylbenzene at pH 7, 2, 11, and then 7.... 164
Figure A6.1 Structure of separated BSA and apo-transferrin..... 167
Figure A6.2 Separations of apo-transferrin (1) and BSA (2). (A) 0.1% TFA in buffers A and B, and (B) 0.1% TFA in buffer A and 0.0875% TFA in buffer B..... 168
Figure A6.3 Mass spectra of apo-transferrin (A1 and B1) and BSA (A2 and B2) from the corresponding peaks in the chromatograms in Figure 1 (A) and (B). 169
Figure A7.1 Structure of separated ginsenoside Re and Rd. 175
Figure A7.2 Separations of ginsenoside Re (1) and ginsenoside Rd (2). 176
Figure A7.3 Mass spectra of ginsenoside Re (A) and ginsenoside Rd (B) from the corresponding peaks (1 and 2) in the chromatogram in Figure A7.1. 177

Chapter 1: Introduction

1.1. A Brief History of HPLC

High performance liquid chromatography (HPLC) is one of the most widely applied analytical techniques for chemical analysis.[1-4] The term "chromatography", which means "color writing", was first introduced in the early 1900s by the Russian scientist, Mikhail S. Tswett.[3-7] Tswett invented classical column (adsorption) chromatography and demonstrated the separations of plant pigments.[1, 5-6] In his experiments, a plant pigment extract was poured onto the top of a column filled with a calcium carbonate adsorbent, and a solvent containing petroleum ether was passed through the column.[5, 7] The mixture was separated, and the components were identified based on their different colors.[1] Interestingly, Tswett's invention of chromatography did not gain wide acceptance and was only adapted by some researchers.[4-5] Later, in the 1930s, chromatography was rediscovered by Edgar Lederer, a scientist in Richard Kuhn's laboratory in Heidelberg, Germany, who studied chromatographic methods for separating carotenoids in egg yolk.[5, 8] This rediscovery of Tswett's works led to an explosion in the development of chromatography.[1]

In 1938, thin layer chromatography was introduced by Izmailov and Schraiber in Ukraine, and in 1951, this technique was further rediscovered in the U.S. by Kirchner.[3, 9-10] In the 1940s, Martin and Synge studied the combination of (adsorption) chromatography and countercurrent solvent extraction (liquid-liquid extraction, LLE) and developed the principles of partition chromatography.[11] Partition chromatography was based on two immiscible solvents and the relative solubility of solutes in these two solvents.[12-13] In 1952, Martin and Synge's work on partition chromatography was recognized with the Nobel Prize in chemistry.[14] Their work

encouraged the development of paper chromatography and gas chromatography (GC), where GC is the precursor of HPLC.[15-16] Significant development in chromatography occurred after 1960.[1] The first HPLC columns were introduced between 1964 to 1965, where the particle sizes in these columns were around 100 μm.[17-18]

Smaller particles in HPLC lead to higher separation efficiencies and faster separations.[17-25] The trend toward smaller particles in HPLC during the last few years, which has led to increased performance, matches Martin and Synge's prediction for the technique in 1941.[11] During the past decade the continued decease in particle size has necessitated the introduction of equipment that can deliver higher pressures.[23] For example, in the 2000s, ultra high performance liquid chromatography (UHPLC) was introduced, which provides the high pressures needed for small particle columns.[20, 24-26] Some of the most recently developed HPLC columns today have efficiencies in excess of 250,000 plate per meter (N/m).[19] These columns come with many types of bonded phases, including mixed-mode options, that provide the user with many different selectivities.[19, 21, 27-29]

1.2. Theory of Chromatography

1.2.1. Plate Theory

In 1942, Martin and Synge developed plate theory, which describes column efficiency using the concept of theoretical plates.[1, 11-12] Plate theory was adapted from the fields of distillation and countercurrent distribution to explain the complete equilibrium process of analytes in stationary and mobile phases in chromatography.[11-12] That is, each individual unit in chromatography can be considered to be one theoretical plate where equilibrium is established,

i.e., one can imagine each complete equilibrium process in a theoretical plate as the condensation and revolatilization processes in distillation or the individual extraction in a countercurrent distribution.[11] Although plate theory contains a number of simplifying assumptions, it is still useful for evaluating different types of separation methods.[12] Some factors derived from plate theory include the number of theoretical plates (N), the plate height (H), the retention factor (k), the selectivity (α), the peak capacity (n), and the resolution (R_s).[1, 7, 12]

1.2.1.1. Number of Theoretical Plates (N)

The measurement of the number of theoretical plates, N, is given in Equation 1.1, where t_R is the elution time of an analyte, and W_b is its baseline peak width.[1, 12] The value of W_b is determined by drawing the tangent line at the inflection points of the peak (on both sides of a peak), and finding the intersection of those tangent lines with the baseline.[1, 7]

$$N = 16\left(\frac{t_R}{W_b}\right)^2 \tag{1.1}$$

Because an ideal chromatographic peak has a Gaussian shape, the baseline peak width, W_b, is equal to 4σ, where σ is the standard deviation of the Gaussian peak profile.[1, 7, 12] Thus, Equation 1.1 can be represented in term of the standard deviation, σ (Equation 1.2).[1, 12]

$$N = \left(\frac{t_R}{\sigma}\right)^2 \tag{1.2}$$

However, there are challenges associated with Equations 1.1 and 1.2. Measuring the number of theoretical plates from a peak by determining its width at the baseline can be challenging, especially if two peaks are not fully separated.[1, 7] Equation 1.2 is also not convenient because it requires the measurement/calculation of the standard deviation of a Gaussian.[1, 12] It is much more

convenient and straightforward simply to measure the half height, $W_{1/2}$, of the peak.[7] In the resulting equation (Equation 1.3), $W_{1/2}$, is approximately equal to 0.588 W_b.[1]

$$N = 5.545 \left(\frac{t_R}{W_{1/2}}\right)^2 \quad (1.3)$$

Equations 1.1 and 1.3 show that in a separation, increasing the retention time or decreasing the peak width of solutes without altering the other parameter results in higher numbers of theoretical plates.[1, 12]

1.2.1.2. Plate Height (H)

The efficiency of a chromatographic separation can also be measured using the plate height, H, which represents the successive equilibriums in a series of segments (theoretical plates) in a chromatographic column.[7, 12, 30] This is also known as the height equivalent of a theoretical plate, HETP, and it is an indication of zone spreading.[12] The plate height, H, is calculated by dividing the column length, L, by the number of theoretical plates, N, (Equation 1.4).[1, 7, 12]

$$H = \frac{L}{N} \quad (1.4)$$

Equation 1.4 shows that for a given column length, higher numbers of theoretical plates result in smaller plate heights.[1, 12]

1.2.1.3. Retention Factor (k)

The retention of solutes in chromatography can be described as the interaction (distribution) of solutes between two phases: a stationary phase and a mobile phase.[1, 11-12]

Stationary phases can be solids or liquids and mobile phases can be liquids, gases, or supercritical fluids.[12] In a separation, one can model the interactions of a solute, A, with the mobile and stationary phases in a column as the following equilibrium:[1, 7, 12]

$$A_{\text{Mobile Phase}} = A_{\text{Stationary Phase}} \tag{1.5}$$

This equilibrium is then described mathematically by an equilibrium constant, the partition coefficient, K:

$$K = \frac{A_s/V_s}{A_m/V_m} \tag{1.6}$$

where A_s and A_m are the number of moles of the analyte in the stationary and mobile phases, respectively, and V_s and V_m are the volumes of the stationary phase and mobile phase, respectively.[1, 12]

The retention factor, k, which was previously known as the capacity factor, is the ratio of the number of moles of solute in the stationary phase to the number of moles of solute in the mobile phase (A_s/A_m) (Equation 1.7). Consequently, from Equation 1.6, it is also equal to K times V_m/V_s, where this quotient is known as the phase ratio, Φ.[1, 7, 12]

$$k = \frac{A_s}{A_m} = K * \Phi \tag{1.7}$$

The fraction of the solute in the stationary phase, p, is:[12]

$$p = \frac{A_S}{A_s + A_m} \tag{1.8}$$

Now, applying Equation 1.7 to Equation 1.8 we obtain Equation 1.9:

$$p = \frac{k}{1+k} \tag{1.9}$$

Because the sum of the fractions of the solute in the stationary phase and mobile phase are one, the fraction of solute in the mobile phase, q, is equal to one minus p:

$$q = \frac{1}{1+k} \tag{1.10}$$

The solute distributes itself between the mobile and stationary phases. Accordingly, the average velocity of the solute A, u_A, is equal to the fraction of solute in the mobile phase multiplied by the average of velocity of the mobile phase, u, plus the fraction of solute in the stationary phase multiplied by the average velocity of the stationary phase.[12] Because the stationary phase is not moving, the average velocity of the solute in the mobile phase, u_A, is simply:

$$u_A = qu \tag{1.11}$$

Because the length, L, of an HPLC column is fixed, the retention time of a solute, t_R, and the time required for the mobile phase to pass through the column (the so called dead time of the column), t_0, are given as follows:[1, 12]

$$t_R = \frac{L}{u_A} \tag{1.12}$$

and

$$t_0 = \frac{L}{u} \tag{1.13}$$

By combining Equations 1.12 and 1.13, t_R can be expressed as:[12]

$$t_R = \frac{t_0 * u}{u_A} \tag{1.14}$$

Because q is equal to u_A/u (Equation 1.11) Equation 1.14 can be expressed as:

$$t_R = \frac{t_0}{q} \tag{1.15}$$

By applying Equation 1.10 to Equation 1.15, the retention factor, k, is found to be:[1, 7, 12, 23]

$$k = \frac{t_R - t_0}{t_0} \tag{1.16}$$

The retention factor, k, is a quantitative measure of the retention of a solute relative to an unretained species, which is typically the unretained solvent or contaminants in the analyte mixture.[1] As a solute is retained to a greater extent on a column, its retention factor increases. Finally note that a previous symbol for the retention factor was k'.

1.2.1.4. Selectivity (α)

The selectivity, α,[1, 12] of two peaks, peak 1 and peak 2, with their relative retention factors, k_1 and k_2, respectively, is:

$$\alpha = \frac{k_2}{k_1} \tag{1.17}$$

In this equation, k_2 is greater than k_1. Clearly, if two eluted peaks have a greater difference in retention factor, their selectivity increases.

1.2.1.5. Resolution (R_s)

The purpose of chromatography is to separate analytes into well distinguished (resolved) peaks.[1, 12] Resolution is the term used to describe the quality of two separated, adjacent peaks. There are three well-known resolution equations: the Said equation, the Purnell equation, and the Knox equation.[12] I will now proceed to derive all three of them.

For the Said equation, we note that the resolution between two peaks is defined as the separation between them ($t_{R2} - t_{R1}$) divided by the average of their widths: 1/2(W_{b1} and W_{b2}) (Equation 1.18).[1, 7, 12, 31]

$$R_s = \frac{t_{R2} - t_{R1}}{\frac{1}{2}(W_{b2} + W_{b1})} \tag{1.18}$$

Because W_b is equal to $(4/N^{1/2})t_R$ by Equation 1.1, Equation 1.18 can be represented as:

$$R_s = \frac{t_{R2} - t_{R1}}{\frac{1}{2}(\frac{4}{\sqrt{N}}t_{R2} + \frac{4}{\sqrt{N}}t_{R1})} \tag{1.19}$$

We rearrange Equation 1.19 and obtain:

$$R_s = \frac{\sqrt{N}}{2}(\frac{t_{R2} - t_{R1}}{t_{R2} + t_{R1}}) \tag{1.20}$$

Of course it is assumed here that N is the same for both peaks, which will in general be a good approximation if the peaks are closely spaced and chemically similar. If we apply $t_R = t_0 (1+k)$ (Equation 1.16) to Equation 1.20, we obtain:[12]

$$R_s = \frac{\sqrt{N}}{2}(\frac{t_0 + t_0k_2 - t_0 - t_0k_1}{t_0 + t_0k_2 + t_0 + t_0k_1}) \tag{1.21}$$

We then divide the second factor of Equation 1.21 by t_0 and we obtain:

$$R_s = \frac{\sqrt{N}}{2}(\frac{k_2 - k_1}{k_2 + k_1 + 2}) \tag{1.22}$$

If we divide the numerator and denominator of the second factor of Equation 1.22 by k_1, we obtain:

$$R_s = \frac{\sqrt{N}}{2}(\frac{\frac{k_2}{k_1} - \frac{k_1}{k_1}}{\frac{k_2}{k_1} + \frac{k_1}{k_1} + \frac{2}{k_1}}) \tag{1.23}$$

Now applying the definition of α as k_2/k_1 (see Equation 1.17) to Equation 1.23, we obtain:

$$R_s = \frac{\sqrt{N}}{2}\left(\frac{\alpha - 1}{\alpha + 1 + \frac{2}{k_1}}\right) \tag{1.24}$$

If we assume $(k_2 + k_1)/2 = k$, and using the fact that $k_2 = \alpha^* k_1$, k_1 can be represented as:[12, 31]

$$k_1 = \frac{2k}{1+\alpha} \tag{1.25}$$

Applying Equation 1.25 to Equation 1.24, we obtain:

$$R_s = \frac{\sqrt{N}}{2}\left(\frac{\alpha - 1}{\alpha + 1 + \frac{2(1+\alpha)}{2k}}\right) \tag{1.26}$$

or

$$R_s = \frac{\sqrt{N}}{2}\left(\frac{\alpha - 1}{\alpha + 1 + \frac{(\alpha+1)}{k}}\right) \tag{1.27}$$

or

$$R_s = \frac{\sqrt{N}}{2}\left(\frac{\alpha - 1}{\alpha + 1\,(1 + \frac{1}{k})}\right) \tag{1.28}$$

or

$$R_s = \frac{\sqrt{N}}{2}\left(\frac{\alpha - 1}{\alpha + 1\,(\frac{k+1}{k})}\right) \tag{1.29}$$

We rearrange Equation 1.29 and obtain Equation 1.30, which is known as the Said equation or "exact" resolution equation:[12]

$$R_s = \frac{\sqrt{N}}{2}\left(\frac{\alpha - 1}{\alpha + 1}\right)\left(\frac{k}{1+k}\right) \tag{1.30}$$

To derive the Purnell equation, we note that if two adjacent peaks have similar peak widths and if we replace the average of the peak width of the two adjacent peaks with the width of the second eluted peak in Equation 1.18, we obtain:[31]

$$R_s = \frac{t_{R2} - t_{R1}}{W_{b2}} \tag{1.31}$$

Because W_{b2} is equal to $(4/N^{1/2})t_{R2}$ by Equation 1.1, Equation 1.31 can be represented as:

$$R_s = \frac{\sqrt{N}}{4} \frac{t_{R2} - t_{R1}}{t_{R2}} \tag{1.32}$$

If we apply $t_R = t_0 (1 + k)$ (Equation 1.16) to Equation 1.32, we obtain:

$$R_s = \frac{\sqrt{N}}{4} \left(\frac{t_0 + t_0 k_2 - t_0 - t_0 k_1}{t_0 + t_0 k_2}\right) \tag{1.33}$$

or

$$R_s = \frac{\sqrt{N}}{4} \left(\frac{k_2 - k_1}{1 + k_2}\right) \tag{1.34}$$

Equation 1.34 can be represented as:

$$R_s = \frac{\sqrt{N}}{4} \frac{k_2 - k_1}{k_2} \frac{k_2}{1 + k_2} \tag{1.35}$$

By dividing the numerator and denominator of the second factor by k_1, we obtain:

$$R_s = \frac{\sqrt{N}}{4} \frac{\frac{k_2}{k_1} - \frac{k_1}{k_1}}{\frac{k_2}{k_1}} \frac{k_2}{1 + k_2} \tag{1.36}$$

We can represent the second factor of Equation 36 in terms of selectivity, α, and we obtain Equation 1.37, which is known as the Purnell equation:[1, 12]

$$R_s = \frac{\sqrt{N}}{4} \frac{\alpha - 1}{\alpha} \frac{k_2}{1 + k_2} \tag{1.37}$$

By a similar approach, the Knox equation can be obtained if we replace the average of the peak widths of the two adjacent peaks with the width of the first eluted peak in Equation 1.18, as follows:[12]

$$R_s = \frac{t_{R2} - t_{R1}}{W_{b1}} \tag{1.38}$$

Because W_{b1} is equal to $(4/N^{1/2})t_{R1}$ by Equation 1.1, Equation 1.38 can be represented as:

$$R_s = \frac{\sqrt{N}}{4} \frac{t_{R2} - t_{R1}}{t_{R1}} \tag{1.39}$$

If we apply $t_R = t_0 (1+k)$ (Equation 1.16) to Equation 1.39, we obtain:

$$R_s = \frac{\sqrt{N}}{4} \left(\frac{t_0 + t_0 k_2 - t_0 - t_0 k_1}{t_0 + t_0 k_1}\right) \tag{1.40}$$

We divide the second factor of Equation 1.40 by t_0 and we obtain:

$$R_s = \frac{\sqrt{N}}{4} \left(\frac{k_2 - k_1}{1 + k_1}\right) \tag{1.41}$$

Equation 1.41 can be represented as:

$$R_s = \frac{\sqrt{N}}{4} \frac{k_2 - k_1}{k_1} \frac{k_1}{1 + k_1} \tag{1.42}$$

By dividing the numerator and denominator of the second factor by k_1, Equation 1.42 can be represented as:

$$R_s = \frac{\sqrt{N}}{4} \frac{\frac{k_2}{k_1} - \frac{k_1}{k_1}}{\frac{k_1}{k_1}} \frac{k_1}{1 + k_1} \tag{1.43}$$

or

$$R_s = \frac{\sqrt{N}}{4} \frac{\frac{k_2}{k_1} - 1}{1} \frac{k_1}{1 + k_1} \quad (1.44)$$

If we multiply k_1 to the third factor of Equation 1.44, we obtain:

$$R_s = \frac{\sqrt{N}}{4} \left(\frac{k_2}{k_1} - 1\right) \frac{k_1}{1 + k_1} \quad (1.45)$$

The second factor of Equation 1.45 can be represented in term of selectivity, α, and we obtain Equation 1.46, which is known as the Knox equation:[12]

$$R_s = \frac{\sqrt{N}}{4} (\alpha - 1) \left(\frac{k_1}{1 + k_1}\right) \quad (1.46)$$

For high efficiency chromatography, e.g., capillary chromatography, where the peak widths of the two adjacent peaks are considered equal, the Purnell and Knox equations are preferred.[31] However, if the peak width of the second peak is greater than the first peak, the Said or "exact" equation has to be used.[12, 31] Comparing these three equations, the Said (or "exact") equation gives the average values of the Purnell and Knox equations, where the Purnell and Knox equations give slightly lower and slightly higher values, respectively, of R_s compared to the Said equation.[12]

1.2.1.6. Peak Capacity (n)

The column peak capacity, n, is described as the number of peaks that can be fitted in a given time interval with a resolution of unity (Equation 1.47), where t_{R2} and t_{R1} are the retention times of the first and the last peaks, respectively, and W_b is the width of the peaks at their bases.[32-33] The "1" term in the equation indicates that the left and right half-widths of the first and last peaks are included, and W_b is the mean peak width.[32]

$$n = 1 + \frac{t_{R2} - t_{R1}}{W_b} = 1 + \frac{\Delta t_R}{W_b} \quad (1.47)$$

Equation 1.47 does not take into account the variation in peak width that occurs as a function of retention time in the separation.[12, 32] In gradient elution, the peak widths are generally similar, especially at small gradient times; but, in most cases the peak width increases with time. In such cases, the peak width is usually measured by averaging a few peak widths.[32] A "sample peak capacity" that correlates the peak capacity and resolution was proposed by Dolan et al. (Equation 1.48).[32]

$$n^* = \frac{t_{R2} - t_{R1}}{W_b} = \frac{\Delta t_R}{W_b} \quad (1.48)$$

In the case of high peak capacities, Equations 1.47 and 1.48 can be considered to be equal.[32]

In the following, we will show the approaches of Giddings and Grushka to derive the peak capacity. In 1967, Giddings approached the issue of peak capacity by using a resolution of unity. If the resolution of two adjacent peaks is one, the difference in retention time between these two peaks can be represented as:[32-34]

$$t_{R2} - t_{R1} = \frac{W_{b2} + W_{b1}}{2} = \frac{4\sigma_2 + 4\sigma_1}{2} \quad (1.49)$$

Since σ is equal to $t_R/N^{1/2}$ by Equation 1.2, $t_R/N^{1/2}$ can be applied to Equation 1.49 to obtain:

$$t_{R2} - t_{R1} = \frac{\frac{4}{\sqrt{N}}(t_{R2} + t_{R1})}{2} \quad (1.50)$$

For convenience, α' (not selectivity) is used to represent $4/N^{1/2}$, so Equation 1.50 can be represented as:

$$t_{R2} - t_{R1} = \frac{\alpha'(t_{R2} + t_{R1})}{2} \quad (1.51)$$

By dividing both sides of Equation 1.51 by t_{R1}, the ratio of retention times for the two adjacent peaks is:

$$\frac{t_{R2}}{t_{R1}} - 1 = \frac{\alpha'}{2}\left(\frac{t_{R2}}{t_{R1}} + 1\right) \tag{1.52}$$

We then rearrange Equation 1.52 to obtain:

$$\frac{t_{R2}}{t_{R1}} = \frac{1+ \alpha'/2}{1- \alpha'/2} \tag{1.53}$$

We can represent the ratio of the first, t_{R1}, and the last eluted peaks, t_{Rn} as:[32]

$$\frac{t_{Rn}}{t_{R1}} = \left(\frac{t_{R2}}{t_{R1}}\right)\left(\frac{t_{R3}}{t_{R2}}\right)\left(\frac{t_{R4}}{t_{R3}}\right)\ldots.\left(\frac{t_{Rn}}{t_{Rn-1}}\right) \tag{1.54}$$

We apply Equation 1.53 to Equation 1.54, and obtain:

$$\frac{t_{Rn}}{t_{R1}} = \left(\frac{1+ \alpha'/2}{1- \alpha'/2}\right)\left(\frac{1+ \alpha'/2}{1- \alpha'/2}\right)\left(\frac{1+ \alpha'/2}{1- \alpha'/2}\right)\ldots.\left(\frac{1+ \alpha'/2}{1- \alpha'/2}\right) = \left(\frac{1+ \alpha'/2}{1- \alpha'/2}\right)^{n-1} \tag{1.55}$$

By taking logarithms of both sides in Equation 1.55, we obtain:

$$\ln\frac{t_{Rn}}{t_{R1}} = (n-1)\ln\left(\frac{1+ \alpha'/2}{1- \alpha'/2}\right) \tag{1.56}$$

We arrange Equation 1.56 and obtain:

$$n = 1 + \frac{\ln\frac{t_{Rn}}{t_{R1}}}{\ln\left(\frac{1+ \alpha'/2}{1- \alpha'/2}\right)} \tag{1.57}$$

In most situations, N is sufficiently large, and α' is relatively small, so Giddings expanded the denominator of Equation 1.57, as follows:[32]

$$\ln\left(\frac{1+\frac{\alpha'}{2}}{1-\frac{\alpha'}{2}}\right) = \alpha' + \frac{1}{3}\alpha'^3 + \cdots \tag{1.58}$$

Giddings retained the first term, α', and discard all other terms, so Equation 1.57 can be represented as Equation 1.59, where α' (not selectivity) is $4/N^{1/2}$:

$$n = 1 + \frac{1}{\alpha'} \ln \frac{t_{Rn}}{t_{R1}} = 1 + \frac{\sqrt{N}}{4} \ln \frac{t_{Rn}}{t_{R1}} \tag{1.59}$$

Equation 1.59 can also be represented in terms of the retention factor for the first peak, k_1, and the last peak, k_n (Equation 1.60):

$$n = 1 + \frac{\sqrt{N}}{4} \ln \frac{1 + k_n}{1 + k_1} \tag{1.60}$$

In 1970, Grushka derived the peak capacity using an infinitesimal treatment to take an account of the variation of W_b with retention time.[32, 35] Similar to the resolution equation that is defined as the change in the retention time of two adjacent peaks divided by the average of the peak widths of these two adjacent peaks (Equation 1.18), Grushka defined the peak capacity as the number of peaks in a small time interval:[32]

$$dn = \frac{dt}{W_b} \tag{1.61}$$

If we replace the peak width, W_b, with 4σ, we obtain:

$$dn = \frac{dt}{4\sigma} \tag{1.62}$$

Since 4σ is equal to $4t/N^{1/2}$, where t is the retention time, Equation 1.62 can be represented as:

$$dn = \frac{\sqrt{N}}{4} \frac{dt}{t} \tag{1.63}$$

Equation 1.63 is integrated to obtain Equation 1.64, where t_{Rn} and t_{Ro} represent the last eluted peak and the dead time peak (not the first peak), respectively:

$$\int_1^n dn = n - 1 = \frac{\sqrt{N}}{4}\int_{t_{R0}}^{t_{Rn}} \frac{dt}{t} \quad (1.64)$$

We arrange Equation 1.64 to obtain:

$$n = 1 + \frac{\sqrt{N}}{4}\ln\frac{t_{Rn}}{t_{R0}} \quad (1.65)$$

Grushka's approach (Equation 1.65) leads to Giddings' peak capacity equation (Equation 1.59).[32] However, unlike Giddings' approach, Grushka chose the dead time peak as the first peak instead of the first eluted peak.[32] If Equation 1.65 is represented in terms of the retention factor, the retention factor of the dead time peak is negligible. Accordingly, it can be simplified (Equation 1.66), where k_n is the retention factor of the last eluted peak:

$$n = 1 + \frac{\sqrt{N}}{4}\ln(1 + k_n) \quad (1.66)$$

Thus, the peak capacity of a column can be predicted when the number of theoretical plates of a column and two chosen peaks with their retention times or retention factors are known.

1.2.2. Rate Theory and the van Deemter Equation

After Martin and Synge, many theories were developed to describe the relationship between plate height and the mobile phase linear velocity.[1, 12] These were classified into the general category of rate theory. If we apply Equation 1.4 to Equation 1.2, we obtain:[12]

$$\frac{L}{H} = \left(\frac{t_R}{\sigma}\right)^2 \quad (1.67)$$

Equation 1.67 can be rearranged to give:

$$H = \left(\frac{L}{t_R^2}\right)\sigma^2 \quad (1.68)$$

A Gaussian peak shape in chromatography is the result of a series of broadening mechanisms, where each such mechanism contributes a variance, σ^2.[1, 12] The σ^2 In Equation 68 represents the total variance contributed from each broadening mechanism, as follows:

$$\sigma^2 = {\sigma_1}^2 + {\sigma_2}^2 + {\sigma_3}^2 + {\sigma_4}^2 + {\sigma_5}^2 \ldots . = \sum {\sigma_i}^2 \quad (1.69)$$

Here ${\sigma_1}^2$, ${\sigma_2}^2$, ${\sigma_3}^2$, ${\sigma_4}^2$, ${\sigma_5}^2$ are contributions from eddy diffusion, longitudinal diffusion, resistance to mobile phase mass transfer, resistance to stationary phase mass transfer, and extra column contributions, etc.[12] For a well-designed conventional HPLC system, the extra column contribution is minimum; however, since the introduction of UHPLC systems for higher efficiency HPLC, extra column broadening has become an issue for narrower or sharper peaks, especially for those eluted earlier in a chromatogram.[1] This issue can be minimized by the use of narrow bore tubing and better column fittings. In general, the extra column contributions are ignored in the following equations and accompanying discussion.

Similar to Equation 1.68, which is a sum of variances, the plate height is the sum of each broadening mechanism.[1, 12] That is, in Equation 1.70, H_E is the contribution due to eddy diffusion, H_L is the contribution from longitudinal diffusion, H_{MP} is the contribution from the resistance to mobile phase mass transfer, and H_{SP} is the resistance to mass transfer in the stationary phase.[12]

$$H_{total} = H_E + H_L + H_{MP} + H_{SP} \quad (1.70)$$

We will now discuss van Deemter theory, which is one of the mostly widely use rate theories in chromatography. The early form of the van Deemter equation was developed in the 1950s by a group of Dutch chemical engineers and is known as the Lapidus and Amundson equation (Equation 1.71), where λ is the eddy diffusion factor, d_p is the particle diameter, Υ is the obstruction factor, and D_m and D_l are the molecular diffusivities of the analyte in the mobile phase

and stationary phase, respectively.[30] In addition, u is the linear velocity of the mobile phase, k is the column capacity ratio (retention factor), and d_f is the stationary phase film thickness.

$$H = 2\lambda d_p + \frac{2\Upsilon D_m}{u} + \frac{8}{\pi^2}\frac{k}{(1+k)^2}\frac{{d_f}^2 u}{D_l} \quad (1.71)$$

A simplied form of the van Deemter equation is commonly used in chromatography:[7, 18, 30, 36]

$$H = A + \frac{B}{u} + Cu \quad (1.72)$$

Here, the C term can be further expressed as a combination of C_s and C_m terms that represent the resistance to mass transfer in the stationary and mobile phases, respectively (Equation 1.73).[1, 12]

$$H = A + \frac{B}{u} + (C_s + C_m)u \quad (1.73)$$

The A term represents eddy diffusion in which analytes go through multiple paths in a column. However, eddy diffusion is a misleading description for the A term because it deals with analytes taking different paths through a column, but does not take diffusion into account in any way.[1, 7, 12] The B term represents longitudinal diffusion, i.e., along and against the direction of flow in the column. The C ($C_s + C_m$) term represents resistance to mass transfer in the stationary phase and mobile phase, where analytes have not instantaneously come to equilibrium in these two phases.[1, 12] In the van Deemter equation, the A term is independent of the linear velocity of the mobile phase, and the B and C terms, on the other hand, are dependent on its linear velocity.[1] For example, the C_s component of the C term is greatly improved by reducing the stationary film thickness.[12] In the case of increasing the linear velocity of the mobile phase, the A term remains constant. In contrast, the B term gets lower and the C term increases.

Although the van Deemter equation is useful for analyzing zone broadening, it is not completely correct because it assumes each term is independent from each other.[1] In 1961,

Giddings pointed out that eddy diffusion and lateral mass transfer in the mobile phase should be considered as one coupled mechanism.[37-38] Knox further addressed this issue and derived an equation, which represents the eddy diffusion and the resistance to mass transfer in the mobile phase.[37] This equation is known as Knox-Bristow equation (Equation 1.74), where, h is the reduced plate height (Equation 1.75) and v is a reduced velocity (Equation 1.76).[18, 20, 37, 39-42]

$$h = Av^{0.33} + \frac{B}{v} + Cv \tag{1.74}$$

$$h = \frac{H}{d_p} \tag{1.75}$$

$$v = \frac{ud_p}{D_m} \tag{1.76}$$

Currently, the Knox and van Deemter equations are the two mostly widely encountered equations in chromatography.[43] However, the van Deemter equation is commonly chosen to determine the minimum plate height and optimum velocity because of its simplicity.

1.3. Manipulating Resolution in HPLC

Different separation conditions can change the resolution, R_s, in HPLC.[1, 7, 12] This is because different conditions affect values of retention factor (k), selectivity (α), and number of theoretical plates (N) in a separation.[1] Of these three terms, the selectivity, α, affects the resolution the most.[31] Increasing the value of the retention factor (k) up to a point (to 10 or maybe 20) also increases the resolution of a separation (see Equations 1.30, 1.37, and 1.46).[7, 12] But beyond this point, it has little effect on resolution. In general, higher values of k result in longer analysis times and broader peaks, both of which are undesirable. Fast separations at high resolution are clearly the most desirable. Other separation conditions, including the type of stationary phase, the mobile

phase composition, temperature, pH, buffer concentration, and ion-pair-reagent concentration, can significantly affect the retention factor (k) and the selectivity (α).[1, 12] Column length, particle size, and flow rate have greater effect on the number of theoretical plates (N). Pressure has little effect on the number of theoretical plates (N).[1]

1.3.1. pH and Temperature Effects on Resolution

pH and temperature also change the resolution in HPLC separations.[44-46] In particular, the retention factor, k, is a function of pH and temperature for ionizable analytes.[47] Many important analytes are acids and bases that require adjustment of pH to get good retention. For example, many pharmaceuticals are obtained in their protonated form and are better retained at higher pH (pH > 10) where they are in their neutral form.[50-51] For acidic analytes, lower pH is preferred, where they are neutral.

Temperature also affects the retention of analytes.[36, 40, 44-46] Indeed, when the retention factor of an analyte is obtained at different temperatures, these data can be used to generate a van't Hoff plot.[40-41] The van't Hoff equation is derived by combining two classical equations, i.e., one that relates the free energy to the enthalpy and entropy of adsorption in a separation, and the other that relates it to the equilibrium constant, K for the process:[44-46]

$$-\mathrm{RT}\ln \mathrm{K} = \Delta \mathrm{H}^0 - \mathrm{T}\Delta \mathrm{S}^0 \tag{1.77}$$

Upon rearrangement, the following equation is obtained:

$$\ln \mathrm{K} = -\frac{\Delta H^0}{RT} + \frac{\Delta S^0}{R} \tag{1.78}$$

In Equation 1.78, the equilibrium constant, K, can be replaced with the retention factor, k, and the phase ratio, Φ:

$$\ln \frac{k}{\Phi} = -\frac{\Delta H^0}{RT} + \frac{\Delta S^0}{R} \quad (1.79)$$

We rearrange Equation 1.79 to obtain:

$$\ln k = -\frac{\Delta H^0}{RT} + \frac{\Delta S^0}{R} + \ln \Phi \quad (1.80)$$

The van't Hoff equation is useful for predicting the order of retention of analytes at different temperatures, allowing coeluting compounds to be separated via temperature.

1.3.2. Effects of Bonded Phases on Resolution

Changing the bonded phase changes the selectivity/retention of analytes in HPLC.[1, 12] This is because different types of stationary phases show different intermolecular interactions with different analytes. The reversed phase stationary phase, which retains analytes through hydrophobic interactions (dispersion forces), is the most commonly used type of HPLC column.[1] When a reversed phase separation is not successful, hydrophilic interaction liquid chromatography (HILIC) and normal phase chromatography may be considered for retaining analytes. Recently, mixed-mode HPLC has attracted much attention.[27] These phases are the combination of hydrophobic-interaction chromatography (HIC) or hydrophilic-interaction chromatography (HILIC) with ion-exchange chromatography (IEC).[27, 48] Compared with traditional reversed and normal phase columns, mixed-mode columns provide multiple retention mechanisms, which are beneficial for amphiphilic analytes that have both hydrophobic and hydrophilic, and perhaps ionic

properties.[27, 29] Some research groups have obtained good separations of proteins using mixed-mode columns.[27-29, 48-49]

1.4. Silica-Based Packing Materials and Their Limitations

Since the 1960s, silica-based materials have dominated the HPLC markets.[50] Because of their advantages of high mechanical strength, solvent capability, easy surface modification, and high reproducibility, silica materials are well adapted for industry.[51] Most high efficiency HPLC columns are made of silica.[19] However, the limitations of pH and temperature range of silica limits these materials in elevated pH and temperature applications.[1, 24, 47, 52-56] Newly developed hybrid columns show improved resistance to degradation at elevated pH. Nevertheless, they are still challenged by higher temperature applications at elevated pH.[24, 53]

1.4.1. Development of Non-Silica Materials for HPLC

Various non-silica-based materials have been introduced into the HPLC market to overcome the drawbacks of silica-based HPLC columns.[53, 57] Polymer and carbon-based HPLC columns have been developed to allow wider pH and temperature ranges in separations. Common polymer-based HPLC particles are prepared from poly(divinylbenzene) (PDVB) microspheres.[58-62] Porous graphitic carbon (PGC) is another carbon-based material found on the HPLC market. The selectivity of PGC columns are different from reversed phase columns and they are suitable for retaining hydrophilic compounds.[63]

1.4.2. Approaches for Making Carbon-Based, Mixed-Mode HPLC Columns in the Linford Group at BYU

The Linford group at BYU has developed nanodiamond/carbon/amine polymer-based materials for HPLC.[50-51, 64-68] They used nanodiamond, carbon, and polymer based materials because they are well known for their chemical and thermal stability under harsh conditions.[64, 69-71] In their early approaches, they used a carbon core that was supplied from an outside vendor.[50] However, these carbon particles had a broad size distribution and were quite porous, which reduced column efficiency. Subsequently, they synthesized their carbon core materials using uniform PDVB microspheres as precursors.[58-61, 72-76] These PDVB microspheres retain their spherical shapes after air oxidation, carbonization, and acid treatment.[74, 77-86] The efficiency of the column was greatly improved as a result of their use of more uniform carbon core materials.[51]

The particles developed by the Linford group have mixed-mode properties that allow them to retain both hydrophobic and hydrophilic analytes. This is because their core-shell materials contain an amine-based polymer that allows them to retain acidic analytes at low pH and basic analytes at high pH. Good separations of bio-molecules, including proteins, have been reported.[27] Quite a few application notes for pharmaceutical compounds, such as tricyclic antidepressants (TCAs), alkaloids, cannabinoids, etc., have been developed using these carbon-based core-shell mixed-mode columns.[48, 87-90] Other related stationary phases have now been developed to provide additional selectivities, and will be discussed in Chapter 4.

1.5. Conclusions

Chromatography plays an important role in chemical analysis. The factors that come out of plate theory and rate theory allow quantitative measurements and comparisons of column efficiency and resolution. The selectivity/retention of ionizable analytes depends on pH and temperature. Different bonded phases provide different selectivties through different intermolecular interactions with analytes. Mixed-mode stationary phases retain analytes that have both hydrophobic and hydrophilic properties. Silica-based columns are challenged by elevated pH and temperature applications. Non-silica (carbon-based) HPLC columns show stability under harsh conditions and the newly developed carbon/nanodiamond/polymer based core-shell mixed-mode HPLC column shows improvements in efficiency for a wide variety of analytes.

1.6. References

1. Snyder, L. R.; Kirkland, J. J.; Dolan, J. W., *Introduction to Modern Liquid Chromatography/Lloyd R. Snyder, Joseph J. Kirkland, and John W. Dolan - Third Edition*. 3rd Edition ed.; John Wiley & Sons, Inc: Hoboken, 2009.
2. Karger, B. L., *J. Chem. Educ.* **1997,** *74* (45-48).
3. Berezkin, V. G., *J. Anal. Chem.* **2007,** *63* (4), 400-404.
4. Livengood, J., *Stud. Hist. Phil. Sci.* **2009,** *40*, 57-69.
5. Ettre, L. S., *LCGC North Am.* **2003,** *21*, 458-467.
6. Abraham, M. H., *J. Chromatogr. A* **2004,** *1061*, 113-114.
7. Dong, M. W., *Modern HPLC for Practicing Scientists*. John Wiley & Sons, Inc.,: Hoboken, 2006.

8. Roberts, G. K.; Russell, C. A., *Chemical History: Reviews of the Recent Literature*. Royal Society of Chemistry: Cambridge, UK, 2005; p 247.

9. Shraiber, M. S., *J. Chromatogr.* **1972,** *73*, 367-370.

10. Ettre, L. S., *Milestones in the Evolution of Chromatography*. ChromSource: 2002; p 220.

11. Martin, A. J. P.; Synge, R. L. M., *Biochem. J* **1941,** *35* (12), 1358-1368.

12. Lee, M. L., *Fundamentals of Analytical Separations*. Brigham Young University: Provo, UT, 2010.

13. Khopkar, S. M., *Basic Concepts of Analytical Chemistry Second Edition*. New Age International (P) Ltd.,: New Delhi, 1998; p 500.

14. Ettre, L. S.; Sakodynskii, K. I., *Chromatographia* **1993,** *35* ((3/4)), 223-231.

15. Davaji, B.; Lee, C. H., *Biosens. Bioelectron.* **2014,** *59*, 120-126.

16. Müller, R. H.; Clegg, D. L., *Anal. Chem.* **1949,** *21* (9), 1123-1125.

17. Kirkland, J. J.; Destefano, J. J., *J. Chromatogr. A* **2006,** *1126*, 50-57.

18. Gritti, F.; Guiochon, G., *Anal. Chem.* **2013,** *85*, 3017-3035.

19. Wang, Y.; Ai, F.; Ng, S.-C.; Tan, T. T. Y., *J. Chromatogr. A* **2012,** *1228*, 99-109.

20. Wu, N.; Clausen, A. M., *J. Sep. Sci.* **2007,** *30*, 1167-1182.

21. Gerber, F.; Krummen, M.; Potgeter, H.; Roth, A.; Siffrin, C.; Spoendlin, C., *J. Chromatogr. A* **2004,** *1036* (2), 127-133.

22. Unger, K. K.; Kumar, D.; Grün, M.; Büchel, G.; Lüdtke, S.; Adam, T.; Schumacher, K.; Renker, S., *J. Chromatogr. A* **2000,** *892*, 47-55.

23. MacNair, J. E.; Lewis, K. C.; Jorgenson, J. W., *Anal. Chem.* **1997,** *69*, 983-989.

24. Pail, V. P.; Tather, R. D.; Devdhe, S. J.; Angadi, S. S.; Kale, S. H., *IRJP* **2011,** *2* (6), 39-44.

25. Fekete, S.; Kohler, I.; Rudaz, S.; Guillarme, D., *J. Pharm. Biomed. Anal.* **2014,** *87*, 105-119.

26. Fekete, S.; Oláh, E.; Fekete, J., *J. Chromatogr. A* **2012,** *1228*, 57-71.

27. Guo, H.; Li, X.; Frey, D. D., *J. Chromatogr. A* **2014,** *1323*, 57-65.

28. Majors, R. E., Improving Protein Separations with Mixed-Mode Chromatography. *LC-GC North America* 2009, pp 14-24.

29. Burton, S. C.; Harding, D. R. K., *J. Chromatogr. A* **1998,** *814*, 71-81.

30. Hawkes, S. J., *J. Chem. Educ.* **1983,** *60*, 393-398.

31. Sandra, P., *J. High. Resolut. Chromatogr.* **1989,** *12* (2), 82-86.

32. Pous-Torres, S.; Baeza-Baeza, J. J.; Torres-Lapasió, J. R.; García-Álvarez-Coque, M. C., *J. Chromatogr. A* **2008,** *1205*, 78-89.

33. Wang, X.; Stoll, D. R.; Schellinger, A. P.; Carr, P. W., *Anal. Chem.* **2006,** *78* (10), 3406-3416.

34. Giddings, J. C., *Anal. Chem.* **1967,** *38* (9).

35. Grushka, E., *Anal. Chem.* **1970,** *42* (11), 1142-1147.

36. Teutenberg, T., *Anal. Chim. Acta.* **2009,** *643* (1-2), 1-12.

37. Knox, J. H., *Anal. Chem.* **1966,** *38* (2), 253-261.

38. Giddings, J. C., *J. Chromatogr. A* **1961,** *5*, 46-60.

39. Villiers, A. d.; Lauer, H.; Szucs, R.; Goodall, S.; Sandra, P., *J. Chromatogr. A* **2006,** *1113*, 84-91.

40. Heinisch, S.; Rocca, J.-L., *J. Chromatogr. A* **2009,** *1216*, 642-658.

41. Guillarme, D.; Heinisch, S.; Rocca, J. L., *J. Chromatogr. A* **2004,** *1052*, 39-51.

42. Li, J.; Carr, P. W., *Anal. Chem.* **1997,** *69*, 2193-2201.

43. Carr, P. W.; Sun, L., *J. Microcolumn Sep.* **1998,** *10* (1), 149-152.

44. Jensen, D. S.; Teutenberg, T.; Clark, J.; Linford, M. R., *LCGC North Am.* **2012,** *30* (12), 1052-1057.

45. Jensen, D. S.; Teutenberg, T.; Clark, J.; Linford, M. R., *LCGC North Am.* **2012,** *30* (11), 992-998.

46. Jensen, D. S.; Teutenberg, T.; Clark, J.; Linford, M. R., *LCGC North Am.* **2012,** *30* (9), 850-862.

47. Kirkland, J. J.; henderson, J. W.; DeStefano, J. J.; Straten, M. A. v.; Claessens, H. A., *J. Chromatogr. A* **1997,** *762*, 97-112.

48. Bobály, B.; Guillarme, D.; Fekete, S., *J. Pharm. Biomed. Anal.* **2015,** *104*, 130-136.

49. Chen, J.; Tetrault, J.; Ley, A., *J. Chromatogr. A* **2008,** *1177*, 272-281.

50. Wiest, L. A.; Jensen, D. S.; Hung, C.-H.; Olsen, R. E.; Davis, R. C.; Vail, M. A.; Dadson, A. E.; Nesterenko, P. N.; Linford, M. R., *Anal. Chem.* **2011,** *83* (14), 5488-5501.

51. Hung, C.-H.; Wiest, L. A.; Singh, B.; Diwan, A.; Valentim, M. J. C.; Christensen, J. M.; Davis, R. C.; Miles, A. J.; Jensen, D. S.; Vail, M. A.; Dadson, A. E.; Linford, M. R., *J. Sep. Sci.* **2013,** *36* (24), 3821-3829.

52. Teutenberg, T., *High Temperature Liquid Chromatography A User's Guide for Method Development*. The Royal Society of Chemistry: Cambridge, 2010.

53. Teutenberg, T.; Hollebekkers, K.; Wiese, S.; Boergers, A., *J. Sep. Sci.* **2009,** *32* (9), 1262-1274.

54. Teutenberg, T.; Tuerk, J.; Holzhauser, M.; Giegold, S., *J. Sep. Sci.* **2007,** *30*, 1101-1114.

55. Nawrocki, J., *J. Chromatogr. A* **1997,** *779*, 29-71.

56. Claessens, H. A.; Straten, M. A. v., *J. Chromatogr. A* **2004,** *1060*, 23-41.

57. Wyndham, K. D.; O'Gara, J. E.; Walter, T. H.; Glose, K. H.; Lawrence, N. L.; Alden, B. A.; Izzo, G. S.; Hudalla, C. J.; Iraneta, P. C., *Anal. Chem.* **2003,** *75* (24), 6781-6788.

58. Bai, F.; Yang, X.; Huang, W., *Macromolecules* **2004,** *37*, 9746-9752.

59. Li, K.; Stöver, H. D. H., *J. Polym. Sci., Part A: Polym. Chem.* **1993,** *31* (13), 3257-3263.

60. Wang, Z.; Jiang, D. D.; McKinney, M. A.; Wilkie, C. A., *Polym. Degrad. Stab.* **1998,** *64*, 387-395.

61. Downey, J. S.; Frank, R. S.; Li, W.-H.; Stover, H. D. H., *Macromolecules* **1999,** *32*, 2838-2844.

62. Lungfiel, K.; Seubert, A., *J. Chromatogr. A* **2014,** *1358*, 117-127.

63. Jensen, D. S.; Gupta, V.; Olsen, R. E.; Miller, A. T.; Davis, R. C.; Ess, D. H.; Zhu, Z.; Vail, M. A.; Dadson, A. E.; Linford, M. R., *J. Chromatogr. A* **2011,** *1218* (46), 8362-8369.

64. Saini, G.; Jensen, D. S.; Wiest, L. A.; Vail, M. A.; Dadson, A.; Lee, M. L.; V., S.; Linford, M. R., *Anal. Chem.* **2010,** *82* (11), 4448-4456.

65. Saini, G.; Wiest, L. A.; Herbert, D.; Biggs, K. N.; Dadson, A.; Vail, M. A.; Linford, M. R., *J. Chromatogr. A* **2009,** *1216*, 3587-3593.

66. Saini, G.; Gates, R.; Asplund, M. C.; Blair, S.; Attavar, S.; Linford, M. R., *Lab Chip* **2009,** *9* (12), 1789-1796.

67. Saini, G.; Yang, L.; Lee, M. L.; Dadson, A.; Vail, M. A.; Linford, M. R., *Anal. Chem.* **2008,** *80* (16), 6253-6259.

68. Hung, C.-H.; Kazarian, A. A.; Dadson, A. E.; Paull, B.; Nesterenko, P.; Linford, M. R., Guidelines for Understanding the Retention Mechanism of the Diamond Analytics Flare Mixed-Mode Column. Diamond Analytics: Orem Utah.

69. Nesterenko, P. N.; Haddad, P. R., *Anal. Bioanal. Chem.* **2010,** *396* (1), 205-211.

70. Nesterenko, P. N.; Fedyanina, O. N., *J. Chromatogr. A* **2010,** *1217* (4), 498-505.

71. Matheson, A.; Nesterenko, P. N., *LC GC Eur.* **2010,** *23* (3), 120-124.

72. Li, W.-H.; Stöver, H. D. H., *Macromolecules* **2000,** *33*, 4354-4360.

73. Downey, J. S. Precipitation Polymerization of Divinylbenzene to Monodisperse Microspheres: An Investigation of the Particle Formation Mechanism. 2000.

74. Hirano, S.-I.; Ozawa, M.; Naka, S., *J. Mater. Sci.* **1981,** *16*, 1989-1993.

75. Lee, K.-C.; WI, H.-A., *Trans. Nonferrous Met. Soc. China* **2011,** *21*, 153-159.

76. Yan, Q.; Bai, Y.; Meng, Z.; Yang, W., *J. Phys. Chem. B* **2008,** *112* (6914-6922).

77. El-Hendawy, A.-N. A., *Carbon* **2003,** *41* (4), 713-722.

78. Mahata, N.; Pereira, M. F. R.; Suárez-García, F.; Martínez-Alonso, A.; Tascón, J. M. D.; Figueiredo, J. L., *J. Colloid Interface Sci.* **2008,** *324* (1-2), 150-155.

79. Samant, P. V.; Gonçalves, F.; Freitas, M. M. A.; Pereira, M. F. R.; Figueiredo, J. L., *Carbon* **2004,** *42* (7), 1321-1325.

80. Moreno-Castilla, C.; Ferro-García, M. A.; Joly, J. P.; Bautista-Toledo, I.; F.Carrasco-Marín; Rivera-Utrilla, J., *Langmuir* **1995,** *11*, 4386-4392.

81. Malik, D. J.; Trochimczuk, A. W.; Ronka, S., *PLoS One* **2012,** *7* (8), e43354.

82. Partouche, E.; Margel, S., *Carbon* **2008,** *46* (5), 796-805.

83. Manocha, S. M., *Sādhanā* **2003,** *28*, 335-348.

84. Streklko-Jr, V.; Malik, D. J.; Streat, M., *Carbon* **2002,** *40*, 95-104.

85. Hirano, S.; Dachille, F.; P. L. Walker, J., *High Temp.- High Pressures* **1973,** *5*, 207-220.

86. Winslow, F. H.; Baker, W. O.; Pape, N. R.; Matreyek, W., *J. Polym. Sci.* **1955,** *16*, 101-120.

87. Singh, B.; Jensen, D. S.; Miles, A. J.; Dadson, A. E.; Linford, M. R. *Probing the Retention Mechanism of the Flare Mixed-Mode Column at Low pH via Acidic Herbicides with Different pK_a Values*; Application Note: DA1000-C; Diamond Analytics: Orem, Utah.

88. Hung, C.-H.; Jensen, D. S.; Miles, A. J.; Zukowski, J.; Dadson, A. E.; Linford, M. R. *FLARE C18 Mixed-Mode Column: Separation of Apo-Transferrin and Bovine Serum Albumin (BSA) by LC-MS*; Application Note: DA1014-A; Diamond Analytics: Orem, Utah.

89. Hung, C.-H.; Davis, T. C.; Jensen, D. S.; Miles, A. J.; Zukowski, J.; Dadson, A. E.; Linford, M. R. *FLARE C18 MIxed-Mode Column: Alkaloids*; Application Note: DA1013-A; Diamond Analytics: Orem, Utah.

90. Hung, C.-H.; Davis, T. C.; Jensen, D. S.; Miles, A. J.; Zukowski, J.; Dadson, A. E.; Linford, M. R. *Flare C18 Mixed-Mode Columns: Tricyclic Antidepressants (TCAs)*; Application Note: DA1001-C; Diamond Analytics: Orem, Utah.

Chapter 2: Improved Efficiency of Reversed Phase Carbon/Nanodiamond/Polymer Core Shell Particles for HPLC Using Carbonized, Poly(divinylbenzene) Microspheres as the Core Materials*

2.1. Abstract

Here we report efficiencies up to 112,000 plates per meter (*N/m*) (a reduced plate height, *h*, of 2.22) for reversed phase, carbon/nanodiamond/aminopolymer particles using conventional injection conditions. This efficiency greatly exceeds our best previously reported value of 71,000 *N/m* (*h* = 3.52). The carbon cores used in this study were derived from carbonized poly(divinylbenzene) (PDVB) spheres that were either made in house via a two step polymerization procedure or obtained commercially. The resulting particles showed good uniformity and were oxidized in nitric acid to increase their dispersability. X-ray photoelectron spectroscopy (XPS) confirms particle oxidation and subsequent aminopolymer deposition. Layer-by-layer (LbL) growth of poly(allylamine) (PAAm) and nanodiamond was demonstrated to produce core-shell particles. After LbL, particles were functionalized, sieved, and packed into columns. Column functionalization and packing were reproducible. Van Deemter curves indicated that the commercially-obtained PDVB spheres outperformed those synthesized in our laboratory. The columns appear to be stable at 120 °C in a pH 11.3 mobile phase. Longer columns (2.1 x 50 mm) than previously reported were packed. Four essential oils were separated by gradient elution.

*This chapter is reproduced with permission from (Hung, C.-H., Wiest, L. A., Singh, B., Diwan, A., Valentim, M. J. C., Christensen, J. M., Davis, R. C., Miles, A. J., Jensen, D. S., Vail, M. A., Dadson, A. E., Linford, M. R) *J. Sep. Sci.* 2013, *36*, 3821-3829. Copyright 2013 WILEY-VCH Verlag GmbH & Co.

2.2. Introduction

Elevated temperatures and extremes of pH are increasingly recognized as offering substantial benefits in liquid chromatography.[1-6] For example, as temperature is raised, mobile phase viscosities and, thus, column back pressures, decrease, allowing conventional HPLC systems to run at higher flow rates. At higher temperatures, analyte diffusion also increases, resulting in faster mass transfer (lower *C*-terms) – van Deemter curves flatten and their minima shift to higher flow rates, which allows faster separations without significant loss of efficiency. Because the polarity of water decreases with increasing temperature, less organic solvent is needed and even pure water may be employed as the mobile phase at sufficiently high temperatures. High pH separations are attractive because analytes with basic groups, which include many pharmaceutical compounds, are better separated and retained in their deprotonated state.[7-8] Conversely, acidic analytes are in general better retained and separated at low pH where they are neutral. Setting the protonation state of an analyte (either fully protonated or deprotonated) is advantageous because the resulting separation will be less sensitive to small changes in mobile phase pH compared to when the analyte is in its buffer region.[9] In spite of the advantages of high temperature and extreme pH separations, there are still relatively few columns that can withstand such forcing conditions.[5]

For many years silica has been the primary support material for HPLC because its mechanical strength, bonding chemistry, batch-to-batch reproducibility, reasonable stability, and reactivity are well known and meet many of the high standards for modern separation science.[9] However, most silica-based bonded-phase materials have relatively low pH and temperature stability. At lower pH values (< 2), silica suffers from hydrolysis of its silane ligands, and at higher pHs (>8), the material is eroded by solubility.[7-9] Using trifunctional silanes or sterically hindered,

monofunctional silanes in bonded phases enhances the lower pH stability of silica.[8] Organic-inorganic hybrid materials, e.g., bridged ethyl hybrids, have also shown significant promise for higher pH applications. For example, hybrid columns were stable up to 100 h when exposed to a pH 10 mobile phase at moderate temperature (50 °C), but then began to degrade. While these results represent considerable advances, improvements are still needed in current stationary phases and supports to fully exploit the advantages of elevated temperature and extreme pH separations.[4-5]

Besides silica-based supports, other competitive materials, such as porous graphitic carbon (PGC), various polymer-based materials, and metal oxides, have drawn attention for applications requiring more extreme conditions. However, in many cases these materials offer quite different selectivities from silica, which has been a barrier to their acceptance.[4-6] Relatively low efficiencies and/or poor peak shapes have also been a criticism of some of these alternative materials.[5-8] For example, the contributions of strongly adsorbing sites on the surfaces of PGC and metal oxide materials can result in distorted peak shapes and tailing in some separations, and some polymer-based materials swell when strong organic solvents are used as the mobile phase.

Diamond and carbon have superior thermal, pH, and mechanical stability and, accordingly, are good candidates for supports for HPLC for use under extreme operating conditions.[10-14] Indeed, newly developed nanodiamond/carbon-based core-shell materials from our group have shown some promising results.[15-19] These materials were prepared via a layer-by-layer (LbL) deposition of an amine-containing polymer, poly(allylamine) (PAAm), and nanodiamond onto carbon cores, which were subsequently functionalized to make weak anion exchange/reversed-phase C18 columns. These columns showed efficiencies of approximately 60,000-71,000 plates per meter (N/m) for various analytes on an HPLC and a UHPLC system (unpublished results), and even

higher efficiencies (100,000-120,000 N/m) in a specialized sandwich-type injection on a UHPLC system.[15] For standard injections, the reduced plate height (h) was higher than expected (h = 3.52), which suggested bed inhomogeneity/packing issues.

Here we report the synthesis, carbonization, and then oxidation of poly(divinylbenzene) (PDVB) microspheres[20-27] that have a tighter particle size distribution (PSD) than the carbon particles used in our previous report. We also report the carbonization and oxidation of commercially available PDVB microspheres. These carbon particles are used as the core particles for LbL deposition of porous polymer/nanodiamond shells. The greater uniformity of the resulting particles appears to be advantageous in column packing (lower A-term). The efficiencies of the resulting columns were tested with a homologous series of alkylbenzene analytes using water and acetonitrile (ACN) as the mobile phase at pH 11.3 with triethylamine (TEA) as pH modifier. Characterization of the pore size distribution of the core-shell materials was done using the Brunauer-Emmett-Teller (BET), method and images of the particles were obtained by scanning electron microscopy (SEM). Gradient separations of various essential oils with these new columns are shown.

2.3. Materials and Methods

2.3.1. Reagents, Solvents, and Instrumentation

Dry acetonitrile (ACN) was obtained at the general facilities of the organic laboratories at BYU; 2,2'-azobisisobutyronitrile (AIBN) (98%, Sigma-Aldrich, St. Louis, MO), divinylbenzene (DVB) (80% divinylbenzene, 20% ethylstyrene, Sigma-Aldrich), inhibitor remover (Sigma-Aldrich product number: 311340, alumina replacement packing for removing *tert*-butylcatechol),

tetrahydrofuran (THF) (Mallinckrodt Baker, Philipsburg, NJ), acetone (Sigma-Aldrich), diethyl ether (≥ 99.0%, Sigma-Aldrich), 5 μm non-porous DVB (Sepax Technologies, Newark, DE), hydrogen peroxide (30%, Fisher Scientific, Pittsburgh, PA), nitric acid (68-70%, Mallinckrodt Baker), sulfuric acid (95-98%, Mallinckrodt Baker), poly(allylamine) (PAAm) 65,000 average M_w (20 wt. % solution in water, Sigma-Aldrich), poly(allylamine) (PAAm) 17,000 average M_w (20 wt. % solution in water, Sigma-Aldrich), 50 nm nanodiamond suspension (10%, 0 - 0.1 μm, Advanced Abrasive, Pennsauken, NJ), 1,2,7,8-diepoxyoctane (97%, Sigma-Aldrich), 1,2-epoxyoctadecane (90%, Alfa Aesar, Ward Hill, MA), methanol (MeOH) (≥ 99.9%, Sigma-Aldrich), 2-propanol (≥ 99.8%, Sigma-Aldrich), xylene (Mallinckrodt Baker, Phillipsburg, NJ), cyclohexanol (J.T. Baker, Phillipsburg, NJ), acetonitrile (CAN) (≥ 99.9%, Sigma-Aldrich), Triton X-100 (electrophoresis grade, Fisher Scientific, Fair Lawn, NJ), and triethylamine (99.50%, Mallinckrodt Baker) were used as received. Purified water was obtained from a Milli-Q Water System (EMD Millipore, Billerica, MA). Analytes from a benzenoid hydrocarbon kit (Sigma-Aldrich) containing ethyl-, butyl-, hexyl-, octyl-, and decylbenzene were diluted in ACN to test column efficiencies.

DVB was polymerized in cylindrical hybridization tubes (35 x 300 mm with screw-caps) that were rotated in a hybridization incubator (Model 400, Robbin Scientific, Sunnyvale, CA). A small benchtop furnace (Model 1400, Barnstead Thermolyne, Dubuque, IA) was used for PDVB air oxidation and a high temperature furnace (Lindberg/Blue M, Thermo Electron, Waltham, MA) with nitrogen purge gas was used for carbonization of PDVB particles. X-ray photoelectron spectroscopy (XPS) was performed in the Surface Science Lab at the University of Utah (Salt Lake City, UT) using an Ultra-DLD Axis spectrometer (Kratos Analytical, Chestnut Ridge, NY). Spectra were collected using a monochromated Al K-alpha source (1486.6 eV), operated at 180

W. Charge compensation was with a low energy electron flood gun, coupled with a magnetic immersion lens. A final binding energy (BE) correction was made by referencing the adventitious C1s signal to 284.8 eV. Pass energies were 160 eV and 40 eV for survey and high-resolution spectra, respectively. XPS was also performed at Brigham Young University (Provo, UT) with an SSX-100 instrument using an Al K-alpha source and a hemispherical analyzer. Charge compensation was with an electron flood gun. Samples were mounted on a double-sided carbon tape attached to silicon wafers. For the layer-by-layer process, a centrifuge (Clinical 200, VWR, Radnor, PA) and a probe sonicator (Model 450, Branson Ultrasonics, Danbury, CT) were used. Scanning electron microscopy (SEM) was performed with either an FEI XL30 SFEG or FEI Helio NanoLab 600 system (FEI, Hillsboro, OR). SEM samples were prepared by placing a few drops from a slurry of particles on an aluminum SEM stub that was dried in an oven. Images were obtained under high vacuum with a spot size of 3.

Surface area and pore size measurements were made with a TriStar II surface area analyzer (Micromeritics Instrument, Norcross, GA). Surface areas were determined by N_2 adsorption at 77 K, where the particles were degassed at 200 °C for 12 h prior to data collection. Particle size distributions (PSD) were measured with an LS 13 320 Multi-Wavelength Particle Size Analyzer (Beckman Coulter, Brea, CA) from a slurry of the particles in the analysis bath of the analyzer. A Haskel air driven pump (Haskel International, Burbank, CA) was used to pack the columns. To test column efficiencies, both HPLC and UHPLC systems were employed. Our HPLC system (Waters, Milford, MA) consisted of a dual wavelength detector (Model No. 2487), a binary HPLC pump (Model No. 1525), a column oven (Model No. 5CH), and the Breeze software (Version 3.3). The injection volume was 5 µL. Our UHPLC system was an Agilent Infinity 1290 (Agilent Technologies, Santa Clara, CA) with a diode array detector (Model No. G4212A), an LC pump

(Model No. G4220A), a column oven (Model No. G1316C), an autosampler (Model No. G4226A), and the Chem Station software (Version B.04.03). The injection volume was 1 μL. Both software packages were able to calculate the efficiencies of analytes in the separations. A high temperature HPLC oven (Polaratherm^{TM} series 9000, Selerity Technologies, Salt Lake, UT) was coupled with the Waters HPLC system for the elevated temperature studies.

2.3.2. Synthesis of Poly(divinylbenzene) (PDVB) Microspheres

PDVB particles were prepared in two steps. The first step followed the reports of Bai et al.[21] and Li et al.,[20] in which 2% AIBN (relative to the weight of DVB and previously recrystallized from methanol) and 2% DVB (relative to total volume of dry ACN) were used to make 3.0 – 3.7 μm PDVB particles. The microspheres were then rinsed with THF, acetone, and diethyl ether to remove any unreacted monomer, soluble polymer, and/or residuals of the initiator. The particles were then filtered on a 0.45 μm membrane filter (Pall Life Sciences, Port Washington, NY), and dried at room temperature under house vacuum overnight.

The second stage of PDVB particle formation followed the report of Li et al.[22] Here, the PDVB microspheres obtained from the first stage of the reaction were divided equally by weight into four hybridization tubes – about 200 mL of the reaction solution was added to each tube for an additional polymerization. The heating process was the same as in the first stage of the polymerization. The final particle size after this second step was 4.0 – 4.8 μm, and the particles were filtered and dried as before. They were then ready for air oxidation, carbonization, and acid oxidation. Commercial PDVB particles (5 μm, non-porous, Sepax Technologies, Newark, DE) were also employed in this study and were used as received.

2.3.3. Air Oxidation, Carbonization, and Oxidation of PDVB

PDVB particles were air oxidized and carbonized according to the procedure of Li et al.[24] PDVB particles synthesized in house were carbonized at 700 °C, while those obtained commercially were carbonized at 900 °C, or in the case of the column used to separate the essential oils at 1050 °C. The purpose of the higher carbonization temperatures was to reduce the particle size to a greater extent. Depending on the particle size obtained from the second stage of the in-house polymerization, the particle diameter decreased after carbonization from 4.0 – 4.8 μm to 2.8 – 3.3 μm. The commercial 5.0 μm PDVB particles decreased in size to ca. 3.6 μm. After carbonization, the particles were again oxidized, where one of two different oxidation reagents was used: nitric acid or piranha solution. The HNO_3 oxidation process followed the reports of Moreno-Castilla et al.[27] and El-Hendawy et al.,[25] and the piranha solution process followed Saini et al.[16] For the HNO_3 and piranha solution processes, the carbonized PDVB was present in the acid solution at ca. 3 wt. %. The HNO_3 process was carried out in 68 – 70 % HNO_3 at 60 °C for 24 h and the piranha solution process was performed using a mixture of concentrated H_2SO_4 and 30% H_2O_2 in a 70/30 (v/v) ratio at 100 °C for 1 h. Caution: both of these solutions are very dangerous and should be handled with great care and with proper protective equipment. After the oxidation processes, the solutions were diluted with Millipore water and the microspheres were captured by filtration through a 0.22 μm nitrocellulose membrane (Sigma-Aldrich). The oxidized particles were then dried under vacuum overnight.

2.3.4. Layer-by-Layer (LbL) Deposition of an Aminopolymer and Nanodiamond on Carbon, and Cross-Linking and Functionalization with a C18 Ligand

Layer-by-layer (LbL) deposition of diamond-polymer composite shells on the carbon core, and subsequent particle functionalization and column packing, were similar to the procedures reported by Wiest et al.[15] Exceptions were that (i) after each deposition of poly(allylamine) (PAAm), the particles were sonicated with a probe sonicator (Model 450, Branson Ultrasonics Corporation, Danbury, CT) for 2 min at 25% output power, and (ii) after completion of the particle synthesis they were filtered through a 40 μm sieve to remove any large agglomerates. If the particles were not sieved through a 40 μm sieve, it is stated below. The mechanism of this LbL procedure is not entirely clear. We previously observed that PAAm may be largely deprotonated under our deposition conditions,[16] and nanodiamond is a complex material. Indeed, studies of nanodiamond have suggested multiple types of oxidized carbon at its surface.[10-14] Thus, nanodiamond deposition on PAAm, and the reverse process of PAAm deposition on nanodiamond, may be the result of (i) electrostatic interactions between carboxylates at the nanodiamond surface and protonated amines on the PAAm, (ii) covalent interactions between carbonyls at the nanodiamond surface and free amines on PAAm, and (iii) hydrogen bonding between hydroxyl groups on the nanodiamond and the amine groups on PAAm. A comprehensive study of the nanodiamond materials used in our particles is nearing completion in our laboratory, which should shed further light on this issue. The shell thicknesses of the particles were determined as the difference between the diameters of the original core particles and the core-shell particles as determined by PSD measurements.

2.3.5. Column Packing

After functionalization, the particles were typically filtered through a 40 μm sieve. If particles were not sieved through a 40 μm sieve, it will be mentioned below. Column packing was performed with a Haskel (Haskel International, Burbank, CA) air-driven fluid pump following the procedure of Wiest et al.[15] In particular, the pressure was increased 1000 psi every 5 min up to its final pressure of 7000 psi. After reaching the maximum pressure, column packing continued until 90 mL of packing solvent had passed through the column. The columns were then rinsed with methanol for 20 min and tested using a mobile phase consisting of 40/60/0.1 H_2O/ACN/TEA (v/v/v), at 0.7 mL/min at 35 °C.

2.3.6. Column Efficiency and Temperature Stability Tests

Elevated temperature stability tests were performed in 5 h cycles at 120 °C using a mobile phase of 60/40/0.1 H_2O/ACN/TEA (v/v/v) at pH 11.3, and at 140 °C using a mobile phase composition of 70/30/0.1 H_2O/ACN/TEA (v/v/v), also at pH 11.3. Before and after each heating cycle, the column was flushed with MeOH for 10 min. The efficiencies of the column before and after each heating cycle were measured using an alkybenzene mixture at 35 °C with a H_2O/ACN/TEA 60/40/0.1 (v/v/v) mobile phase at pH 11.3 and 0.7 mL/min.

2.4. Results and Discussion

2.4.1. Carbon Core Particle Preparation from Poly(divinylbenzene) (PDVB) Microspheres

In our previous study,[15] core particles showed disperate morphologies/shapes and final core-shell particles had fairly large particle size distributions (PSD), e.g., d90/d10 = 1.63, which

appeared to translate into a relatively high reduced plate height (h = 3.52). Accordingly, our first goal was to prepare core particles that would be similar in size to those we previously studied (3 μm), but with a tighter PSD and better morphologies to improve packing and achieve lower values of h. Figure 2.1 shows SEM results from the two-step polymerization process used in the preparation of polydivinylbenzene (PDVB) microspheres.[20-22] The particles were ca. 3.3 μm after the first step/polymerization (Figure 2.1A), ca. 4.0 μm after the second (Figure 2.1B), and ca. 2.8 μm after carbonization and filtration (Figure 2.1C), which was close to our goal. Some particles of submicron dimensions were also formed in the second polymerization (see Figure 2.1B), but during carbonization, they decreased in size. In practice, they were removed by filtration (see Figure 2.1C) and also during the layer-by-layer process so that at the end of 30 LbL cycles they are no longer present. PDVB particles (5.0 μm) were also obtained from a commercial supplier. After carbonization, they were reduced in size to ca. 3.6 μm (see Figure 2.1D). Based on scanning electron microscopy (SEM), the commercially obtained, carbonized PDVB particles were more uniform than the in house prepared particles (compare Figures 2.1C and 2.1D), but both of these types of particles appeared to be of higher quality and uniformity than those we had employed previously. Brunauer-Emmett-Teller (BET) data were taken on the commercially obtained particles before and after carbonization. As expected, the surface area and pore diameter of the PDVB were low before carbonization: 1.60 ± 0.35 m^2/g and 6.62 ± 0.32 nm, respectively. However, after carbonization, small pores (less than 25 Å) appeared, significantly increasing the surface area and decreasing the pore diameter to 445.18 ± 39.86 m^2/g and 1.95 ± 0.01 nm, respectively. Interestingly, after LbL functionalization (vide infra), the surface area of the particles was drastically reduced, suggesting that the pores had been completely or nearly completely sealed off.

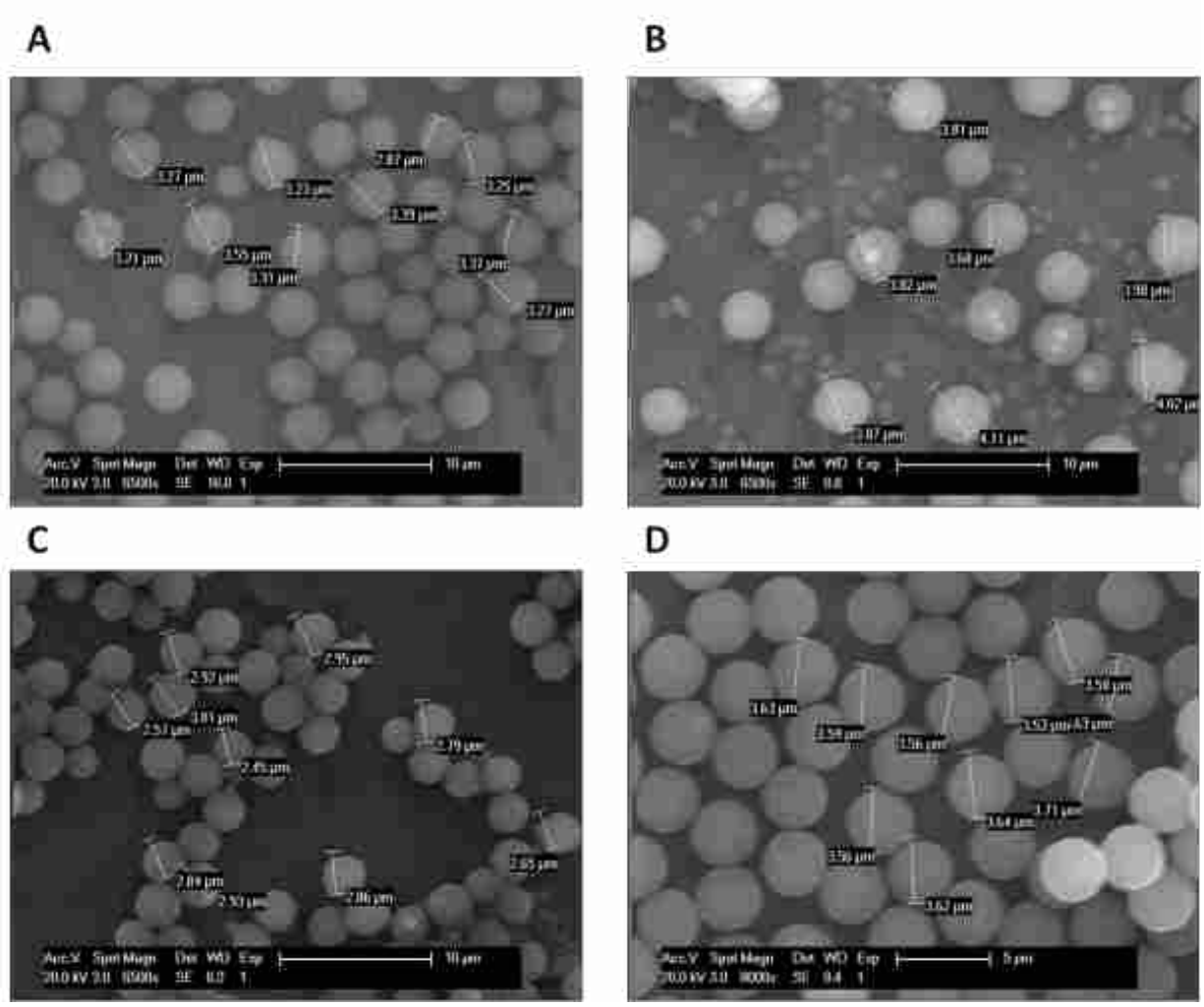

Figure 2.1 SEM images (taken with an FEI XL30 SFEG) of PDVB microspheres after (A) the first step in the particle synthesis (ca. 3.3 µm particle diameters), (B) the second step in the synthesis (ca. 4.0 µm diameters), (C) carbonization and filtration (ca. 2.8 µm diameters) – some particles of submicron dimensions are present in the lower right corner of this image, and (D) oxidation and carbonization of commercially obtained 5.0 µm PDVB particles (ca. 3.6 µm diameters).

2.4.2. Oxidation of the Carbon Core for Improved Poly(allylamine) (PAAm) Deposition and Layer-by Laer (LbL) PAAm/Nanodiamond Growth

After preparation of the carbonized PDVB particles, LbL deposition of PAAm and nanodiamond were attempted. However, the hydrophobicity of the particles did not allow their suspension in the solvents used for the PAAm and nandiamond depositions. Accordingly, it was convenient to oxidize the surfaces of the particles to increase their surface free energy/hydrophilicity/dispersability. X-ray photoelectron spectroscopy (XPS), which probes the upper ca. 10 nm of a material, had given an oxygen-to-carbon (O/C) ratio of 0.10 for the carbonized particles (see Figure 2.2 and Table 2.1). This value was lower than that for the carbon particles employed in our previous study (0.17), which had been provided by an outside source and showed good dispersability,[15] i.e., we expected a correlation between the XPS O/C ratio of the particles and their dispersability. After treatment of the carbonized PDVB particles with nitric acid,[25, 27] their XPS O/C ratio increased substantially (to 0.24) (see Figure 2.2 and Table 2.1), and their C 1s narrow scan (not shown) showed more signal at higher binding energies, which is consistent with increased oxidation of the particle surfaces. Oxidation in piranha solution (a mixture of concentrated sulfuric acid and concentrated hydrogen peroxide), which we had previously used to clean core diamond particles,[16] also raised the XPS O/C ratios of the carbon particles. Ultimately, the nitric acid approach was found to be somewhat easier to apply in this study, and most of the results presented herein are from particles oxidized in this fashion. XPS confirmed the deposition

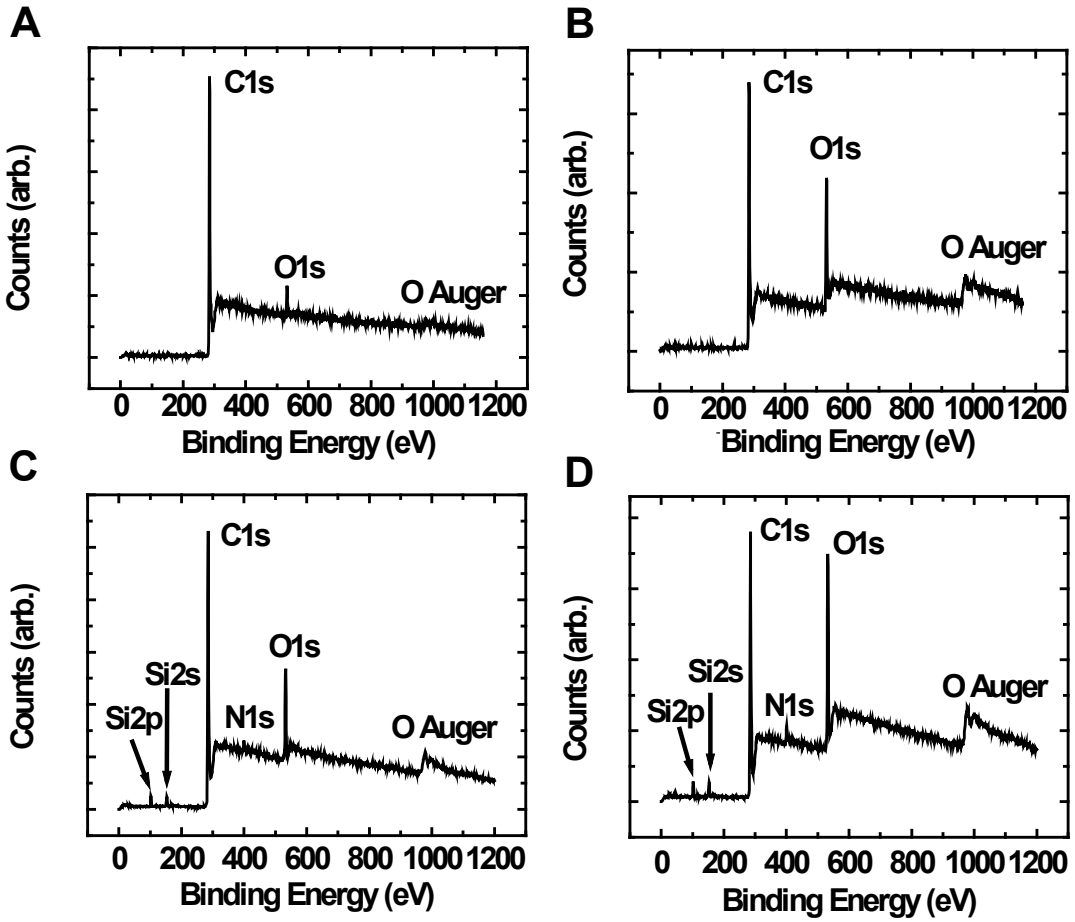

Figure 2.2 XPS survey spectra of (A) carbon core particles, (B) nitric acid-treated carbon core particles, (C) carbon core particles coated with PAAm, and (D) nitric acid-treated carbon core particles coated with PAAm. The actual O/C ratios for (A) and (B) are 0.05 and 0.25, respectively (see Table 2.1).

Table 2.1 XPS data. The oxygen to carbon (O/C) and nitrogen to carbon (N/C) ratio for (A) carbon core, (B) nitric acid-treated carbon core, (C) carbon core coated with PAAm, and (D) nitric acid-treated carbon core coated with PAAm.

XPS samples	O/C	SD	N/C	SD
(A) Carbon core[a)]	0.10	0.06[b)]	0	
(B) Carbon core + 60 ˚C nitric acid for 24 h[a)]	0.24	0.02	0.004	0.001
(C) Carbon core + PAAm[c)]	0.12		0.025	
(D) Carbon core + 60 ˚C nitric acid for 24 h + PAAm[c)]	0.24		0.036	

[a)] These XPS measurements were done at Brigham Young University. [b)] The amount of oxygen seemed to vary a fair amount on the carbonized particles. After three separate carbonizations, the percent carbon and oxygen for the samples were 95.1% C, 4.9% O; 92.6% C, 7.4% O; and 86.2% C, 13.8% O. [c)] These XPS measurements were done at the University of Utah.

of PAAm onto oxidized and unoxidized carbon particles, but, as expected, suggested greater deposition, as evidenced by a larger N 1s signal (see Figure 2.2 and Table 2.1), on the oxidized particles. A small amount of silicon was also observed on the PAAm-coated particles. It is unclear whether this contamination is due to the glass/silica vessels used during particle preparation and carbonization, to the particle mounting during XPS analysis, or to polydimethylsiloxane (PDMS) contamination.[28]

After successful acid oxidation of the core particles (both those prepared in house and the commercial ones), LbL deposition of PAAm and nanodiamond was attempted as described previously.[15] Figure 2.3 shows SEM images of shell growth on both types of particles after deposition of 5, 15, and 25 bilayers of PAAm and nanodiamond. The images point to a growing, porous nanodiamond/polymer composite coating on the core carbon particles. Indeed, Figure 2.3G shows the average particle diameter from measurements on ca. 30 – 40 particles from each image as a function of the number of bilayers. Overall there appears to be relatively consistent growth in the particles (an increase in diameter of about 40 nm per bilayer). However, there also appear to be regions of limited growth and others of more accelerated growth. These phenomena have been reproduced and are under further study. Figure 2.3H is a plot of the 95% confidence intervals in Figure 2.3G as a function of the number of bilayers deposited. The particle size distribution appears to remain nearly constant for the first 10 bilayers, after which it appears to increase fairly steadily.

2.4.3. Improved Particle Size Distribution (PSD) by Sieving and Column Packing

PSD measurements were performed after deposition of 30 bilayers of PAAm and nanodiamond on HNO_3-treated in-house synthesized (2.8 μm) and commercial (3.6 μm) carbon

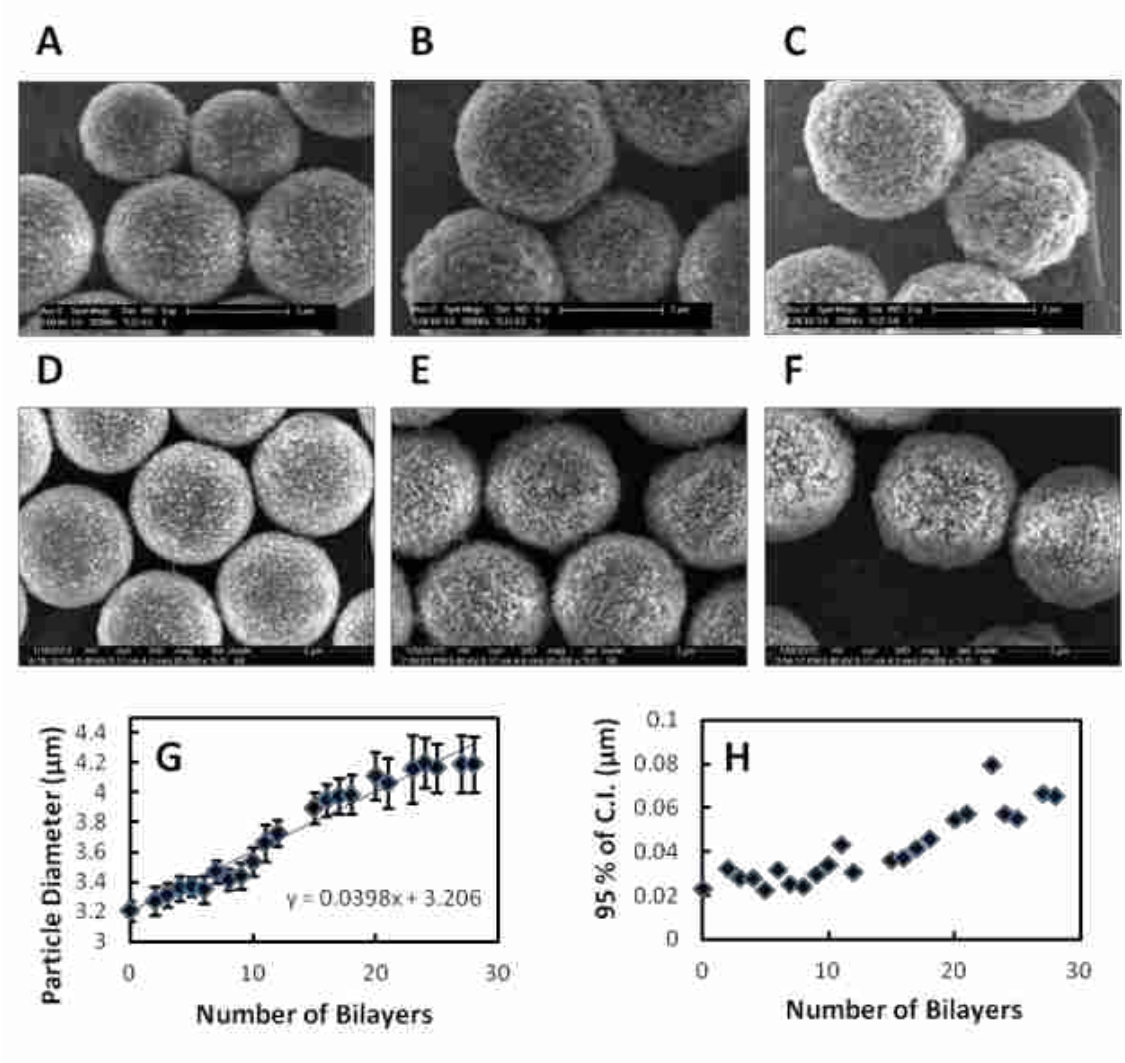

Figure 2.3 SEM images (taken with an FEI XL30 SFEG) of (A) 5, (B) 15, and (C) 25 bilayers of PAAm/nanodiamond on in-house prepared carbonized PDVB particles, and SEM images (taken with an FEI Helio NanoLab 600) of (D) 5, (E) 15, and (F) 25, bilayers of PAAm/nanodiamond on commercially obtained, carbonized PDVB. Both kinds of particles were pretreated in nitric acid at 60 °C for 24 h. (G) Growth curve for the LbL process on the commercially obtained, carbonized particles (error bars are standard deviations of measurements on 30 - 40 particles), and (H) 95% confidence intervals (C.I.) of the data in (G). See Figure 2.4 for additional images. The starting diameter for the particles in (G) and (H) was ca. 3.2 µm, which suggests some heterogeneity in the carbonization process, c.f., Figure 2.1.

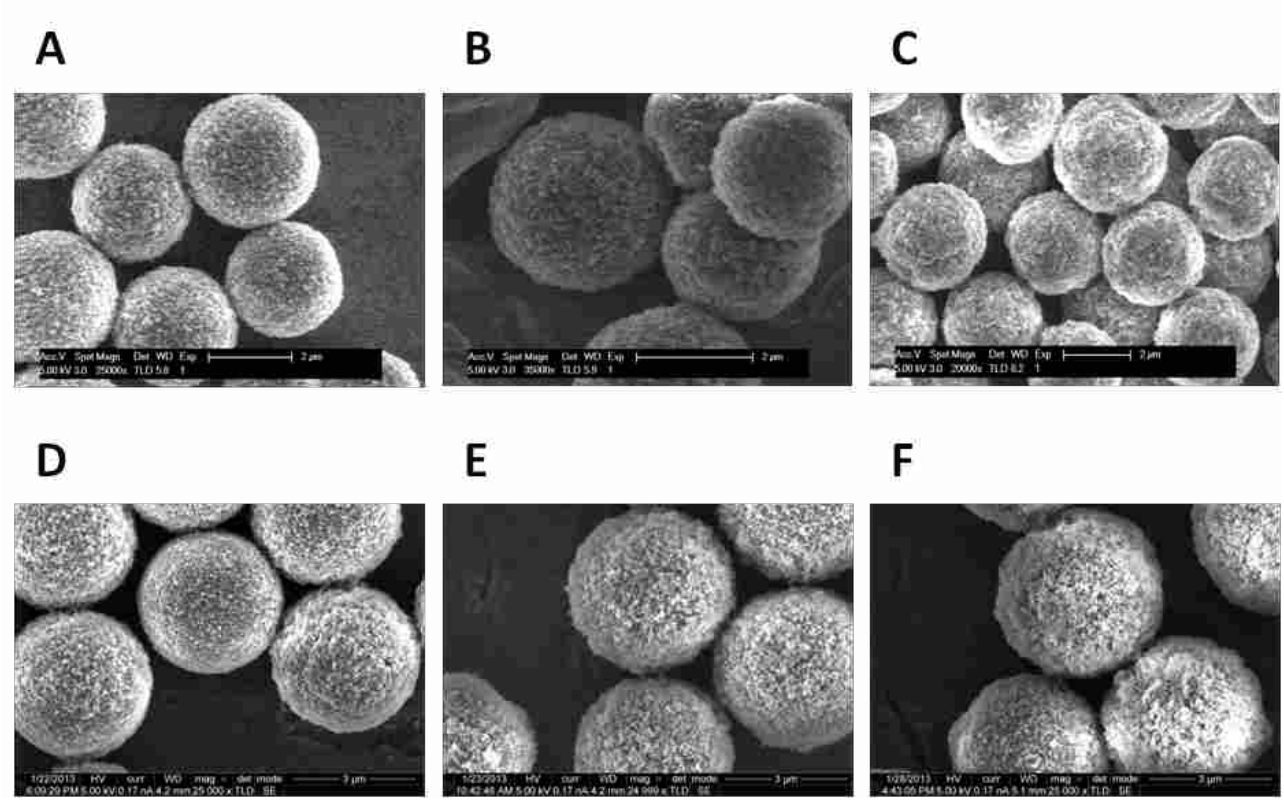

Figure 2.4 SEM images (taken with an FEI XL30 SFEG) of (A) 10, (B) 20, and (C) 30 bilayers of PAAm/nanodiamond on in-house prepared carbonized PDVB particles. SEM images (taken with an FEI Helio NanoLab 600) of (D) 10, (E) 20, and (F) 28, bilayers of PAAm/nanodiamond on commercially obtained, carbonized PDVB particles. Both kinds of particles were treated in nitric acid at 60 °C for 24 h prior to PAAm/nanodiamond deposition.

core particles. After deposition of PAAm and nanodiamond, the particles had increased in size to ca. 3.3 and 4.0 μm, respectively – the increase in particle diameter (ca. 0.4 – 0.5 μm) was nearly the same in both cases. Unfortunately, some agglomerates (ca. 100 μm and larger) were present in both the particles made from the in-house synthesized as well as the commercial PDVB. Fortunately, these could be removed by passing the particles through a 40 μm sieve. PAAm-nanodiamond coated particles made from commercial 5 μm PDVB particles also showed tighter d90/d10 values after sieving (1.36 vs. 1.42 for the in house synthesized carbon cores), and the PSDs of both types of sieved particles were better than the d90/d10 value of 1.63 previously obtained.[15] Representative PSDs for these particles are shown in Figure 2.5.

As before, the resulting particles were functionalized/crosslinked using 1,2-epoxyoctadecane and 1,2,7,8-diepoxyoctane to make a weak anion exchange/reversed-phase material.[15] The three types of particles mentioned in the previous paragraph were then packed via a slow increase in pressure (200 psi/min) to a final pressure of 7000 psi using 1% (v/v) aqueous Triton X-100 as the packing solvent.[15] Prior to packing, the particles that had been sieved before functionalization (See Figure 2.5B - C) were resieved through a 40 μm sieve, and the particles that showed agglomerates (see previous paragraph and Figure 2.5A) underwent sedimentation. The sieving process appears to be more effective here as the backpressures for the packed, in-house derived particles were 1271 psi with sieving and 2329 psi with sedimentation but no seiving. As expected, the particles based on the larger commercial cores (and final size) showed an even lower backpressure of 729 psi (See Table 2.2).

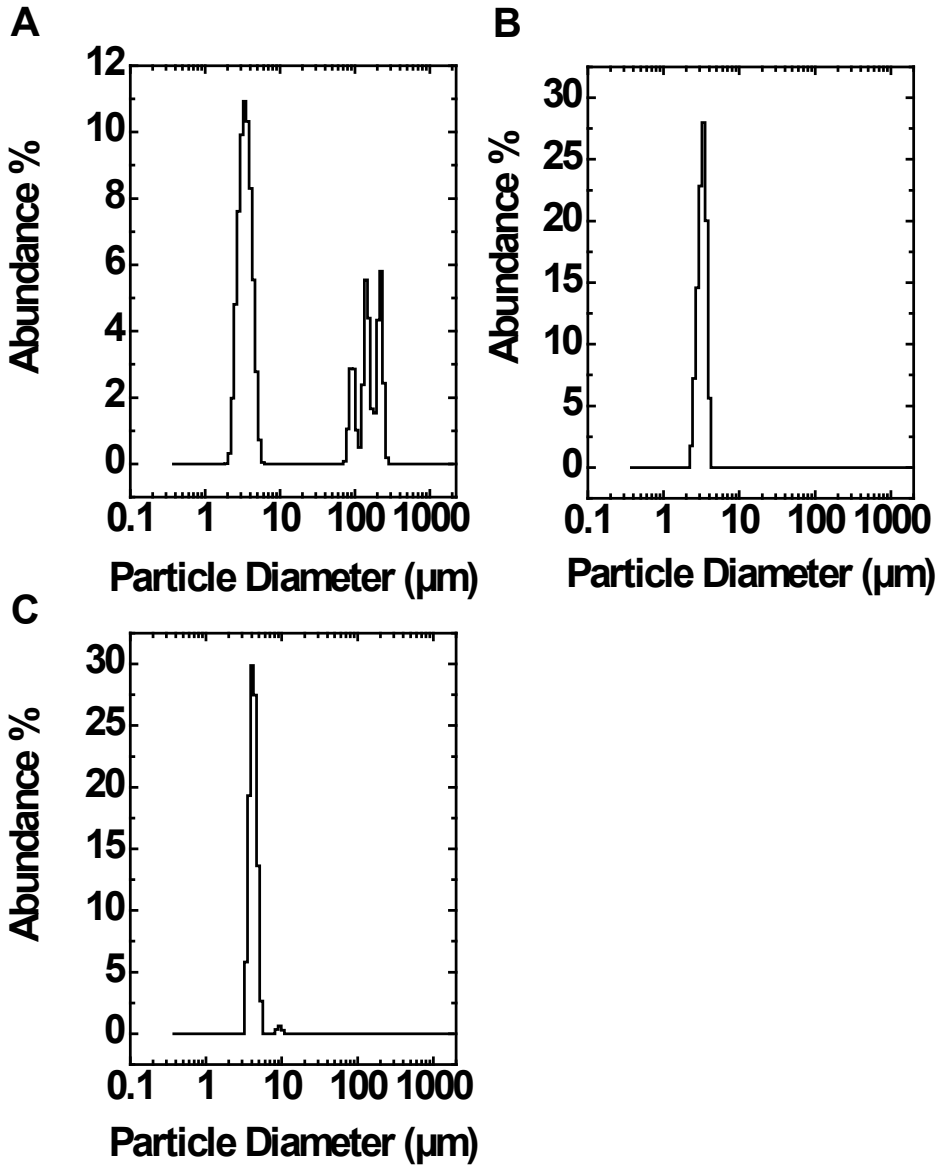

Figure 2.5 Particle size distributions (PSD) of nitric acid-treated carbon-core particles after deposition of 30 bilayers of PAAm and nanodiamond: (A) particles from cores prepared in-house, (B) particles as in (A) after passage through a 40 µm sieve (d90/d10: 1.42), (C) particles from carbonized, commercial 5 µm PDVB starting material after passage through a sieve as in (B) (d90/d10: 1.36).

Table 2.2 Efficiencies obtained with a conventional HPLC system for decylbenzene on three columns prepared with commercial, 5 µm particles. Mobile phase: 40/60/0.1 H_2O/ACN/TEA (v/v/v), flow rate: 0.7 mL/min, 35 °C.

Column ID	N/m	*k*	$Asym_{10\%}$	Psi
Commercial, Sieved #1	91,000	8.66	1.11	729
Commercial, Sieved #2	93,000	8.91	1.16	659
Commercial, Sieved #3	96,000	8.69	1.17	659
Average ± SD	93,000 ± 3,000	8.75 ± 0.14	1.15 ± 0.03	682 ± 40
%RSD	3.2	1.6	2.6	5.9

2.4.4. Brunauer-Emmett-Teller (BET) Measurements on Particles

Table 2.3 presents BET (surface area and pore diameter) results from our columns. The surface areas of these materials are modest (ca. 15 – 25 m^2/g) and the pore diameters of the materials are relatively large (ca. 50 – 70 nm). Obviously, these pore sizes are well suited for separation of proteins and other large molecules, which will be attempted in the future. Efforts are underway to increase the surface areas and decrease the pore diameters of these particles. This might be accomplished by using smaller nanodiamonds, although this approach may come at a cost of more deposition steps.

2.4.5. Reproducibility of Particle Functionalization and Packing

The reproducibility of our functionalization and packing procedures was evaluated. Three samples of the same sieved, PAAm/nanodiamond particles (the particles in Figure 2.5C) were derivatized with epoxides and packed under identical conditions. Quite reproducible chromatograms of a series of alkyl benzenes were obtained from the columns. In these separations, efficiencies for decyl benzene ranged from 91,000 to 96,000 N/m, retention factors (*k*) were very similar (%RSD of 1.56), peak asymmetries ($Asym_{10\%}$) were low and similar (< 1.2), and column back pressures were also low and similar (see Table 2.2 and Figure 2.6).

2.4.6. van Deemter Studies

Plate height, *H*, versus mobile phase linear velocity, *v*, curves were generated to determine the *A*-, *B*-, and *C*-terms of the van Deemter equation for the columns prepared in this study. This work was performed on a UHPLC system to minimize extra column contributions to

Table 2.3 BET data of particles giving surface areas and pore diameters.

Column ID	Core size (μm)	Final particle size (μm)	Shell thickness (μm)	Surface area (m^2/g)	Pore diameter (nm)
In House, Not Sieved	ca.2.8	ca.3.3[a)]	0.25	24	68
In House, Sieved	ca.2.8	ca.3.3	0.25	21	59
Commercial, Sieved #1	ca.3.6	ca.4.0	0.20	15	51

[a)] Average diameter of isolated particles, excluding agglomerates.

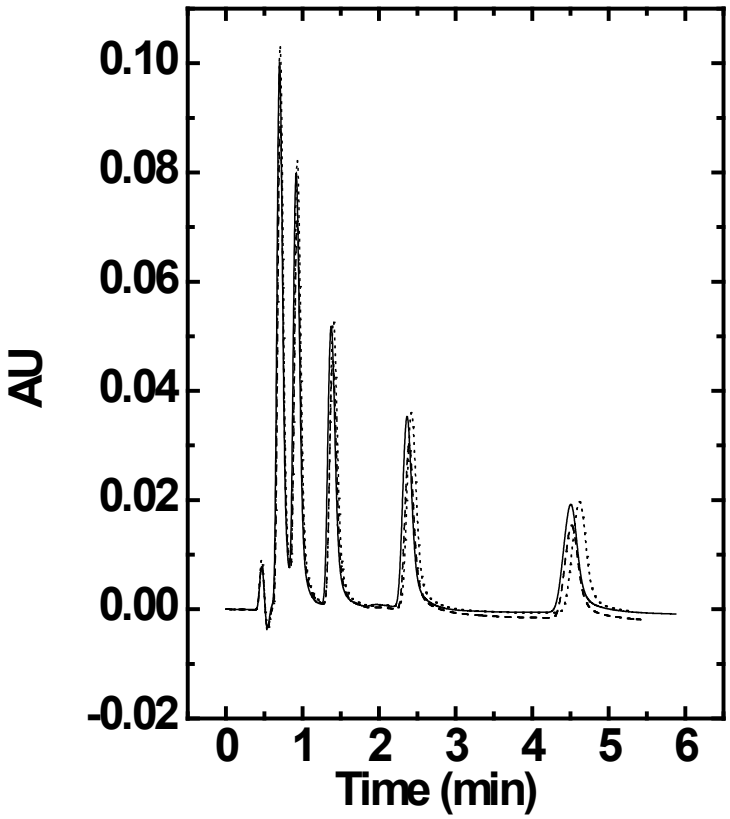

Figure 2.6 Reproducibility of three columns prepared from commercial, PDVB 5 µm particles with final particle size of 4 µm (see Figure 2.5C). The columns are designated as: "Commercial, Sieved, #1" (solid line), "Commercial, Sieved, #2" (dotted line), and "Commercial, Sieved, #3" (dashed line). From left to right analytes were ethyl, butyl, hexyl, octyl, and decylbenzene. Mobile phase: 40/60/0.1 H_2O/ACN/TEA (v/v/v), flow rate: 0.7 mL/min, 35 °C.

band broadening. Results immediately suggested that the newer, more uniform particles could be packed more efficiently than the previous ones.[15] Figure 2.7 shows the van Deemter plot for decylbenzene with *A*, *B*, and *C* terms of 4.97, 0.31, and 37.8, respectively, for the column of "Commercial, Sieved #1" and Table 2.4 gives a comparison of *A*, *B*, *C*, and *H*, and also the corresponding reduced values (*a*, *b*, *c*, and *h* – the previously values divided by the particle diameter) for different columns prepared in this study. Kirkland et al.[29] noted that high-quality columns show reduced plate heights in the range of 2 - 2.5 with USP Tailing Factors of less than 1.2 for non-polar analytes. The columns, Commercial, Sieved #1, #2, and #3, had an *h* between 2 and 2.5 with tailing factors of about 1.0 to 1.4 for alkylbenzene analytes. Given the imprecision in our laboratory procedures – particle synthesis, packing, etc., these values are consistent with reasonably high quality columns. In our previous studies, we obtained efficiencies of 56,000 N/m (*h* = 4.46) for butylbenzene and 71,000 N/m (*h* = 3.52) for diisopropylphenol on a traditional HPLC system, and 100,000 – 120,000 N/m (*h* = ca. 2.3) for different alkyl benzenes using a specialized sandwich-type injection on a UHPLC system. In this study, column efficiencies greater than 90,000 N/m were achieved using a traditional HPLC system (see Table 2.2) and efficiencies of ca. 100,000 – 110,000 N/m were achieved with a UHPLC system (see Table 2.4). These data were obtained via standard injection procedures – a sandwich injection was not necessary to obtain these high efficiencies. The column with the lowest efficiency in Table 2.4 was the "In-House, Not Sieved" column. As noted, the particles in this column had been sedimented, but not sieved as were the particles for the other columns in Table 2.4. The reduced terms *a* and *b* are especially low for the particles made from the commercial PDVB. However, with sieving, the *c* terms are comparable for the in-house synthesized and commercially obtained PDVB – based columns.

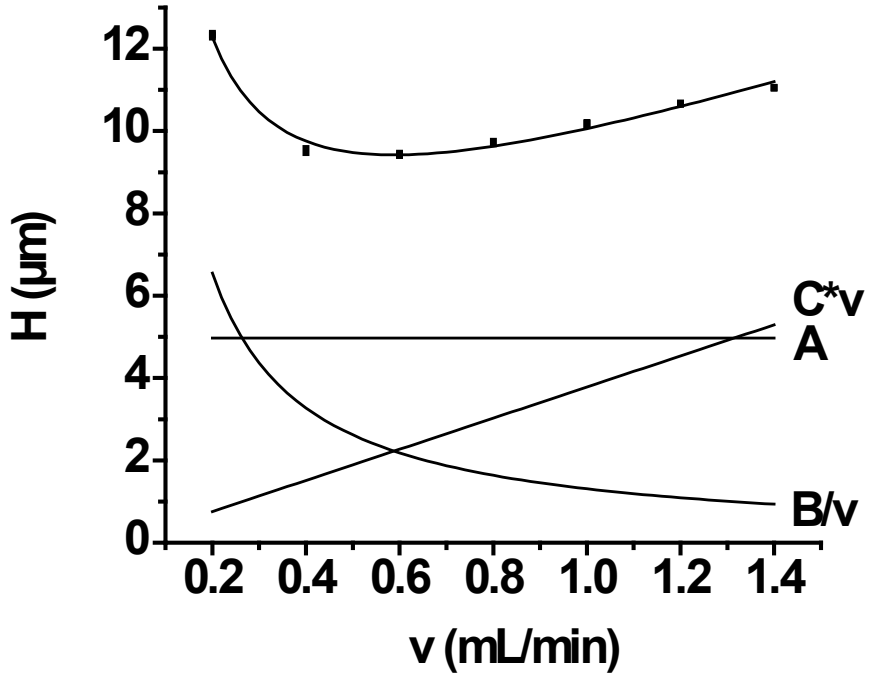

Figure 2.7 van Deemter plot for decylbenzene with *A*, *B*, and *C* terms of 4.97, 1.31, and 3.78. Column: Commercial, Sieved #1 (see Table 2.2 and Figure 2.6). Mobile phase and temperature: 40/60/0.1 H_2O/ACN/TEA (v/v/v), 35 °C.

Table 2.4 The *A*-, *B*-, *C*-terms, and plate heights (*H*) from the van Deemter equation for the columns: "in-house, not sieved," "in-house, sieved," and "commercial, sieved #1, #2, and #3." The reduced values of *A*, *B*, *C*, and *H* (divided by d_p) are also given. Efficiencies were obtained using a UHPLC system with triplicate injections at each linear velocity (0.02 – 0.14 cm/s, inclusive, at 0.02 cm/s increments). The analyte was decylbenzene with a mobile phase of 40/60/0.1 H_2O/ACN/TEA v/v/v, pH 11.3, at 35 °C.

Column ID	d_p (μm)	d90/d10[b)]	*A* (μm)	*B* (μm* cm/s)	*C* (μm* s/cm)	H (μm)	Optimal linear velocity (cm/s)	*a*	*b* (cm/s)	*c* (s/cm)	h	N/m
In-house, not sieved	ca. 3.3[a)]	N/A[c)]	6.06	0.180	43.8	11.57	0.08	1.84	0.0545	13.3	3.51	86,000
In-house, sieved	ca. 3.3	1.42	5.58	0.168	27.7	9.88	0.07	1.69	0.0509	8.39	2.99	101,000
Commercial, sieved #1	ca. 4.0	1.36	4.97	0.131	37.8	9.43	0.06	1.24	0.0328	9.45	2.36	106,000
Commercial, sieved #2	ca. 4.0	1.36	4.51	0.107	47.3	8.89	0.04	1.13	0.0268	11.8	2.22	112,000
Commercial, sieved #3	ca. 4.0	1.36	4.41	0.138	45.7	9.48	0.06	1.10	0.0345	11.4	2.37	105,000

[a)] Average diameter of isolated particles, excluding agglomerates. [b)] Data obtained from a PSD analyzer [c)] Data not available because of the presence of agglomerates.

2.4.7. Elevated Temperature Stability

In our previous report, columns were tested and found to be stable up to 80 °C at pH 11.3.[15] In this study, we have extended this temperature range to 120 and 140 °C, also at pH 11.3, where chromatograms were taken before and after two heating cycles, each of which consisted of five hours of mobile phase flowing through the column at the temperature in question. The ca. 3.6 μm particles used for this column were prepared from ca. 3.3 μm for in-house-prepared carbon core particles that had been oxidized with piranha solution. These particles were not sieved prior to packing and had a PSD similar to those shown in Figure 2.5A. Table 2.5 and Figure 2.8 show that there is a ca. 5% increase in retention and a 10% decrease in efficiency for some alkyl benzene analytes after the two heating cycles at 120 °C. After two heating cycles at 140 °C, there is a ca. 10% increase in retention and a ca. 25% loss in N/m. These results suggest that the column is quite stable at 120 °C and pH 11.3, but that its performance begins to degrade to a greater degree at higher temperature. It is noteworthy, however, that in no case was a catastophic decrease in column performance observed (see Figure 2.8) as Teutenberg has found in some of his column stabilty studies,[5] i.e., peak shapes and overall chromatograms remained fairly reasonable.

2.4.8. Packing Longer Columns

Longer and narrower columns (2.1 x 50 mm instead of 4.6 x 30 mm) were packed using particles prepared in the same way as those used to make the columns corresponding to Figure 2.6. These columns showed a decrease in efficiency (N/m) of ca. 20% (down to 89,000 N/m with decyl benzene) compared to the wider bore columns (see Table 2.6), which was expected

Table 2.5 *k* and N/m before and after heating cycles (all were 5 h) for decylbenzene at 120 °C and 140 °C.

Temperature (˚C)	Heating cycle	pH	Mobile Phase (H_2O/ACN/TEA, v/v/v)	Flow rate (mL/min)	*k* (Before)	*k* (After)	N/m (Before)	N/m (After)
120	I	11.3	60/40/0.1	0.7	34.4	35.5	90,000	82,000
120	II	11.3	60/40/0.1	0.7	37.8	36.2	86,000	81,000
140	I	11.3	70/30/0.1	0.7	42.5	41.5	80,000	73,000
140	II	11.3	70/30/0.1	0.7	41.5	46.6	73,000	59,000

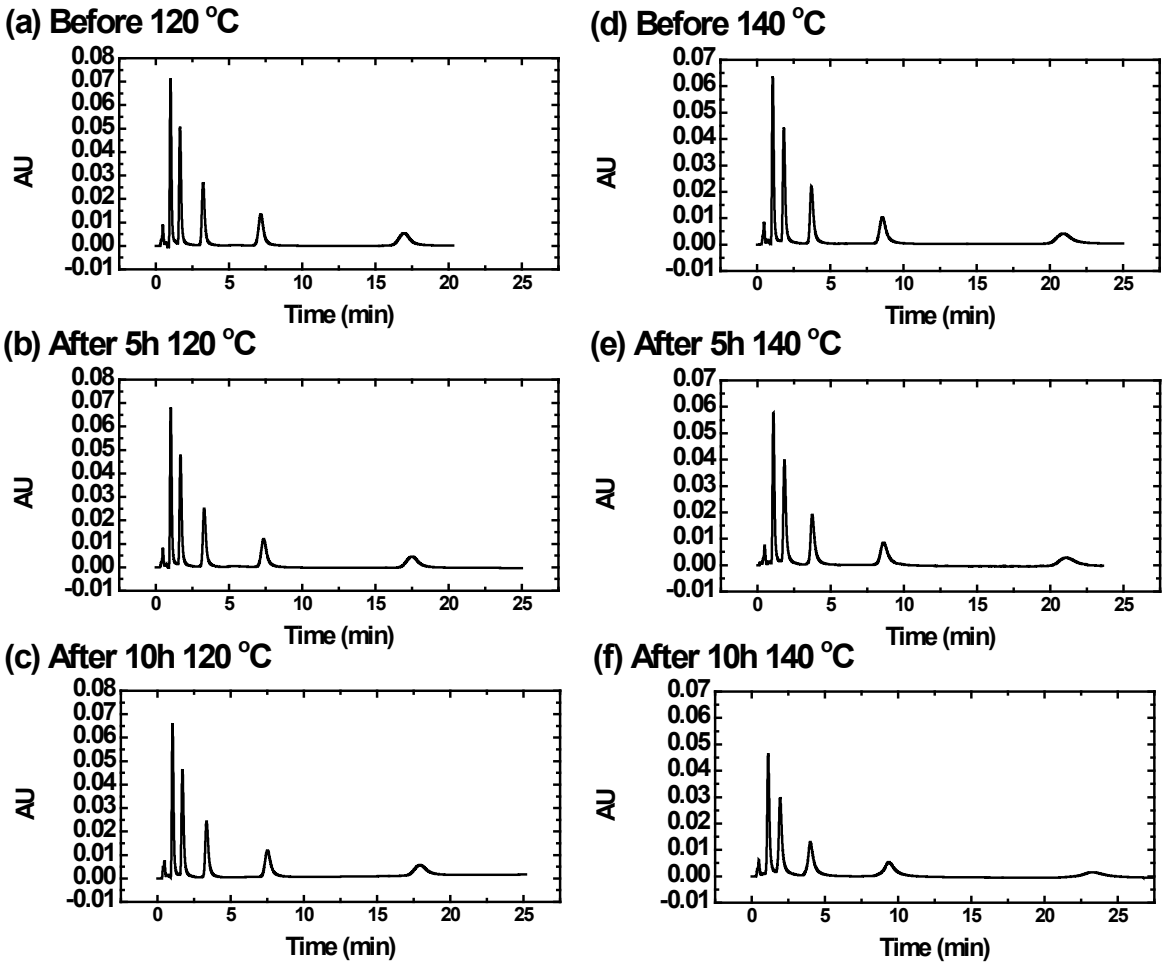

Figure 2.8 Chromatograms of an alkybenzene test mixture (ethyl-, butyl-, hexyl-, octyl-, and decylbenzene) taken at 35 °C with 60/40/0.1 H_2O/ACN/TEA (pH 11.3) (v/v/v) at 0.7 mL/min before [(a) and (d)] and after [(b), (c), (e), and (f)] stability tests (5 h each) on the same column. The same mobile phase and conditions were used for the 120 °C purges. For the 140 °C purges, the mobile phase was 70/30/0.1 H_2O/ACN/TEA (pH 11.3) (v/v/v) at 0.7 mL/min. The mobile phase was made up twice – before and after the 140 °C experiments, which accounts for the small shifts in retention.

Table 2.6 Retention factors (*k*), tailing factors, asymmetries **(**$Asym_{10\%}$), and efficiencies (N/m) of 2.1 x 50 mm columns obtained with a UHPLC system.

Compound	*k*	Tailing factor	$Asym_{10\%}$	N/m
Ethylbenzene	0.52	1.38	1.35	43,000
Butylbenzene	1.07	1.29	1.41	55,000
Hexylbenzene	2.21	1.20	1.30	72,000
Octylbenzene	4.66	1.09	1.17	85,000
Decylbenzene	9.87	1.08	1.08	89,000

because of increased wall effects in the narrower column.[30] However, because of its increased length, this column showed more plates (*N*) overall than the shorter, 30 mm "Commercial, Sieved #1" column: 4450 N vs. 3180 N, respectively, which led to the high quality separation shown in Figure 2.9.

2.4.9. Applications

A 4.6 x 30 mm column made from carbonized, commercial PDVB particles that had been sieved after LbL was used to separate four essential oils: eucalyptus, lavender, melaleuca, and peppermint (see Figure 2.10).[31-34] Sample preparation was "dilute and shoot" – analytes were dissolved in ACN and injected directly. All separations were gradient elutions. In most cases peak shapes seemed quite good. Peak widths in the separations appear to be roughly constant, which is expected for gradient elution. Also as expected in the separation of complex mixtures, not all components appear to be completely resolved. Separations of other classes of compounds should be possible on these columns; the Flare column by Diamond Analytics is based on the technology described herein and has been shown to separate acidic herbicides at low pH,[35] and β2-agonists, amphetamines, and tricyclic antidepressants at elevated pH.[36-37]

2.5. Conclusions

In this chapter, efficiencies up to 112,000 N/m (h = 2.22) are reported for reversed phase, core-shell, carbon/nanodiamond/aminopolymer particles using conventional injection conditions, which greatly exceeds the previous value of 71,000 N/m (h = 3.52).[15] The carbon core particles

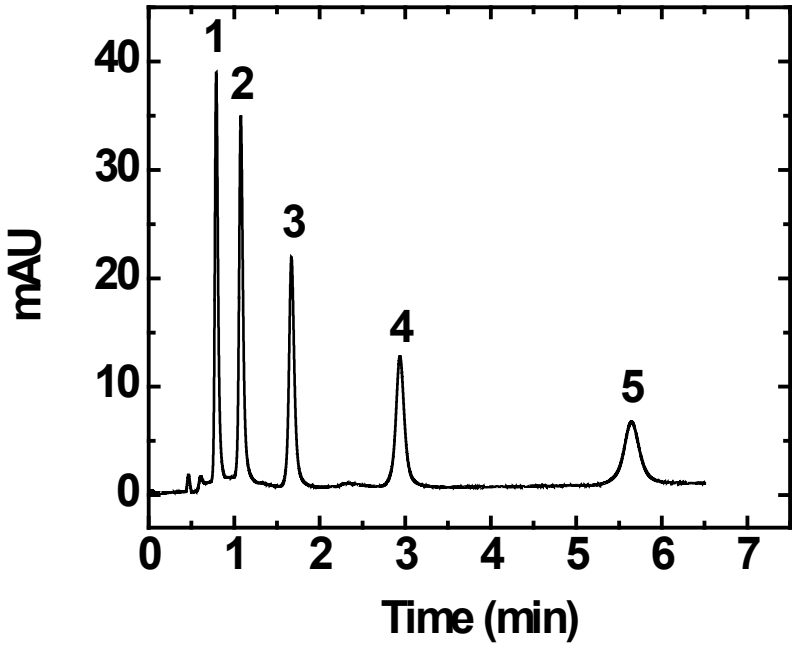

Figure 2.9 UHPLC separation of alkylbenzene analytes (1. ethyl- 2. butyl- 3. hexyl- 4. octyl- and 5. decyl-benzene) using a 2.1 x 50 mm column packed with the particles prepared in the same way as those for Figure 2.6. The mobile phase was 40/60 H_2O/ACN at 35˚C with a flow rate of 0.15 mL/min. The efficiency of the decylbenzene was 89,000 N/m with a tailing factor of 1.08.

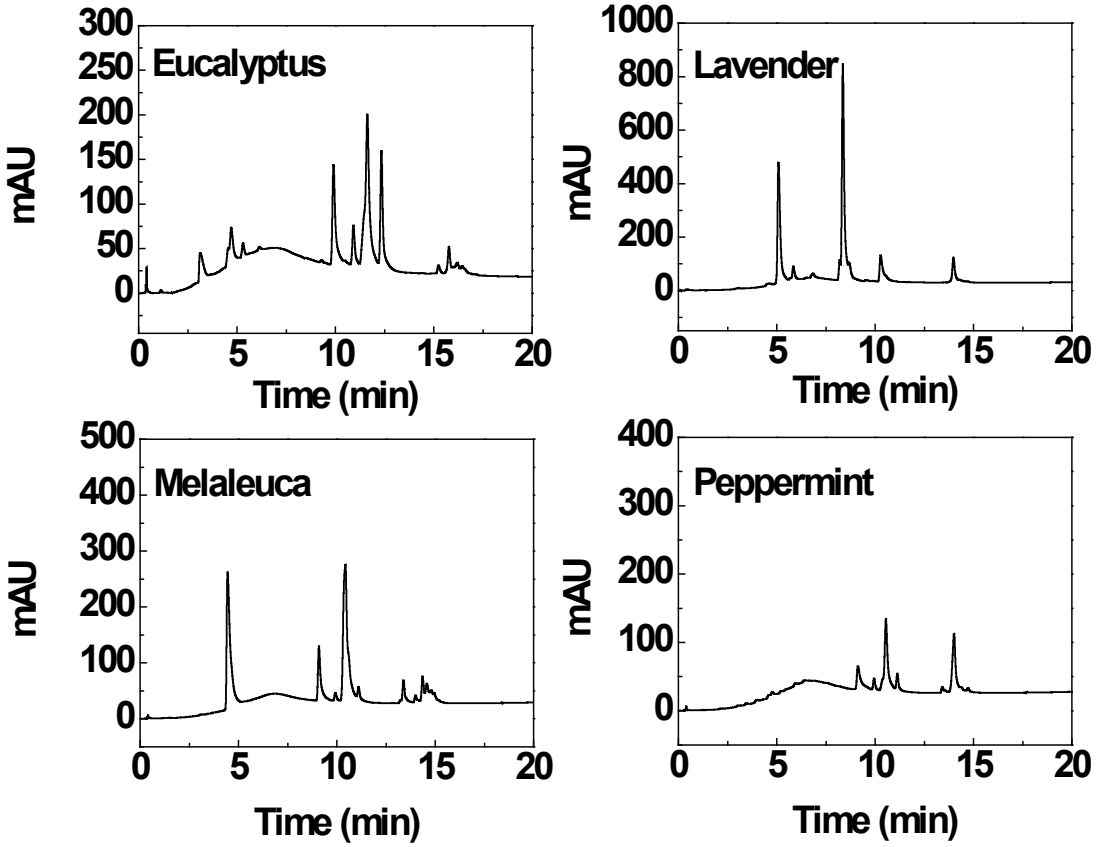

Figure 2.10 Separation of eucalyptus, lavender, melaleuca, and peppermint essential oils under gradient elution. Linear gradient from 90/10 H_2O/ACN at 0 min to 0/100 H_2O/ACN at 30 min. The flow rate was 0.6 mL/min at 35 ˚C with UV detection at 210 nm.

used in this study were derived from carbonized PDVB particles. They showed good uniformity and were oxidized in nitric acid to increase their dispersability. Layer-by-layer growth of PAAm and nanodiamond was demonstrated to produce core-shell particles. After LbL, particles were functionalized, sieved, and packed into columns. Column functionalization and packing were reproducible. Van Deemter curves indicated that the commercially-obtained PDVB spheres outperformed those synthesized in our laboratory. The columns appear to be reasonably stable at 120 °C in a pH 11.3 mobile phase. Longer columns (2.1 x 50 mm) than previously reported were packed. Four essential oils were separated by gradient elution.

This work was financially supported by Diamond Analytics, a US Synthetic Company, Orem, UT, USA. We also acknowledge the Department of Chemistry and Biochemistry and College of Physical and Mathematical Sciences at Brigham Young University for their support of this work. Essential Oils (peppermint, lavender, melaleuca, and eucalyptus) were obtained as a generous gift from dōTERRA, Orem, UT.

Conflict of interest statement: The technology represented by this and earlier related publications has been licensed by Brigham Young University to Diamond Analytics. Authors on this paper will receive royalties from sales of products that employ this technology in accord with that licensing agreement.

2.6. References

1. Jensen, D. S.; Teutenberg, T.; Clark, J.; Linford, M. R., *LCGC North Am.* **2012,** *30* (12), 1052-1057.

2. Jensen, D. S.; Teutenberg, T.; Clark, J.; Linford, M. R., *LCGC North Am.* **2012,** *30* (11), 992-998.

3. Jensen, D. S.; Teutenberg, T.; Clark, J.; Linford, M. R., *LCGC North Am.* **2012,** *30* (9), 850-862.

4. Teutenberg, T.; Tuerk, J.; Holzhauser, M.; Giegold, S., *J. Sep. Sci.* **2007,** *30*, 1101-1114.

5. Teutenberg, T.; Hollebekkers, K.; Wiese, S.; Boergers, A., *J. Sep. Sci.* **2009,** *32* (9), 1262-1274.

6. Teutenberg, T., *High Temperature Liquid Chromatography A User's Guide for Method Development*. The Royal Society of Chemistry: Cambridge, 2010.

7. Kirkland, J. J.; Henderson, J. W.; DeStefano, J. J.; van Straten, M. A.; Claessens, H. A., *Journal of Chromatography A* **1997,** *762*, 97-112.

8. Wyndham, K. D.; O'Gara, J. E.; Walter, T. H.; Glose, K. H.; Lawrence, N. L.; Alden, B. A.; Izzo, G. S.; Hudalla, C. J.; Iraneta, P. C., *Anal. Chem.* **2003,** *75* (24), 6781-6788.

9. Snyder, L. R.; Kirkland, J. J.; Dolan, J. W., *Introduction to Modern Liquid Chromatography/ Lloyd R. Snyder, Joseph J. Kirkland, and John W. Dolan - Third Edition*. John Wiley & Sons, Inc: Hoboken, 2009.

10. Nesterenko, P. N.; Fedyanina, O. N., *J. Chromatogr.* **2010,** *1217* (4), 498-505.

11. Nesterenko, P. N.; Haddad, P. R., *Anal. Bioanal. Chem.* **2010,** *396* (1), 205-211.

12. Fedyanina, O. N.; Nesterenko, P. N., *Russ. J. Phys. Chem. A* **2010,** *84* (3), 476-480.

13. Matheson, A.; Nesterenko, P. N., *LC GC Eur.* **2010,** *23* (3), 120-124.

14. Mochalin, V. N.; Shenderova, O.; Ho, D.; Gogots, Y., *Nat. Nanotechnol.* **2012,** *7*, 11-23.

15. Wiest, L. A.; Jensen, D. S.; Hung, C.-H.; Olsen, R. E.; Davis, R. C.; Vail, M. A.; Dadson, A. E.; Nesterenko, P. N.; Linford, M. R., *Anal. Chem.* **2011,** *83* (14), 5488-5501.

16. Saini, G.; Jensen, D. S.; Wiest, L. A.; Vail, M. A.; Dadson, A.; Lee, M. L.; V., S.; Linford, M. R., *Anal. Chem.* **2010,** *82* (11), 4448-4456.

17. Saini, G.; Yang, L.; Lee, M. L.; Dadson, A.; Vail, M. A.; Linford, M. R., *Anal. Chem.* **2008,** *80* (16), 6253-6259.

18. Saini, G.; Gates, R.; Asplund, M. C.; Blair, S.; Attavar, S.; Linford, M. R., *Lab Chip* **2009,** *9* (12), 1789-1796.

19. Saini, G.; Wiest, L. A.; Herbert, D.; Biggs, K. N.; Dadson, A.; Vail, M. A.; Linford, M. R., *J. Chromatogr. A* **2009,** *1216*, 3587-3593.

20. Li, K.; Stöver, H. D. H., *J. Polym. Chem.* **1993,** *31* (13), 3257-3263.

21. Bai, F.; Yang, X.; Huang, W., *Macromolecules* **2004,** *37*, 9746-9752.

22. Li, W.-H.; Stover, H. D. H., *Macromolecules* **2000,** *33*, 4354-4360.

23. Hirano, S.-I.; Ozawa, M.; Naka, S., *J. Mater. Sci.* **1981,** *16*, 1989-1993.

24. Li, L.; Song, H.; Chen, X., *Mater. Lett.* **2008,** *62* (2), 179-182.

25. El-Hendawy, A.-N. A., *Carbon* **2003,** *41* (4), 713-722.

26. Partouche, E.; Margel, S., *Carbon* **2008,** *46* (5), 796-805.

27. Moreno-Castilla, C.; Ferro-García, M. A.; Joly, J. P.; Bautista-Toledo, I.; F.Carrasco-Marín; Rivera-Utrilla, J., *Langmuir* **1995,** *11*, 4386-4392.

28. Yang, L.; Shirahata, N.; Saini, G.; Zhang, F.; Pei, L.; Asplund, M. C.; Kurth, D. G.; Ariga, K.; Sautter, K.; Nakanishi, T.; Smentkowski, V.; Linford, M. R., *Langmuir* **2009,** *25* (10), 5674-5683.

29. Kirkland, J. J.; Destefano, J. J., *J. Chromatogr.* **2006,** *1126* (1-2), 50-57.

30. Shalliker, R. A.; Broyles, B. S.; Guiochon, G., *J. Chromatogr. A* **2000,** *888*, 1-12.

31. Wiest, L. A.; Jensen, D. S.; Miles, A. J.; Dadson, A. E.; Linford, M. R. *Flare Mixed-Mode Column: Eucalyptus Essential Oil*; DA1002-A; Diamond Analytics: Orem, Utah.

32. Wiest, L. A.; Jensen, D. S.; Miles, A. J.; Dadson, A. E.; Linford, M. R. *Flare Mixed-Mode Column: Lavender Essential Oil*; DA1002-B; Diamond Analytics: Orem, Utah.

33. Wiest, L. A.; Jensen, D. S.; Miles, A. J.; Dadson, A. E.; Linford, M. R. *Flare Mixed-Mode Column: Melaleuca Essential Oil*; DA1002-C; Diamond Analytics: Orem, .

34. Wiest, L. A.; Jensen, D. S.; Miles, A. J.; Dadson, A. E.; Linford, M. R. *Flare Mixed-Mode Column: Peppermint Essential Oil*; DA1002-D; Diamond Analytics: Orem.

35. Singh, B.; Jensen, D. S.; Miles, A. J.; Dadson, A. E.; Linford, M. R. *Probing the Retention Mechanism of the Flare Mixed-Mode Column at Low pH via Acidic Herbicides with Different pK_a Values*; DA1000-C; Diamond Analytics: Orem, Utah.

36. Wiest, L. A.; Jensen, D. S.; Miles, A. J.; Dadson, A. E.; Linford, M. R. *Flare Mixed-Mode Column: β_2-Agonists and Amphetamines*; DA1003-A; Diamond Analytics: Orem, Utah.

37. Hung, C.-H.; Davis, T. C.; Jensen, D. S.; Miles, A. J.; Zukowski, J.; Dadson, A. E.; Linford, M. R. *Flare C18 Mixed-Mode Columns: Tricyclic Antidepressants (TCAs)*; DA1001-A; Diamond Analytics: Orem, Utah.

Chapter 3: Multi-Instrument Characterization of Poly(divinylbenzene) Microspheres for Use in Liquid Chromatography: As Received, Air Oxidized, Carbonized, and Acid Treated*

3.1. Abstract

We report a multi-instrument characterization of the carbon particles in carbon/polymer/nanodiamond core-shell materials used for high performance liquid chromatography. These particles are prepared by the carbonization/pyrolysis of poly(divinylbenzene) (PDVB) microspheres. Scanning electron microscopy showed that the particles (4.9 μm initially) decreased in size after air oxidation (to 4.4 μm) and again after carbonization (down to 3.5 μm), but remained highly spherical. Brunauer-Emmett-Teller measurements showed low surface areas initially (as received: 1.6 m^2/g, after air oxidation: 2.6 m^2/g), but high values after carbonization (445 m^2/g). Fourier transform infrared spectroscopy revealed the changes in the functional groups after air oxidation (C=O and C-O stretches appear), carbonization (carbon-oxygen containing moieties disappear), and acid treatment (reintroduction of carbon-oxygen containing moieties). X-ray photoelectron spectroscopy (XPS) and elemental analysis revealed the surface and bulk oxygen contents before and after treatments. By XPS the atom percent oxygen for the as received, air oxidized, carbonized, and acid treated particles are 8.7, 16.6, 3.7, and 13.8, respectively, and by elemental analysis, the percent oxygen in the materials

*This chapter was taking from a manuscript accepted by Surface and Interface Analysis: which has granted permission for its use here.

is 0.6, 8.1, 0.9, 16.9, respectively. A principal components analysis of time-of-flight secondary ion mass spectrometry data identified ions that were enhanced in the different materials, where almost 90% of the variation in the analyzed peak areas was captured by two principle components. X-ray diffraction and Raman spectroscopy suggested that the carbonized PDVB was disordered. Thermogravimetric analysis showed significant differences between the differently treated PDVB microspheres. This work applies directly to a commercial product and the process for preparing it.

3.2. Introduction

Carbon-based materials are well known for their chemical, thermal, and mechanical stability. Accordingly, they are often suitable for applications under harsh conditions.[1-7] They can be made from natural materials, such as wood or coal.[8-11] They can also be prepared by the pyrolysis of polymers, such as polyacrylonitrile (PAN).[11-12] Prior to carbonization, natural materials may be treated with a dehydrating reagent to limit the formation of tar and alter their pyrolytic decomposition.[9] They may also be treated thermally with a reactive gas, e.g., H_2O, CO_2, air, or O_2, which may have the positive effect of removing disorganized, amorphous carbon that may reduce the porosity of the materials.[9, 12-13] To increase its oxygen content, the carbon may be treated with an oxidizing agent, such as an oxygen plasma, nitric acid, or hydrogen peroxide.[3, 12-14] Oxygen-containing moieties on the surface of carbon increase its surface free energy, hydrophilicity, and dispersability.[1, 8, 13-16] These may include carboxyl groups, carbonyls, quinones, phenols, carboxylic anhydrides, and lactones.[8, 13, 15-17] Nitric acid-treatment of carbon has been reported to enhance the carboxylic acid content of the surface of carbon[14, 17], where the final functional group profile depends on the concentration of nitric acid and the reaction temperature.[13-14] Carboxyl groups allow subsequent functionalization of the material through, for

example, esterification.[14] The high surface area of porous (activated) carbon makes it suitable for many applications that include energy storage, catalysis, water purification, and chemical separations, e.g., liquid chromatography.[2-3, 8, 11-13, 15-16, 18-21]

Some of us have studied the preparation and properties of carbon/polymer/nanodiamond core-shell particles for high performance liquid chromatography (HPLC).[1, 4-7] These particles exhibit excellent pH and thermal stability. Of course, silica-based materials are the workhorse of modern liquid chromatography.[22-23] However, its more restricted pH range, especially at elevated temperatures, limits its use.[22-24] Excluding polymeric particles, the porous graphitic carbon (PGC) column (Hypercarb ®) invented by Knox and Gilbert has been the most successful carbon-based material for HPLC on the market.[24-25] PGC shows extraordinary pH and temperature stability. It also has a unique retention mechanism, i.e., a polar retention effect on graphite (PREG) that results from charge-induced dipoles on the graphitic surface.[2, 26] Because the retention mechanism of PGC is different from that of silica-based materials, PGC can be used as an orthogonal phase to retain and separate polar compounds that elute quickly from reversed phase columns. In our previous papers, we reported core-shell particles for HPLC from carbon cores, an amine containing polymer, and nanodiamond.[1, 4, 7] These materials were functionalized with C18 chains to create a mixed-mode column (a reversed-phase material with anion exchange properties). This phase showed unique selectivity. It could separate acidic analytes at low pH and basic analytes at high pH. Chromatographic efficiencies of ca. 112,000 plates per meter (N/m) with 4 μm particles (a reduced plate height of 2.22) were reported.[1] These materials were stable under harsh conditions, e.g., pH 11.3 and 120 °C.

In this study, we focus on the characterization of the carbon core materials used in our new core-shell particles for liquid chromatography. These particles are prepared by carbonizing

poly(divinylbenzene) (PDVB) microspheres.[12-13, 17, 27-33] Following the reports of Li et al.[29] and Winslow et al.[33], the PDVB was air oxidized before carbonization to enhance its ability to be crosslinked, and also to prevent it from melting and fusing together during carbonization. After carbonization, a nitric acid treatment was used to increase the oxygen content of the particles, which improved their dispersibility and affinity for the amine-containing polymer (poly(allylamine) (PAAm)).[13, 17, 32] To understand the physical and chemical changes that take place in the materials during these processes, the following analytical tools were employed: scanning electron microscopy (SEM), Brunauer-Emmett-Teller (BET) nitrogen adsorption, Fourier transform infrared spectroscopy (FTIR), X-ray photoelectron spectroscopy (XPS), elemental analysis, time-of-flight secondary ion mass spectrometry (ToF-SIMS), X-ray diffraction (XRD), and Raman spectroscopy. A principal components analysis (PCA) was used to analyze the negative ion ToF-SIMS data.

While it is true that others have studied the oxidation/carbonization of PDVB, the following appear to be unique features of this work. (1) There is a real world application for the carbon materials described here. That is, the carbon microspheres studied herein form the basis for the core particles of prototype core-shell particles that are now in a commercial high performance liquid chromatography column. (2) While the chemistries associated with the different processes employed herein are known, we believe that this is the first report of the full process of oxidizing highly uniform PDVB microspheres, carbonizing them, and then acid treating them. These steps were studied under different reaction conditions. (3) We undertook a sophisticated, multi-instrument characterization of our materials using SEM, BET, FTIR, XPS, elemental analysis ToF-SIMS, XRD, and Raman, and we compare the results from the multiple methods. For example, SEM showed that the particles enjoyed a very high degree of sphericity, which remained after all

of the chemical and thermal treatments reported herein. BET showed that the particles exhibited extremely low surface area prior to carbonization, and extremely high surface area thereafter. For the FTIR analysis, both diamond and Ge ATR crystals were employed to vary the depth of penetration (sampling depth) of the light. The combination of XPS and elemental analysis proved to be particularly powerful. The results from these two techniques were often anti-correlated, showing that in some cases surface compositions differed substantially from bulk compositions. Little ToF-SIMS characterization of these types of materials has been reported in the literature, and two different chemometrics analyses of the negative ion ToF-SIMS data are presented. For the principle components analysis (PCA), we report scores and loadings, and the Hotelling T^2 vs. Q residuals plots. The results from the ToF-SIMS/PCA analysis agree well with and help clarify the expected material chemistry. A cluster analysis of the ToF-SIMS data clearly separates the spectra from different samples. Finally, XRD and Raman indicated strongly disordered materials. The composite picture painted by this series of techniques leads to a much more clear and elegant understanding of these materials, which is important for their application in chromatography where they serve as core particles that are surrounded by a porous, composite layer of amine-containing polymer and nanodiamond.

3.3. Experimental

3.3.1. Reagents and Solvents

PDVB microspheres (5 μm, non-porous) were obtained from Sepax Technologies (Newark, DE), and nitric acid (68-70%) was obtained from Mallinckrodt Baker (Phillipsburg, NJ). High purity water was obtained from a Milli-Q Water System (EMD Millipore, Billerica, MA).

3.3.2. Instrumentation

The air oxidation of PDVB was performed in a small bench-top furnace (Model 1400, Barnstead Thermolyne, Dubuque, IA), and the carbonization took place in a high temperature furnace (Lindberg/Blue M, Thermo Electron, Waltham, MA, temperature ramp set at 1 °C/min) that was purged with nitrogen gas. An FEI XL30 SFEG scanning electron microscope (SEM) with spot size of 3 was used for surface/materials imaging. Samples for SEM were prepared from suspensions of particles placed on aluminum SEM stubs.

Brunauer-Emmett-Teller (BET) nitrogen adsorption data were obtained using a TriStar II surface area analyzer (Micromeritics Instrument, Norcross, GA) to measure the surface areas and pore sizes of the particles. Prior to data collection, samples were degassed at 200 °C for 12 h and the surface areas were measured by N_2 adsorption at 77 K.

Fourier transform infrared spectroscopy coupled with an attenuated total reflectance accessory (FTIR-ATR) was performed with a single bounce 'Smart Orbit' diamond crystal plate accessory in a Nicolet 6700 instrument (Thermo Fisher Scientific). This apparatus probed the air oxidation of PDVB from 25 °C to 250 °C and the carbonization of PDVB from 300 °C to 900 °C. An FTIR instrument (Nicolet iS50 FTIR, Thermo Fisher Scientific, Waltham, MA) coupled with a single bounce 'Smart iTR' germanium crystal plate was used to measure the carbonized PDVB before and after nitric acid-treatment at the Olympia, WA site of Thermo Fisher Scientific.

X-ray photoelectron spectroscopy (XPS) was performed with an SSX-100 photoelectron spectrometer (serviced by Service Physics, Bend, OR) using Al K-alpha X-rays and a hemispherical analyzer. An electron flood gun was used for charge compensation. Samples were prepared by placing a small amount of a slurry of particles on a shard of silicon that was heated to

ca. 60 °C on a hot plate to remove the solvent. Samples were sent to ALS Environmental (Tucson, AZ) for elemental analysis.

An ION-TOF IV ToF-SIMS instrument (ION-TOF, Münster, Germany) probed the samples with a 25 keV Ga^+ source over a 150 x 150 μm^2 area. An electron flood gun was used for charge compensation. Each sample was measured at two spots in both positive and negative polarity. A principle components analysis (PCA) of the negative ion mode ToF-SIMS data was performed using the PLS_Toolbox 4.2 (Eigenvector Research, Wenatchee, WA) in MATLAB. The spectral data (integrated peak regions) were organized row-wise in a matrix, and then normalized and autoscaled. Normalization is a row operation performed on the data from an individual spectrum, i.e., each spectral region was divided by the sum of the peak areas for that spectrum. Autoscaling consists of subtracting the mean of the values in each column from each value in the column (mean centering), and then dividing each mean centered value in the column by the standard deviation of the numbers in that column.

A PANalytical X'Pert Pro diffractometer with a Cu X-ray source and an X'Celerator detector was used to obtain X-ray diffraction (XRD) data. The samples were scanned from 4 - 100° 2θ using a step size of 0.017° 2θ at a rate of 0.01°/s (200 s total exposure time per step). Automatic slits were used to keep an 8 mm beam footprint on the thin layer (0.1 mm) of each sample to improve the intensity of the signals. The PANalytical Highscore Plus software was then used to correct the data for the increasing number of photons allowed by the automatic slits at higher angles, making the peak height ratios more directly comparable to those in other studies.

Raman microscopy with a 100x objective and 50 μm confocal pinhole was performed with a 532 nm laser at the Seattle, WA site of Thermo Fisher Scientific using a DXR Raman microscope

spectrometer. At least two spots per sample were analyzed, and the laser power at the sample was 0.5 – 1 mW. A full range grating was used in the measurement.

Thermogravimetric analyses (TGA) for differently treated PDVB samples were performed using a Netzsch STA 409 PC instrument. For these experiments, ca. 20 mg of the PDVB samples were heated in an alumina crucible in an inert gas (He) at a rate of 5 °C/min from room temperature to 1200 °C. Baseline corrections were performed using the empty alumina crucibles.

3.3.3. Air Oxidation, Carbonization, and Acid-Oxidation of Poly(divinylbenzene) (PDVB)

Following the reports of Li et al.[28] and Winslow et al.[32], commercially obtained 5 μm PDVB particles (Sepax Technologies, Newark, DE) were oxidized by heating in the air from room temperature up to 250 °C at a rate of ca. 20 °C /min. The particles were then held at the target temperature (50 - 250 °C) for 6 h. The PDVB that had been air oxidized at 250 °C was then carbonized by inserting the particles in the furnace, quickly raising its temperature to 250 °C, and then slowing increasing the temperature at 1 °C /min to a target temperature between 300 and 900 °C.[12, 29-30] The particles were then held at the target temperature for 6 h. After carbonization, the particles were acid-treated with nitric acid to oxidize the surfaces (see refs.[31] and [17]). The acid treatment process was performed with a ca. 3 wt. % solution of the particles in a HNO_3 solution (68 – 70 %) at 60 °C for 24 h.[1] After the acid-treatments, the solutions were diluted with Millipore water and filtered through a 0.22 μm nitrocellulose membrane (Sigma-Aldrich). The resulting oxidized particles were then vacuum dried overnight.

3.4. Results and Discussion

3.4.1. SEM of PDVB Microspheres

Commercially obtained, 5 μm, PDVB particles have a uniform particle size distribution (PSD), which makes them appropriate candidates for an HPLC application because particle homogeneity contributes to uniform packing and improved performance in HPLC.[33] SEM was used to monitor the particles in their as-received form, and after their thermal and chemical treatments. Figure 3.1a shows the SEM of an as-received PDVB microsphere. For these SEM measurements, at least fifty particles were individually imaged and their diameters were measured and averaged. Errors here are the standard deviations of these measurements. In their as-received state, the particles were very uniform: 4.88 ± 0.09 μm (see Figure 3.1, panels a and d). After air oxidation at 250 °C, the particle diameter decreases by ca. 0.4 μm to 4.44 ± 0.08 μm (see Figure 3.1, panels b and d). Winslow et al. similarly observed volume shrinkage after the air oxidation of their divinylbenzene/ethylvinylbenzene copolymer.[32] Somewhat unexpectedly, Li and coworkers report *no* decrease in particle size in a similar process.[28] However, they worked with particles that had a broad size distribution, so any change in diameter may have been less obvious than for the particles we employed. After air oxidation, the PDVB particles were carbonized in the presence of

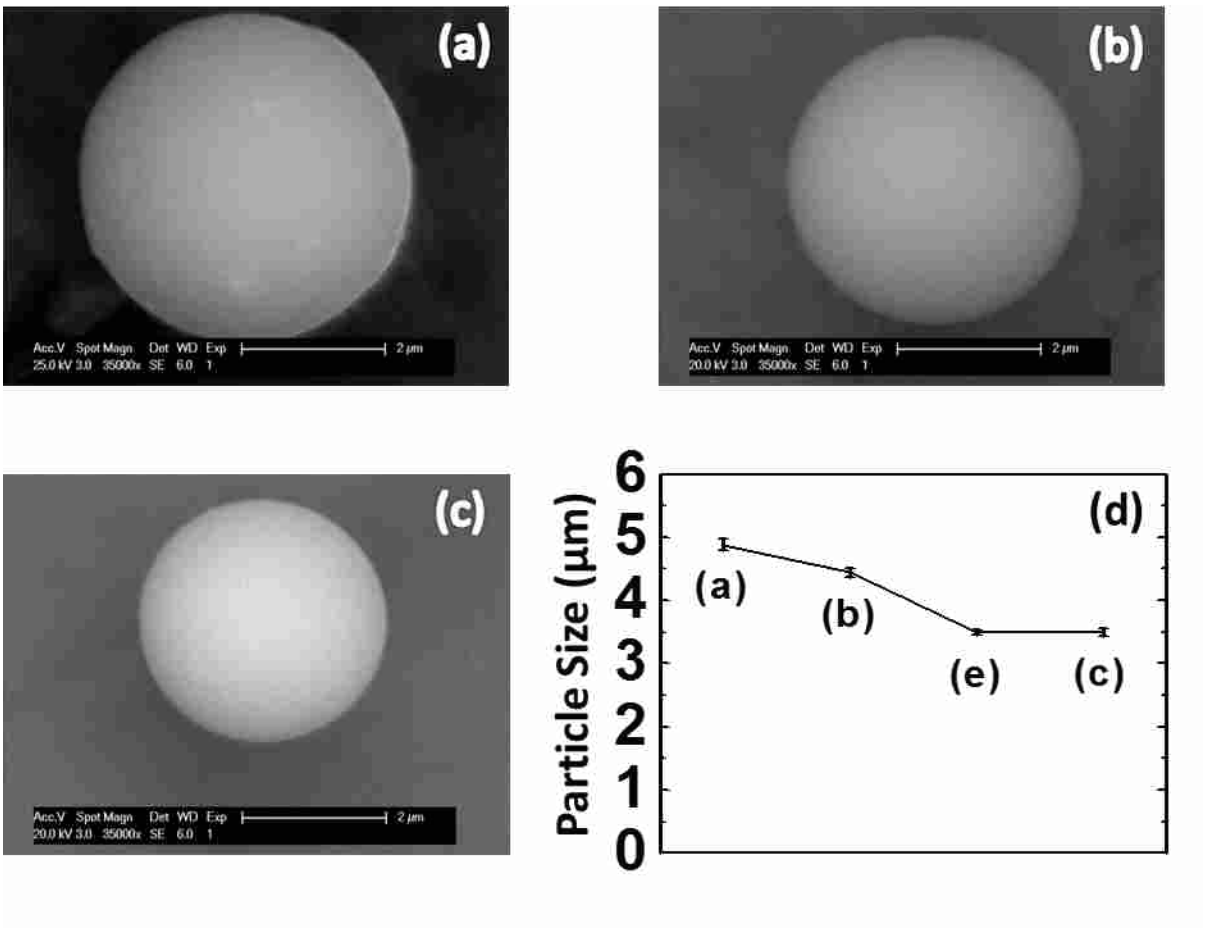

Figure 3.1 SEM images of (a) commercially obtained, as-received, PDVB microspheres, (b) PDVB microspheres that were air oxidized at 250 °C, and (c) air oxidized (at 250 °C), carbonized (at 900 °C), acid treated PDVB microspheres. (d) Average particle diameters of PDVB particles before and after various treatments. The labels (a) – (c) correspond to the particles represented in the panels of this figure. Label (e) corresponds to measurements of air oxidized (at 250 °C), carbonized (at 900 °C) PDVB microspheres. Error bars, which are standard deviations, are given in the text.

an inert atmosphere. SEM after this process showed them to be essentially perfect spheres, like those in Figure 3.1 and panels b and c (see also Figure 3.2). As expected, upon carbonization the particle size decreased further to 3.50 ± 0.04 μm (see Figure 3.1d). This decrease is resonable as more C-C bonds are formed during the process and hydrogen is lost.[32] These carbonized PDVB particles were then treated with nitric acid to oxidize their surfaces. After acid treatment, the particle size (3.50 ± 0.06 μm) was similar to that of the carbonized PDVB particles (see Figure 3.1, panels c and d). In summary, Figure 3.1 and its accompanying analysis show that the particles remain highly spherical for all steps in the process, with no loss of uniformity, i.e., percent relative standard deviations of 1.8%, 1.8%, 1.1%, and 1.7%, respectively.

3.4.2. BET

The surface area (m^2/g), pore volume (cm^3/g), and pore size (nm) of the PDVB particles before and after each treatment are given in Table 3.1. The as-received and air oxidized (at 250 °C) particles show reasonably similar surface areas, pore volumes, and pore sizes. These surface areas are quite low and not far from the theoretical surface area for the particles (1.91 m^2/g), which was calculated using a density of PDVB nanoparticles (1.18 g/cm^3) reported by Ethirajan et al.[34] However, after carbonization at 900 °C, the surface area and pore volume of the particles increased dramatically, indicating that the particles had become quite porous.[9, 32] Nitric acid treatment did not substantially change the properties of these particles.

Figure 3.2 SEM image of carbonized PDVB.

Table 3.1 BET surface area measurements of as-received PDVB, PDVB air oxidized at 250 °C, PDVB air oxidized at 250 °C and then carbonized at 900 °C, and PDVB air oxidized at 250 °C, carbonized at 900 °C, and then treated with nitric acid. The errors (standard deviations) on the as-received PDVB and also on the nitric acid treated particles correspond to three measurements performed on the same batch of particles. The measurements following air oxidation and carbonization were performed on at least three different batches of particles.

BET Samples	Surface area (m^2/g)	Pore volume (cm^3/g) (< 485 Å)	Pore size (nm)
As received PDVB	1.60 ± 0.35[a]	0.002 ± 0.001	6.62 ± 0.32[a]
PDVB air oxidized at 250 °C	2.6 ± 1.1	0.004 ± 0.002	6.42 ± 0.79
PDVB carbonized at 900 °C	445 ± 40[a]	0.217 ± 0.018	1.95 ± 0.01[a]
Nitric acid-treated, carbonized PDVB	495 ± 13	0.242 ± 0.006	1.95 ± 0.00

[a]The data were reported previously.[1]

3.4.3. FTIR

Fourier transform infrared spectroscopy (FTIR) proved to be a powerful technique for monitoring the functional groups on PDVB particles. Here, an attenuated total reflectance accessory (FTIR-ATR) provided a convenient way for direct sample analysis. Figure 3.3 shows the FTIR-ATR results for the air oxidation of PDVB microspheres at different temperatures. At 25 °C, the materials show sharp signals at ca. 710, 795, 833, 901, 1510, and 1600 cm^{-1} corresponding to various modes of the aromatic rings.[21, 35-37] The peaks at 987, 1015, 1410, and 1630 cm^{-1}, where all but the 987 cm^{-1} peak are fairly small, are due to residual vinyl groups in the material.[38-39] When the temperature was increased from 25 °C to 200 °C, bands attributable to the C=O (ca. 1729 cm^{-1}) and C-O (ca. 1270 cm^{-1}) stretches grow in, where the C=O stretch appeared at a lower temperature than the C-O stretch. At 250 °C, both of these bands were large and dominant in the corresponding spectrum. A peak at 758 cm^{-1} also grows in during this process, and the signal at 1600 cm^{-1} increases in intensity during heating. In general, the bands attributable to the aromatic rings and vinyl groups decrease in intensity. Thus, FTIR confirms the oxidation of PDVB and its chemical transformation to an oxidized material when it is heated to 250 °C.[28, 32] PDVB appears to enjoy good chemical stability to ca. 100 °C. Reasonable stability is suggested to 150 °C, although there is already evidence of oxidation at this temperature.

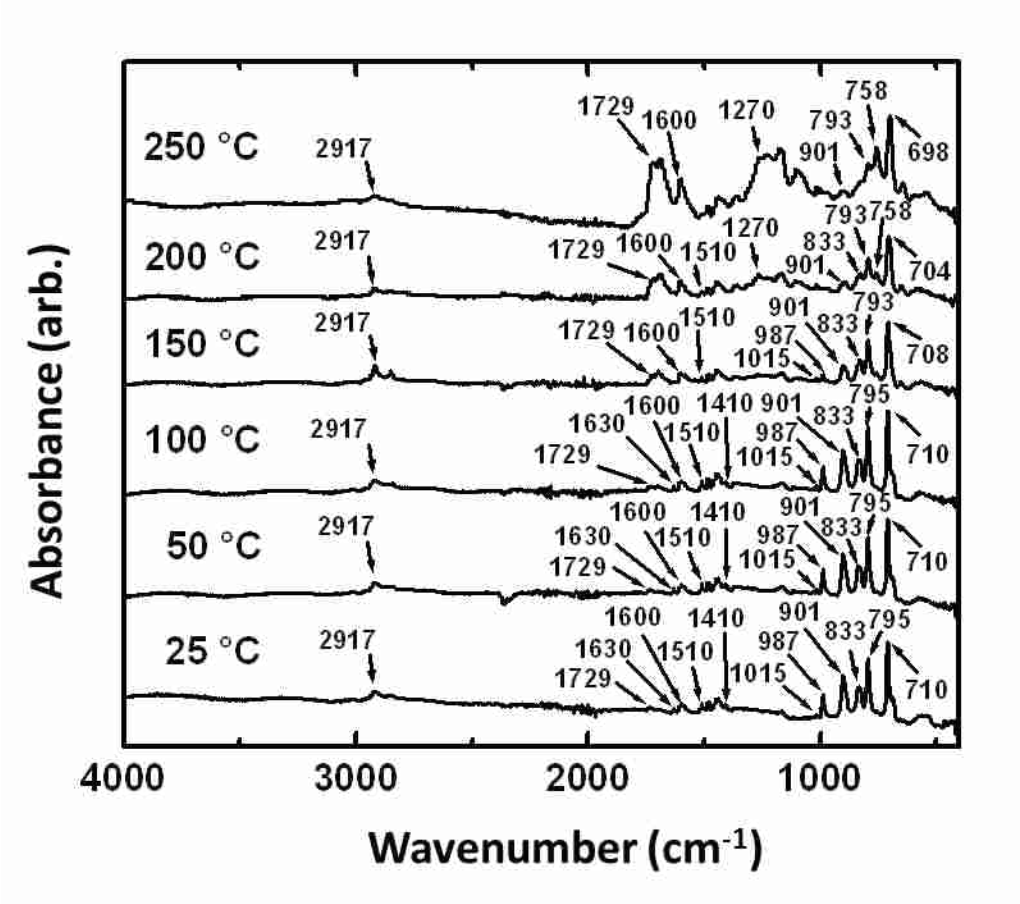

Figure 3.3 FTIR-ATR of PDVB after air oxidation at temperatures ranging from 25 – 250 °C. These spectra are not on the same scale.

Figure 3.4 shows FTIR-ATR spectra of PDVB that had first been air oxidized at 250 °C and then carbonized at 300 – 900 °C. At 300 °C, C=O (ca. 1729 cm^{-1}) and C-O-C (ca. 1270 cm^{-1}) stretches are present, but they have disappeared by 500 °C. At 700 °C, any FTIR signals attributable to molecular functional groups have disappeared, where these result are consistent with other reports of the carbonization of PDVB.[21, 32, 40] Also at 700 °C, and at 900 °C, the particles absorb strongly with decreasing photon energy, i.e., decreasing wavenumber.[16, 41] For this strongly absorbing carbon, the particles were also probed with an ATR accessory with a germanium crystal. The higher refractive index of Ge compared to diamond limits the penetration depth of the evanescent waves into the sampled material[41-42], i.e., ATR with a higher refractive index crystal is more surface sensitive. Figure 3.4 (inset) shows the FTIR-ATR spectra of PDVB particles carbonized at 900 °C before (a) and after (b) nitric acid treatment. Prior to this treatment, the spectrum (a) is featureless, which was the case for the 900°C material probed with the diamond crystal ATR accessory. However, after acid treatment (b), bands appear that suggest oxidation of the material vis-à-vis an O-H band (ca. 3250 cm^{-1}), a C=O band (ca. 1700 cm^{-1}), and a C-O-C band (ca. 1250 cm^{-1}). Interestingly, these signals do not show up when the same material is probed using a diamond crystal ATR accessory. This oxidation is consistent with other reports of nitric acid treated carbon materials.[14, 17] The introduction of the carbonyl group would clearly be advantages for the adhesion of the basic polymer (polyallylamine) in the layer-by-layer (LbL) process used to make our core-shell materials for HPLC.[1, 4-7]

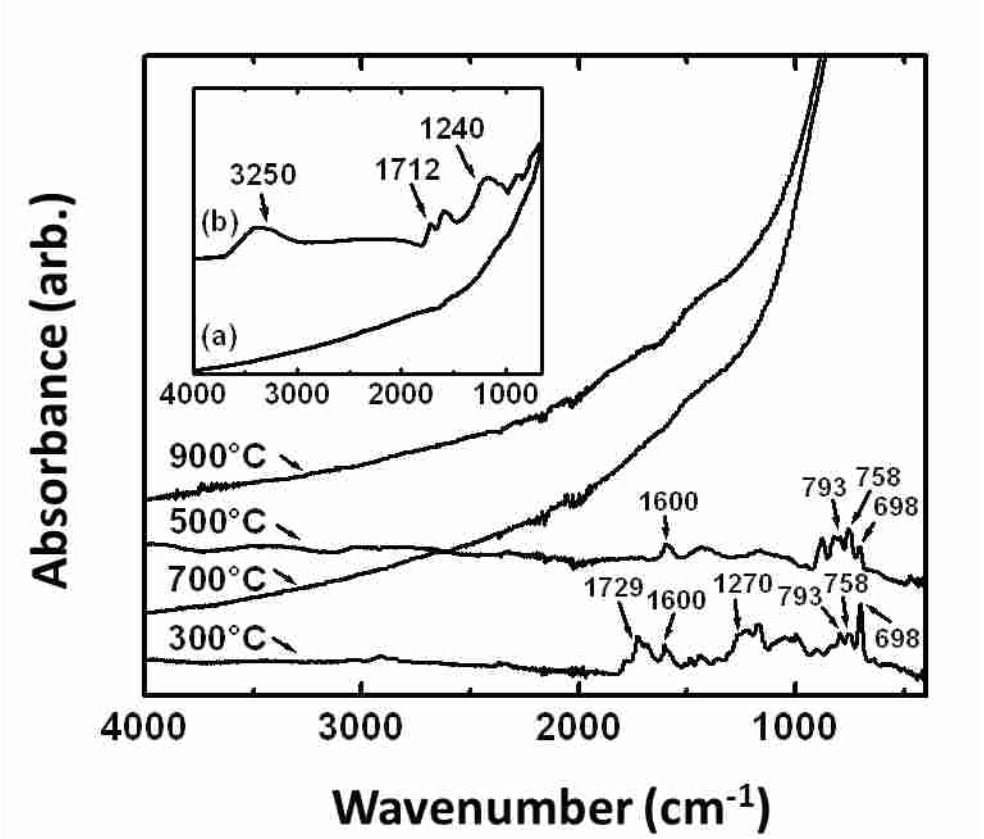

Figure 3.4 FTIR-ATR spectra of PDVB after air oxidation at 250 °C followed by carbonization at 300 – 900 °C. These spectra were taken with a single bounce ATR accessory with a diamond crystal. The spectra in the inset were taken with a single bounce ATR accessory that had a Ge crystal. Spectrum (a) is of the same 900 °C material used to obtain the '900°C' spectrum in the main figure. Spectrum (b) is of this '900°C' material after treatment with nitric acid.

3.4.4. XPS and Elemental Analysis

X-ray photoelectron spectroscopy (XPS) and elemental analysis were used to evaluate the elemental compositions of the PDVB microspheres before and after their various treatments (see Tables 3.2 and 3.3). These techniques probe the materials in different ways. XPS is sensitive to the upper ca. 10 nm of a material. In contrast, elemental analysis is a bulk technique. Before air oxidation, PDVB showed ca. 9% oxygen by XPS and ca. 1% by elemental analysis. Because XPS cannot detect hydrogen, the atomic percentage of oxygen in the materials by elemental analysis was also calculated without the contribution from hydrogen (see Table 3.3). These results indicate that the surfaces of the PDVB microspheres are considerably more oxidized than their interiors. Li and coworkers also observed some oxidized material on untreated PDVB microspheres.[28] After air oxidation at 250 °C, the oxygen content of the material increased in both analyses: to ca. 17% by XPS and ca. 14% by elemental analysis. These results suggest that the degree of oxidation of the particles has become nearly the same in their interiors and at their surfaces. Because BET did not suggest a significant increase in particle surface area (see Table 3.1), these results point to diffusion of oxygen into the particles and their subsequent oxidation, which appears to be nearly as efficient as the surface oxidation. After carbonization at 900 °C, XPS and elemental analysis show ca. 4 and 0.9 at. % oxygen on the particle surfaces and interiors, respectively. Because radical processes are expected at our carbonization temperatures, we speculate that the greater amount of oxygen in the near surface regions of the particles is due to fewer opportunities for radical-radical recombination.[9] After nitric acid treatment, the particles show more oxygen in their interiors than at their surfaces. We attribute this phenomenon to the very high surface area of the carbonized particles (see Table 3.1).[3] Somewhat surprisingly, XPS shows a fairly high degree of nitrogen (ca. 3%) in the as-received particles. The amount of surface nitrogen (by XPS) then decreases after air

Table 3.2 XPS of as-received PDVB microspheres, PDVB air oxidized at 250 °C, PDVB air oxidized at 250 °C and carbonized at 900 °C, and PDVB air oxidized at 250 °C, carbonized at 900 °C, and treated with nitric acid.

PDVB Microspheres	C 1s (at. %)	N 1s (at. %)	O 1s (at. %)
As-received	88.2 ± 2.3	3.1 ± 1.4	8.7 ± 0.9
Air Oxidized at 250 °C	82.2 ± 2.8	1.2 ± 0.2	16.6 ± 2.6
Carbonized at 900 °C	96.3 ± 1.4	0[a]	3.7 ± 1.4
Acid-treated after carbonization	85.5 ± 0.5	0.7 ± 1.0	13.8 ± 0.5

[a]No signal observable.

Table 3.3 Elemental analysis of as-received PDVB microspheres, PDVB air oxidized at 250 °C, PDVB air oxidized at 250 °C and carbonized at 900 °C, and PDVB air oxidized at 250 °C, carbonized at 900 °C, and treated with nitric acid. The first and second values in the ”Oxygen (at. %)” column are values for that element when hydrogen is either considered or not considered in the calculation, respectively.

PDVB Microspheres	Carbon (at. %)	Hydrogen (at. %)	Nitrogen (at. %)	Oxygen (at. %)
As-received	48.06 ± 0.43	51.36 ± 0.52	0.02 ± 0.02	0.58 ± 0.11/1.18 ± 0.21
Air Oxidized at 250 °C	49.30 ± 0.86	42.61 ± 2.45	0.05 ± 0.01	8.05 ± 1.61/13.96 ± 2.20
Carbonized at 900 °C	98.65 ± 0.05	<0.05[a]	0.50 ± 0.01	0.86 ± 0.04/0.86 ± 0.04
Acid-treated after carbonization	70.84 ± 2.72	11.80 ± 1.27	0.44 ± 0.00	16.93 ± 1.45/19.20 ± 1.92

[a]This result was obtained from both analyses performed on this material.

oxidation to ca. 1%, and none can be detected after carbonization (see Table 3.2). As expected, a small amount of nitrogen (less than 1%) is then found by XPS after the nitric acid treatment. Interestingly, these first three XPS results are anti-correlated to their elemental analysis results. That is, the as-received and air oxidized PDVB show almost no nitrogen by elemental analysis, which indicates that the nitrogen found by XPS is localized at the surfaces of the particles. The amount of nitrogen observed by elemental analysis then increases to ca. 0.5% after carbonization, which indicates that this nitrogen is found in the interiors of the particles and *not* at their surfaces. The amount of nitrogen in the particles then drops slightly after acid treatment, where both techniques show comparable levels of this element. These results underscore the importance of using material analysis methods that probe at different length scales.

3.4.5. ToF-SIMS Including Chemometrics (PCA and Cluster Analysis) of the Data

Time-of-flight secondary ion mass spectrometry (ToF-SIMS) is an important surface analytical tool that is complementary to XPS. Often the strengths of XPS, are the weaknesses of SIMS, and vice versa. For example, ToF-SIMS is much less quantitative than XPS but in general it provides more chemical information. ToF-SIMS cannot provide the direct, chemical state information about elements that XPS can through chemical shifts, but it is sensitive to hydrogen, which XPS cannot detect. Chemometrics tools have been widely applied to better understand SIMS spectra because the spectra (i) are often complex, and (ii) usually contain sets of peaks that are correlated because they are derived from the same sets of chemical species. Various chemometrics tools, including principle components analysis (PCA) and cluster analysis, have been widely used to analyze ToF-SIMS data.[43-49] PCA reduces the dimensionality of data sets so that the relationships between the spectra in it can be better understood/visualized. In PCA, one

'plots' each spectrum as a single point in a hyperspace, where the axes of this space correspond to the different peaks used in the analysis. In effect, these axes are then rotated to find a new axis that accounts for the greatest degree of variation in the data. This new axis is the first principle component (PC1). PC1 is then fixed while the remaining axes are rotated to find the axis that accounts for the second largest degree of variation in the data. This is the second principle component (PC2). This process is continued in multiple dimensions. The projections of the original data points (spectra) on the new axes (principle components, PCs) are their scores. The contributions of the old axes to the new axes are their loadings. Scores reveal the relationships between the original spectra (data points).

Figure 3.5 shows the results from a PCA analysis of the negative ion ToF-SIMS spectra of PDVB, PDVB air oxidized at 250 °C, PDVB air oxidized at 250 °C and then carbonized at 900 °C, and PDVB air oxidized at 250 °C, carbonized at 900 °C, and then treated with nitric acid. Nearly 90% of the variation in the data is captured by the first two principle components, where the bulk of this variation is captured by PC1: PC1 captures ca. 70% of the variation and PC2 ca. 19%. The scores plot in Figure 3.5a shows that the different spectra separate well along PC1 (notice the projections of the data points (spectra) along the x-axis in Figure 3.5a), and that the spectra of the as-received and carbonized PDVB materials separate quite well on PC2. The loadings plots in Figures 3.5b – c indicate the chemical basis for the separation between these spectra in the scores plot. The H^- and CH_2^- peaks show negative/lower loadings on both PC1 and PC2, which is consistent with both the chemistry of the PDVB starting material and its scores on PC1 and PC2, i.e., PDVB is rich in hydrogen and contains CH_2 groups between its monomer units, and the PDVB spectra show negative scores on both PC1 and PC2. The CH^- and CH_3^- ions show strongly negative loadings on PC1 and strongly positive loadings on PC2, which indicates that they come

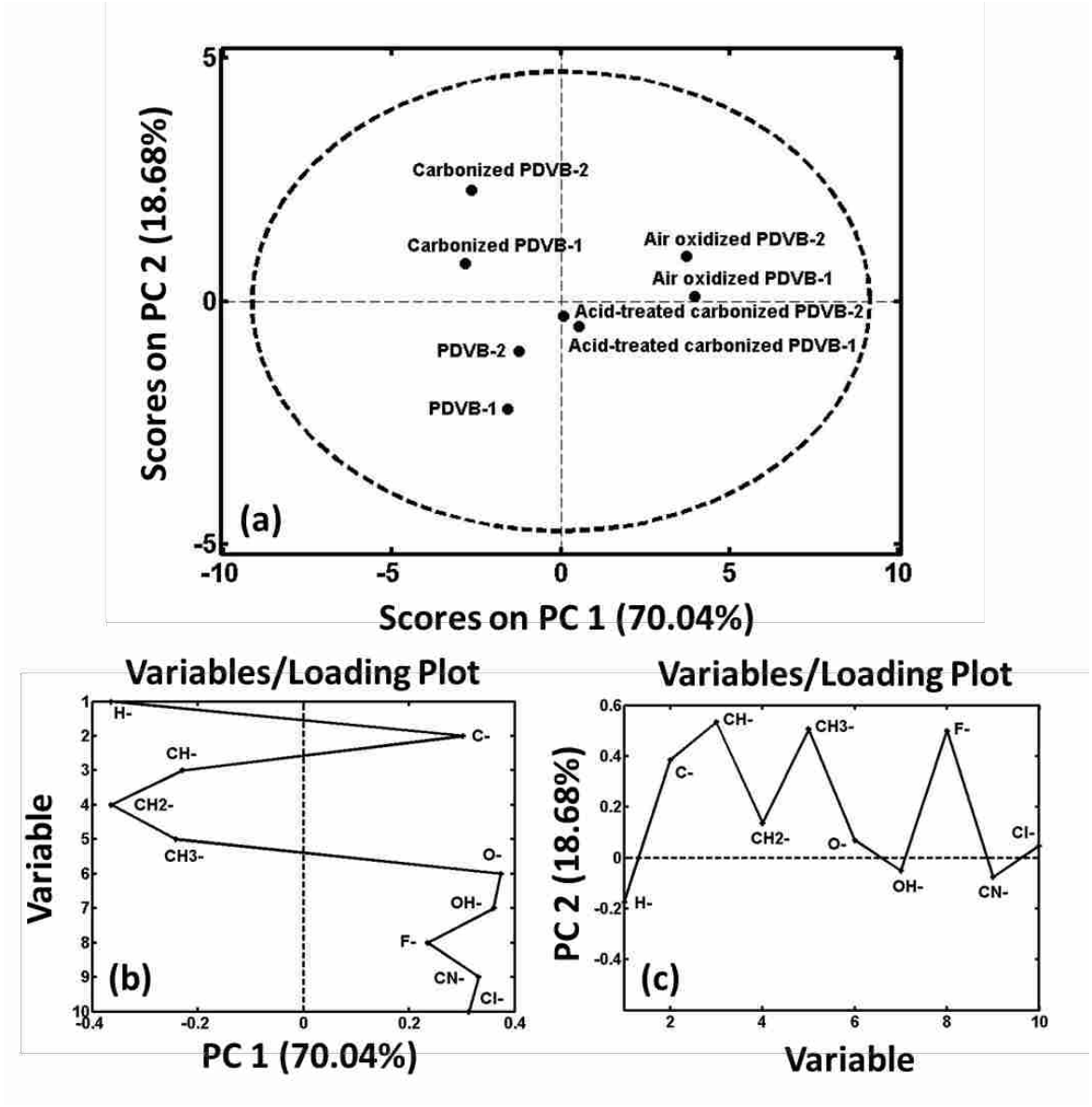

Figure 3.5 Principle components analysis of selected peak areas from the negative ion spectra of PDVB microspheres before and after various treatments. (a) Plot of the scores on PC1 and PC2. (b) Loadings on PC1. (c) Loadings on PC2.

preferentially from the carbonized PDVB samples (negative scores on PC1 and positive scores on PC2). The strongly positive loadings of the O^- and OH^- ions on PC1 are clearly consistent with the expected oxidized state of the acid treated and air oxidized materials, i.e., these spectra show scores that are substantially to the right (more positive) than those of the more reduced materials. ToF-SIMS is extremely sensitive to halogen contamination, and CN^- is readily formed in SIMS from nitrogen-containing organic materials.[44, 50-51] Accordingly, the presence of these signals does not necessarily imply that there is a large amount of F^-, Cl^-, or nitrogen in the samples they come from.

Another possible way of viewing these PCA results is to only consider PC1, which of course captures most of the variation in the spectra. If one proceeds in this way, one sees a set of peaks with negative loadings on PC1 that seem to be indicative of a more reduced material, and there is a set of peaks with positive loadings on PC1 that seem to point to a more oxidized material. The scores on PC1 from the different materials then follow their expected oxidation/reduction states: PDVB shows more negative scores on PC1 (is in a more reduced state), air oxidized PDVB shows more positive scores on PC1 (is in a more reduced state), the carbonized PDVB then shows more negative scores on PC1 (is in a more reduced state), and the acid-treated, carbonized PDVB shows more positive scores on PC1 (is in a more oxidized state). These results are in good agreement with the chemistries of these materials. Finally, a plot of the Hotelling T^2 vs. Q residuals was generated for this data. All of the spectra were within the expected 95% confidence limits (see Figure 3.6). A cluster analysis of this same data is also shown (see dendrogram in Figure 3.7). This analysis clusters replicate spectra while separating the spectra from different materials.

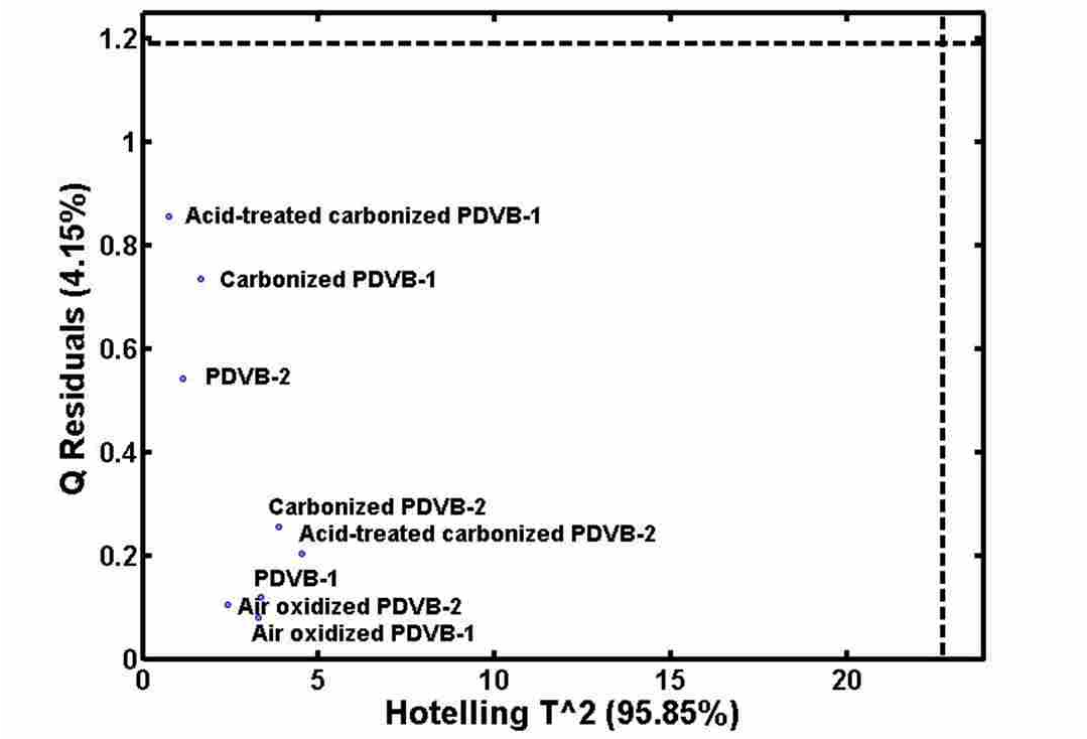

Figure 3.6 T^2 and Q residuals of scores plot of ToF-SIMS data.

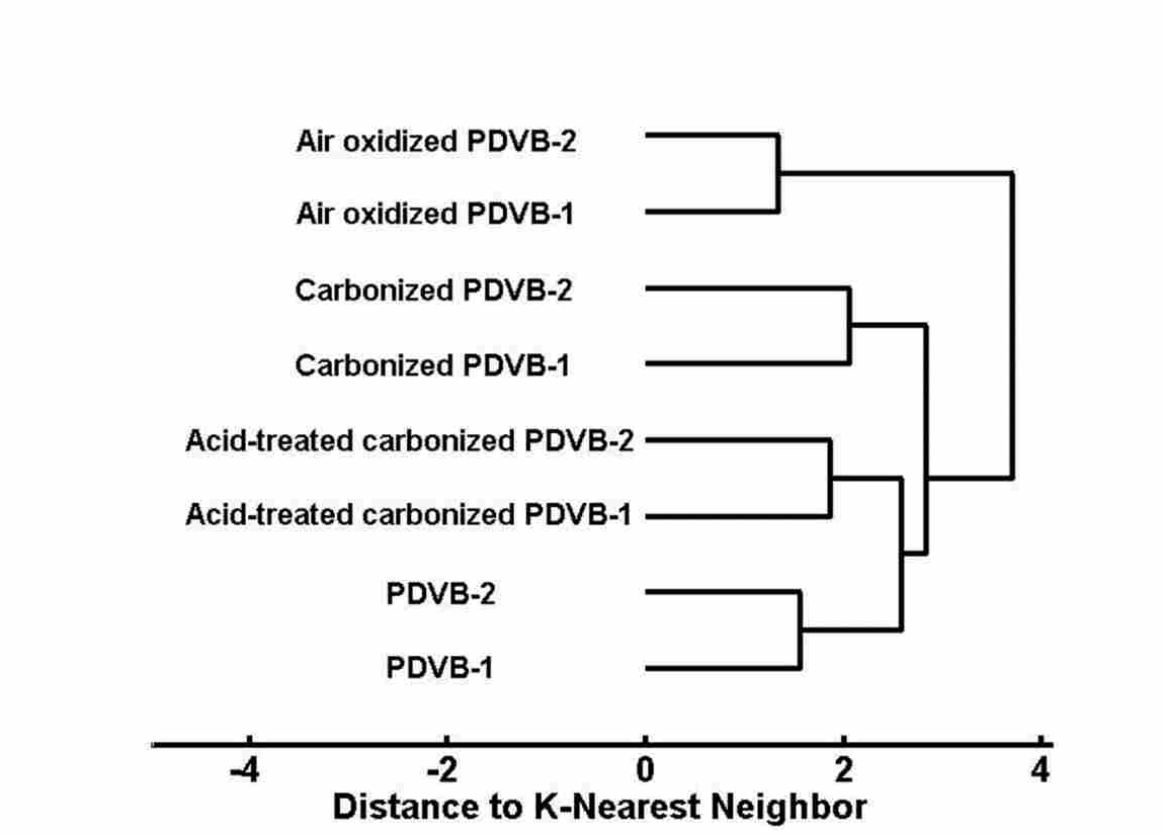

Figure 3.7 Cluster analysis of the same negative ion spectra used in the PCA analysis shown in Figure 3.5.

3.4.6. XRD and Raman

The PDVB, PDVB air oxidized at 250 °C, PDVB air oxidized at 250 °C and carbonized at 900 °C, and PDVB air oxidized at 250 °C, carbonized at 900 °C, and treated with nitric acid were probed by X-ray diffraction (XRD). Figure 3.8 shows the resulting XRD scans. The peaks are rather broad for all of the samples, indicating low crystallinity. As expected, the results for PDVB and air oxidized PDVB are quite similar (Figure 3.8a and b), both exhibiting a broad peak at ca. 18°, corresponding to a d-spacing of roughly 4.9 Å between disorderly graphene-like layers. These results are similar to those of Winslow et al.[32] who reported a d-spacing of 4.68 Å for PDVB. After carbonization, XRD suggests that some ordering towards the graphite structure has taken place in the material, though the carbon remains heavily disordered (see Figures 3.8c and d). The original broad peak at just under 20° shifts to a higher value, ca. 23° (a d-spacing of 3.9 Å compared to graphite's 3.4 Å), and a distinct broad peak at ca. 43° also appears, a single broad echo of the graphite peaks at 42° and 44°. For comparison, the diffraction pattern for graphite is shown at the bottom of the Figure (3.8e). Hasegawa and coworkers[21, 40] also observed the 23° and 43° broad peaks in their XRD patterns of carbonized PDVB, similarly noting that this indicates a turbostratic graphite structure wherein the stacking of the graphene layers are highly disordered.[52]

The samples were also probed by Raman spectroscopy. Raman and FTIR are complementary vibrational spectroscopies. Of the two, Raman is more suitable for identifying non-polar groups, such as C=C and C-C stretches. Figure 3.9 (a) shows the Raman spectrum of PDVB. Partouche and Margel[12] previously identified the peaks in their Raman spectrum of PDVB, and our material shows a similar pattern of signals. The most prominent signals in the spectrum are at 1000 and 1630 cm^{-1}, which correspond to the ring breathing mode and the C=C

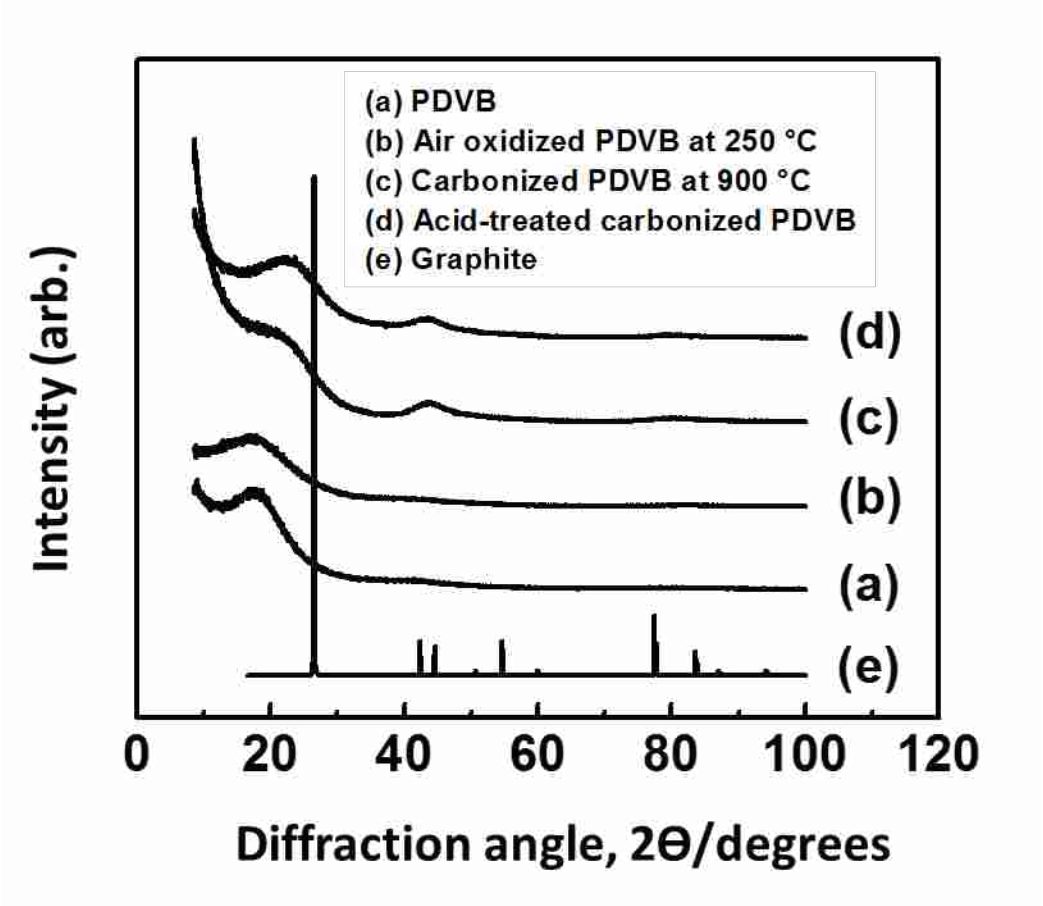

Figure 3.8 XRD data of (a) PDVB, (b) PDVB air oxidized at 250 °C, (c) PDVB air oxidized at 250 °C and carbonized at 900 °C, (d) PDVB air oxidized at 250 °C, carbonized at 900 °C, and treated with nitric acid, and (e) graphite.

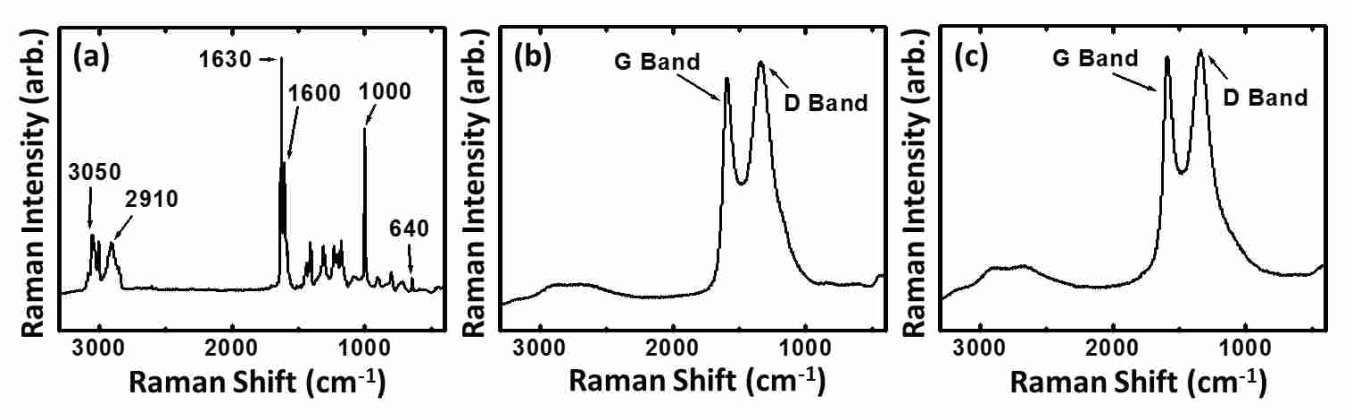

Figure 3.9 Raman data of (a) PDVB, (b) PDVB air oxidized at 250 °C and carbonized at 900 °C, and (c) PDVB air oxidized at 250 °C, carbonized at 900 °C, and treated with nitric acid.

vinyl mode, respectively. The bands between 2800 to 3100 cm^{-1} are C-H stretching modes, where the bands below 3000 cm^{-1} correspond to aliphatic stretches and the bands higher than 3000 cm^{-1} correlate to aromatic C-H stretches.[53] Figure 3.9 (b - c) shows the Raman spectra for carbonized (at 900 °C) and acid-treated, carbonized PDVB. While these spectra are radically different from the spectrum for the untreated PDVB, they are nearly identical to each other, suggesting that the carbonized PDVB only changes in a superficial way when it is acid treated. The D (disordered) and G (graphite) bands at ca. 1320 cm^{-1} and 1580 cm^{-1}, respectively, are identified in the spectra.[54-58] Consistent with the XRD analyses, these Raman spectra displaying both G and D bands suggest that the carbonized and acid-treated, carbonized PDVB samples consist of disordered graphite.[57-58]

3.4.7. TGA

Mass changes as a function of temperature for the differently treated PDVB microspheres were monitored by thermogravimetric analyses (TGA) under an inert gas (He). The most significant weight loss was observed for the as-received PDVB material (63% mass loss from 380 to 475 °C, Figure 3.10a). Air oxidized PDVB also underwent a weight loss in the same temperature range, but not to the same degree (38% mass loss from 380 to 475 °C, Figure 3.10b). Similar to the observation of Li et al.,[29] these data suggest that air oxidation of PDVB increases its thermal stability and allows a larger fraction of it to be carbonized. For PDVB microspheres air oxidized at 250 °C and carbonized at 900 °C (Figure 3.10c), TGA showed almost no mass loss up to ca. 600 °C, and a small decrease in mass at 700 °C (ca. 3 % mass loss). Between 700 and 900 °C, a ca. 15% mass loss was observed and there was ca. 5% mass loss between 900 to 1200 °C. For the materials represented in Figures 3.10b and 3.10c, the rate of mass loss is moderate after 900 °C. Accordingly, this seemed like a reasonable temperature for carbonization of the material. For

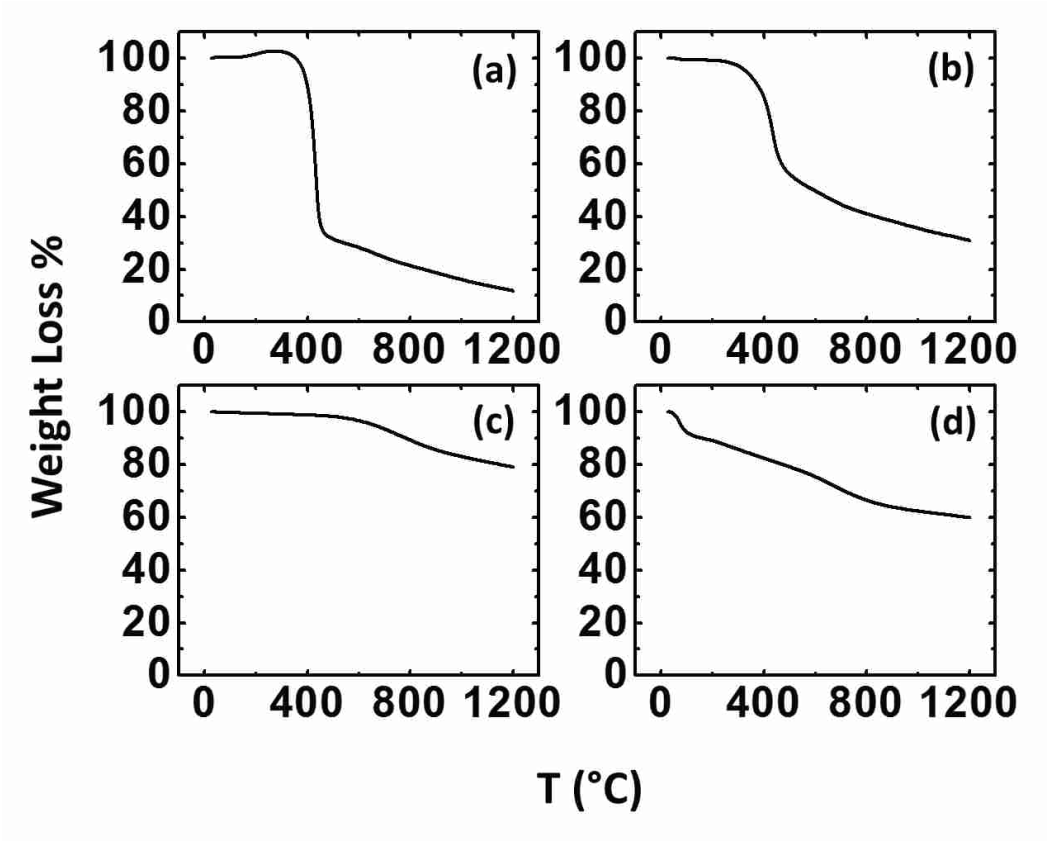

Figure 3.10 TGA of (a) PDVB, (b) PDVB air oxidized at 250 °C, (c) PDVB air oxidized at 250 °C, and carbonized at 900 °C, and (d) PDVB air oxidized at 250 °C, carbonized at 900 °C, and treated with nitric acid.

PDVB microspheres that were air oxidized at 250 °C, carbonized at 900 °C, and treated with nitric acid, significantly more mass is lost in the TGA process compared to the samples that were not acid treated (a ca. 40 % loss of mass took place from room temperature to 1200 °C, see Figure 3.10d). Thus, the acid treatment of the materials appears to destabilize them. Further studies of TGA coupled with mass spectrometry would be helpful to identify the gases evolved from these materials.

3.5. Conclusions

We report a comprehensive characterization of microspheres of PDVB, air oxidized PDVB, carbonized PDVB, and acid-treated carbonized PDVB using a series of analytical methods. Some of the key findings here are:

- By SEM, the particles decreased in size after air oxidation and did so to an even greater extent after carbonization. In all cases, the particles remained highly spherical.
- BET showed very low particle porosity initially and very high porosity after carbonization.
- FTIR showed that the surface functional groups change with temperature. The presence of oxygen-containing moieties clearly indicated material oxidation.
- In a complementary fashion, XPS and elemental analysis revealed the surface and bulk oxygen contents of the materials.
- PCA of the negative ion ToF-SIMS spectra grouped them according to the variables (ions) responsible for their chemical differences.
- XRD and Raman indicated that the carbonized PDVB particles were composed of disordered graphite.

- These data provide valuable information that facilitates the reasonable application of these particles in a chromatography column.
- TGA showed that the air oxidized PDVB is more thermally stability than the untreated PDVB, and that mass loss from acid treated, carbonized PDVB is greater than from the same material that was not treated with acid.

Acknowledgements

We acknowledge Diamond Analytics, a US Synthetic Company (Orem, UT, USA) for funding in this work. We also appreciate the ongoing support of the Department of Chemistry and Biochemistry and the College of Physical and Mathematical Sciences at Brigham Young University.

Conflict of Interest

Some of the authors of this work are employed at Diamond Analytics, which has commercialized HPLC columns based on carbonized PDVB particles. Some of the authors on this work from BYU will receive royalties from the sale of these columns.

3.6. References

1. Hung, C.-H.; Wiest, L. A.; Singh, B.; Diwan, A.; Valentim, M. J. C.; Christensen, J. M.; Davis, R. C.; Miles, A. J.; Jensen, D. S.; Vail, M. A.; Dadson, A. E.; Linford, M. R., *J. Sep. Sci.* **2013,** *36* (24), 3821-3829.

2. Jensen, D. S.; Gupta, V.; Olsen, R. E.; Miller, A. T.; Davis, R. C.; Ess, D. H.; Zhu, Z.; Vail, M. A.; Dadson, A. E.; Linford, M. R., *J. Chromatogr. A* **2011,** *1218* (46), 8362-8369.

3. Mahata, N.; Pereira, M. F. R.; Suárez-García, F.; Martínez-Alonso, A.; Tascón, J. M. D.; Figueiredo, J. L., *J. Colloid Interface Sci.* **2008,** *324* (1-2), 150-155.

4. Saini, G.; Jensen, D. S.; Wiest, L. A.; Vail, M. A.; Dadson, A.; Lee, M. L.; Shutthanandan, V.; Linford, M. R., *Anal. Chem.* **2010,** *82* (11), 4448-4456.

5. Saini, G.; Wiest, L. A.; Herbert, D.; Biggs, K. N.; Dadson, A.; Vail, M. A.; Linford, M. R., *J. Chromatogr. A* **2009,** *1216* (16), 3587-3593.

6. Saini, G.; Yang, L.; Lee, M. L.; Dadson, A.; Vail, M. A.; Linford, M. R., *Anal. Chem.* **2008,** *80* (16), 6253-6259.

7. Wiest, L. A.; Jensen, D. S.; Hung, C.-H.; Olsen, R. E.; Davis, R. C.; Vail, M. A.; Dadson, A. E.; Nesterenko, P. N.; Linford, M. R., *Anal. Chem.* **2011,** *83* (14), 5488-5501.

8. Benaddi, H.; Bandosz, T. J.; Jagiello, J.; Schwarz, J. A.; Rouzaud, J. N.; Legras, D.; Béguin, F., *Carbon* **2000,** *38*, 669-674.

9. Manocha, S. M., *Sādhanā* **2003,** *28* (1-2), 335-348.

10. Verheyen, V.; Rathbone, R.; Jagtoyen, M.; Derbyshire, F., *Carbon* **1995,** *33* (6), 763-772.

11. Malik, D. J.; Trochimczuk, A. W.; Ronka, S., *PLoS One* **2012,** *7* (8), e43354.

12. Partouche, E.; Margel, S., *Carbon* **2008,** *46* (5), 796-805.

13. Silva, A. M. T.; Machado, B. F.; Figueiredo, J. L.; Faria, J. L., *Carbon* **2009,** *47* (7), 1670-1679.

14. Bazuła, P. A.; Lu, A.-H.; Nitz, J.-J.; Schüth, F., *Microporous Mesoporous Mater.* **2008,** *108* (1-3), 266-275.

15. Figueiredo, J. L.; Pereira, M. F. R.; Freitas, M. M. A.; Órfão, J. J. M., *Carbon* **1999,** *37*, 1379-1389.

16. Figueiredo, J. L.; Pereira, M. F. R.; Freitas, M. M. A.; Órfão, J. J. M., *Ind. Eng. Chem. Res.* **2007,** *46* (12), 4110-4115.

17. El-Hendawy, A.-N. A., *Carbon* **2003,** *41* (4), 713-722.

18. Shen, W.; Li, Z.; Liu, Y., *Rec. Pat. Chem. Eng.* **2008,** *1*, 27-40.

19. Wan, Y.; Min, Y.-L.; Yu, S.-H., *Langmuir* **2008,** *24* (9), 5024-5028.

20. Domingo-García, M.; López Garzón, F. J.; Pérez-Mendoza, M. J., *J. Colloid Interface Sci.* **2002,** *248* (1), 116-122.

21. Hasegawa, J.; Kanamori, K.; Nakanishi, K.; Hanada, T., *C. R. Chim.* **2010,** *13* (1-2), 207-211.

22. Teutenberg, T.; Hollebekkers, K.; Wiese, S.; Boergers, A., *J. Sep. Sci.* **2009,** *32* (9), 1262-1274.

23. Wyndham, K. D.; O'Gara, J. E.; Walter, T. H.; Glose, K. H.; Lawrence, N. L.; Alden, B. A.; Izzo, G. S.; Hudalla, C. J.; Iraneta, P. C., *Anal. Chem.* **2003,** *75* (24), 6781-6788.

24. Teutenberg, T.; Tuerk, J.; Holzhauser, M.; Giegold, S., *J. Sep. Sci.* **2007,** *30*, 1101-1114.

25. West, C.; Elfakir, C.; Lafosse, M., *J. Chromatogr. A* **2010,** *1217*, 3201-3216.

26. Melmer, M.; Stangler, T.; Premstaller, A.; Lindner, W., *J. Chromatogr. A* **2010,** *1217*, 6092-6096.

27. Bai, F.; Yang, X.; Huang, W., *Macromolecules* **2004,** *37* (26), 9746-9752.

28. Li, K.; Stöver, H. D. H., *J. Polym. Sci. A Polym. Chem.* **1993,** *31* (13), 3257-3263.

29. Li, L.; Song, H.; Chen, X., *Mater. Lett.* **2007,** *62* (2), 179-182.

30. Hirano, S.; Dachille, F.; P. L. Walker, J., *High Temp.- High Pressures* **1973,** *5*, 207-220.

31. Hirano, S.-I.; Ozawa, M.; Naka, S., *J. Mater. Sci.* **1981,** *16*, 1989-1993.

32. Moreno-Castilla, C.; Ferro-García, M. A.; Joly, J. P.; Bautista-Toledo, I.; F.Carrasco-Marín; Rivera-Utrilla, J., *Langmuir* **1995,** *11* (11), 4386-4392.

33. Winslow, F. H.; Baker, W. O.; Pape, N. R.; Matreyek, W., *J. Polym. Sci. A Polym. Chem.* **1955,** *16* (82), 101-120.

34. Kirkland, J. J.; Destefano, J. J., *J. Chromatogr. A* **2006,** *1126*, 50-57.

35. Ethirajan, A.; Baeten, L.; Conradi, M.; Ranieri, K.; Conings, B.; Boyen, H.-G.; Junkers, T., *Polym. Chem.* **2013,** *4*, 4010-4016.

36. Chaiyasat, P.; Chaiyasat, A.; Boontung, W.; Promdsorn, S.; Thipsit, S., *Mater. Sci. Appl.* **2011,** *2* (8), 1007-1013.

37. Nanjundan, S.; Selvamalar, C. S. J.; Jayakumar, R., *Eur. Polym. J.* **2004,** *40* (10), 2313-2321.

38. Zhou, M. H.; Ha, C.-S.; Cho, W.-J., *J. Appl. Polym. Sci.* **2001,** *81* (5), 1277-1285.

39. Hubbard, K. L.; Finch, J. A.; Darling, G. D., *React. Funct. Polym.* **1999,** *42*, 279-289.

40. Karagoz, B.; Durmaz, Y. Y.; Gacal, B. N.; Bicak, N.; Yagci, Y., *Des. Monomers Polym.* **2009,** *12* (6), 511-522.

41. Hasegawa, G.; Kanamori, K.; Nakanish, K.; Hanada, T., *Carbon* **2010,** *48*, 1757-1766.

42. Do, T.-T.; Celina, M.; Fredericks, P. M., *Polym. Degradation Stab.* **2002,** *77* (3), 417-422.

43. Harrick, N. J., *Internal Reflection Spectroscopy*. Wiley-Interscience: New York, 1967; p 327.

44. Gupta, V.; Madaan, N.; Jensen, D. S.; Kunzler, S. C.; Linford, M. R., *Langmuir* **2013,** *29*, 3604-3609.

45. Yang, L.; Shirahata, N.; Saini, G.; Zhang, F.; Pei, L.; Asplund, M. C.; Kurth, D. G.; Ariga, K.; Sautter, K.; Nakanishi, T.; Smentkowski, V.; Linford, M. R., *Langmuir* **2009,** *25* (10), 5674-5683.

46. Brulet, M.; Seyer, A.; Edelman, A.; Brunelle, A.; Fritsch, J.; Ollero, M.; Laprévote, O., *J. Lipid Res.* **2010,** *51*, 3034-3045.

47. Kim, Y.-P.; Hong, M.-Y.; Kim, J.; Oh, E.; Shon, H. K.; Moon, D. W.; Kim, H.-S.; Lee, T. G., *Anal. Chem.* **2007,** *79* (4), 1377-1385.

48. Berman, E. S. F.; Kulp, K. S.; Knize, M. G.; Wu, L.; Nelson, E. J.; Nelson, D. O.; Wu, K. J., *Anal. Chem.* **2006,** *78*, 6497-6503.

49. Urquhart, A. J.; Taylor, M.; Anderson, D. G.; Langer, R.; Davies, M. C.; Alexander, M. R., *Anal. Chem.* **2008,** *80*, 135-142.

50. Yang, L.; Lua, Y.-Y.; Jiang, G.; Tyler, B. J.; Linford, M. R., *Anal. Chem.* **2005,** *77* (14), 4654-4661.

51. Saini, G.; Gates, R.; Asplund, M. C.; Blair, S.; Attavar, S.; Linford, M. R., *Lab Chip* **2009,** *9*, 1789-1796.

52. Zhang, F.; Sautter, K.; Larsen, A. M.; Findley, D. A.; Davis, R. C.; Samha, H.; Linford, M. R., *Langmuir* **2010,** *26* (18), 14648-14654.

53. Li, Z. Q.; Lu, C. J.; Xia, Z. P.; Zhou, Y.; Luo, Z., *Carbon* **2007,** *45* (8), 1686-1695.

54. Sears, W. M.; Hunt, J. L.; Stevens, J. R., *J. Chem. Phys.* **1981,** *75* (4), 1589-1602.

55. Wang, Y.; Alsmeyer, D. C.; McCreery, R. L., *Chem. Mater.* **1990,** *2*, 557-563.

56. Vidano, R. P.; Fischbach, D. B.; Willis, L. J.; Loehr, T. M., *Solid State Commun.* **1981,** *39* (2), 341-344.

57. Schwan, J.; Ulrich, S.; Batori, V.; Ehrhardt, H., *J. Appl. Phys.* **1996,** *80* (1).

58. Robertson, J., *Mat. Sci. Eng. R* **2002,** *37*, 129-281.

59. Sun, W. H.; Wang, S. T.; Zhang, J. C.; Chen, K. M.; Qin, G. G.; Tong, Y. Z.; Yang, Z. J.; Zhang, G. Y.; Pu, Y. M.; Zhang, Q. L.; Li, J.; Lin, J. Y.; Jiang, H. X., *J. Appl. Phys.* **2000,** *88* (10), 5662-5665.

Chapter 4: Separation of Cannabinoids on Three Different Mixed-Mode Columns Containing Carbon/Nanodiamond/Amine-Polymer Superficially Porous Particles*

4.1. Abstract

Three mixed-mode HPLC columns packed with superficially porous carbon/nanodiamond/amine-polymer particles were used to separate mixtures of cannabinoids. Columns evaluated included: (i) reversed phase (C18), weak anion exchange, 4.6 x 33 mm, 3.6 μm, and 4.6 x 100 mm, 3.6 μm, (ii) reversed phase, strong anion exchange (quaternary amine), 4.6 x 33 mm, 3.6 μm, and (iii) hydrophilic interaction liquid chromatography, 4.6 x 150 mm, 3.6 μm. Different selectivities were achieved under various mobile phase and stationary phase conditions. Efficiencies and peak capacities were as high as 54,000 N/m and 56, respectively. The reversed phase mixed-mode column (C18) retained tetrahydrocannabinolic acid strongly under acidic conditions and weakly under basic conditions. Tetrahydrocannabinolic acid was retained strongly on the reversed phase, strong anion exchange mixed-mode column under basic polar organic mobile phase conditions. The hydrophilic interaction liquid chromatography column retained polar cannabinoids better than the (more) neutral ones under basic conditions. A longer reversed phase (C18) mixed-mode column (4.6 x 100 mm) showed better resolution for analytes (and a contaminant) than a shorter column. Fast separations were achieved in less than five minutes and sometimes two minutes. A real world sample (bubble hash extract) was also analyzed by gradient elution.

*This chapter has been submitted to Journal of Separation Science and is under review.

4.2. Introduction

Cannabinoids are some of the most controversial and consumed illicit drugs in the world.[1-4] However, they are also reported to provide cancer patients relief from nausea and pain.[5] The main psychoactive compound in cannabinoids is delta 9-tetrahydrocannabinol (Δ^9-THC).[3, 6-7] It interacts with the human cannabinoid type-1 (CB1) and type-2 (CB2) receptors, which are the most abundant G proteins in the central nervous system that trigger psychoactive effects.[7] Concerns have also been raised about synthetic cannabinoids because of their stronger effects.[6-8]

The increased legalization of cannabis in the U.S. has raised concerns for driving safety.[9-10] However, the determination of cannabinoid levels in possibly stoned drivers is challenging.[10] Cannabinoids are lipophilic and are quickly absorbed into brain and fatty tissue, so that the analysis of blood (serum) samples may not reveal the amount of drug used.[3, 10-12] In addition, the metabolites of cannabinoids can be detected days or weeks after consumption, so using these metabolites to determine responsibility in traffic accidents may not be reasonable.[3, 10-11] Common techniques for cannabinoid detection include immunoassays, gas chromatography mass spectrometry (GC/MS), and liquid chromatography mass spectrometry (LC/MS).[1-4, 9, 13-15] Cannabinoids have also been separated by HPLC with electrochemical detection.[16] Immunoassays have the drawback of showing false positives that need to be verified using chromatographic techniques.[3] GC/MS analysis is time consuming because of sample preparation (derivatization) and it remains a challenge to detect both acidic and neutral cannabinoids.[1-2, 17] LC shows advantages over GC in detecting both neutral and acidic cannabinoids.[1-2]

Currently, mixed-mode HPLC columns have attracted much attention because they provide different selectivities for analytes that have both hydrophilic and hydrophobic properties. Mixed-mode columns are typically a combination of reversed phase chromatography, hydrophobic-

interaction chromatography (HIC), or hydrophilic-interaction chromatography (HILIC) with ion-exchange chromatography (IEC).[18] For cannabinoid analysis, an anionic mixed-mode column could be advantageous for separating anionic (acidic) cannabinoids from the neutral ones.

In our previous papers, we have reported carbon/nanodiamond/amine-polymer based superficially porous particles for HPLC.[19-22] Carbon/polymer based materials show significant stability at high pH and elevated temperatures.[23-24] For most silica-based HPLC columns, high pH and elevated temperature applications remain a challenge.[23, 25] In addition to their alkyl ligands, carbon/polymer based columns have amine groups in the stationary phase, which provide mixed-mode properties useful in the retention/separations of various analytes, including proteins.[26-30] The stationary phase can be either protonated (positively charged) at lower pH (pH < 10) to interact anionic (acidic) analytes or deprotonated (neutral) at higher pH (pH > 10) to retain neutral or basic analytes (see Figure 4.1).[28-30] However, unlike the protonation of an isolated, molecular amine, amines in a polymer may behave differently. This is because the protonation of an amine in a polymer may be affected by the protonation state or states of its neighbors. As pH decreases, the fraction of protonated amines in the polymer increases and the anionic interaction between the stationary phase and acidic analytes is also increased.

In this report, cannabinoids were analyzed using different types of mixed-mode HPLC columns packed with carbon/nanodiamond/amine-polymer-based superficially porous particles. The columns tested here showed unique selectivities for the separation of cannabinoids and include a shorter (4.6 x 33 mm) and longer (4.6 x 50 mm and 4.6 x 100 mm) versions of a reversed phase (C18) mixed-mode material, a reversed phase (C18+) mixed-mode column (4.6 x 33 mm) with

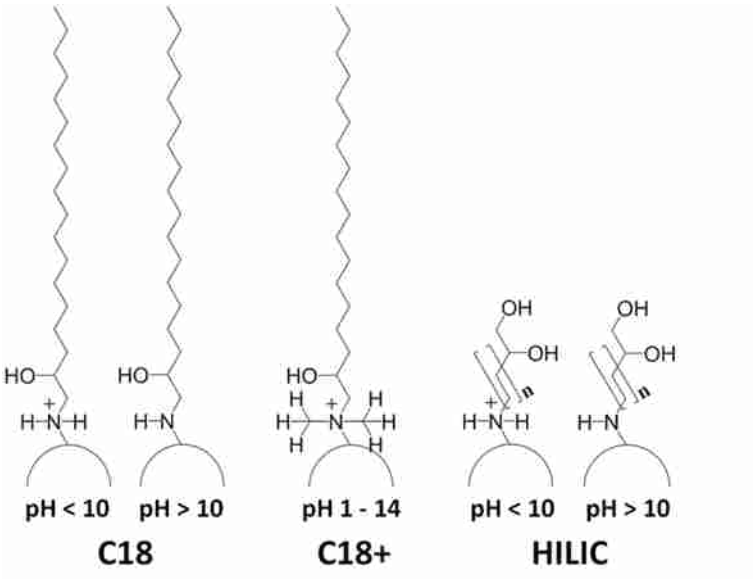

Figure 4.1 Mixed-mode bonded phases (C18, C18+, and HILIC) tested in this study.

permanently positively charged (quaternary) amines, and a hydrophilic interaction liquid chromatography (HILIC) mixed-mode column (4.6 x 150 mm) (see Figure 4.1). To the best of our knowledge, this is the first report of the use of a polar organic mobile phase (POMP) without water to retain polar cannabinoids, which was performed on the reversed phase (C18+) mixed-mode column. We also believe that this is also the first report of the separation of cannabinoids by HILIC. The mobile phase and elution methods were adjusted to properly elute the cannabinoids. The analytes tested in this study included delta 9-tetrahydrocannabinol (Δ^9-THC), cannabidiol (CBD), cannabinol (CBN), tetrahydrocannabinolic acid (THCA), and cannabidiolic acid (CBDA) (see Figure 4.2). A separation of cannabinoids in a real world (bubble hash) extract is also demonstrated in this study.

4.3. Experimental

4.3.1. Reagents

Acetonitrile (ACN) HPLC grade, methanol (MeOH) HPLC grade and methyl-tert-butyl ether were obtained from Fisher Scientific (Pittsburgh, PA). Formic acid (88+ %) and tetramethylammonium hydroxide (25 %, w/w in methanol) were obtained from Alfa Aesar (Ward Hill, MA). Ammonium hydroxide (28-30%) was obtained from Spectrum Chemical (New Brunswick, NJ). Purified water was obtained from a Milli-Q unit from Millipore (Billerica, MA). Cannabis analytes (ca. 1 mg/mL in ethanol) were obtained from Lipomed (Cambridge, MA) and diluted with methanol to make analyte mixtures. A sample of a high THC medical marijuana concentrate known as bubble hash was prepared for cannabinoid testing at Tested Labs (Falmouth, ME) using an ice water extraction technique. Tested Labs is a cannabis and medical marijuana testing lab for patients, caregivers and dispensaries (http://www.testedlabs.com). Details regarding

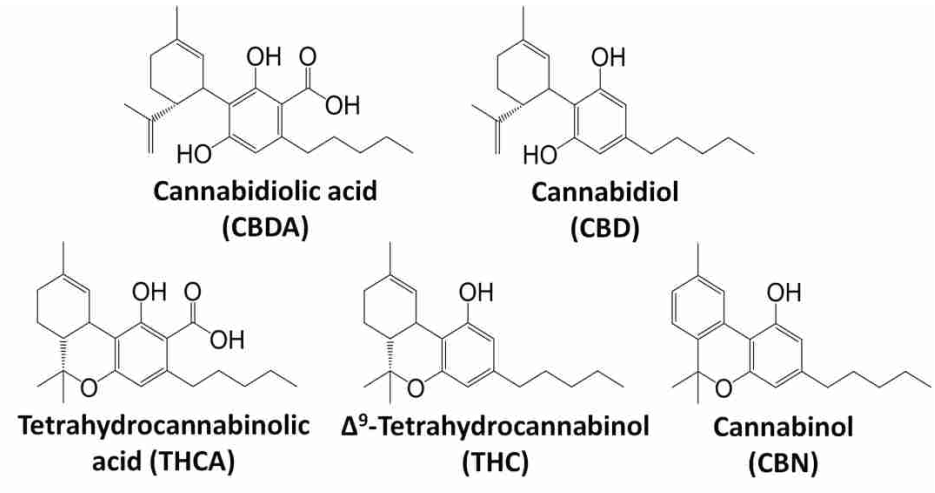

Figure 4.2 Chemical structures of cannabinoids tested in this study [1].

the ice water extraction technique can be found in the report of Jensen et al.[31] For HPLC, 50 mg of this sample with 20 mL of analytical grade ethyl alcohol was sonicated for 20 min in a 50 mL test tube. This "concentrate" sample was then centrifuged at 10000 rpm, and a particulate free aliquot of this extract was transferred by pipette to an autosampler vial for HPLC.

4.3.2. Instrumentation

Mixed-mode columns were manufactured by Diamond Analytics (Orem, Utah). The development of the materials for the reversed phase (C18) mixed-mode HPLC column has been reported.[19-21] The reversed phase (C18+) mixed-mode column (4.6 x 33 mm) was made by further reaction of the reversed phase (C18) material using an end-capping reagent that quaternized the amine groups in the amine-containing polymer. The hydrophilic interaction liquid chromatography (HILIC) mixed-mode HPLC column (4.6 x 33 mm) was prepared in the same manner as the reversed phase (C18) mixed-mode HPLC column, except that only the crosslinker was employed (no C18 ligands), and as a finishing step a small endcapper that contained a diol group was bound to the surface. An Agilent 1200 HPLC system (Agilent Technologies, Santa Clara, CA) equipped with a UV detector set at 230 nm was used for this study. An HP/Agilent 1050 HPLC system (Hewlett-Packard, Palo Alto, CA) equipped with a DAD detector set at 230 nm and an autosampler was used to analyze cannabinoids in the bubble hash or "concentrate" sample. This separation was performed at Tested Labs.

4.3.3. Method Development

The following parameters were adjusted and/or considered during mobile phase development to optimize the separations: temperature (from 30 – 65 °C), column length (4.6 mm x 33, 50, 100, and 150 mm), flow rate (1.0 – 1.5 mL/min), isocratic or gradient conditions, gradient time (4.5 – 16 min), and mobile phase compositions (noted in figure captions). Optimized separations are reported herein.

4.4. Results and Discussion

4.4.1. Separation on a Reversed Phase (C18) Mixed-Mode Column under Acidic Conditions

Figure 4.3A shows a fast gradient separation of a cannabinoid mixture containing acidic THCA and neutral CBD, THC, and CBN using a reversed phase (C18) mixed-mode column (see Figure 4.4 for zoomed in views of CBD, THC, and CBN in Figure 4.3A). For this and the other separations reported herein, please see the figure captions for peak capacities or efficiencies. The concentrations of the cannabinoids in this analyte mixture were adjusted to reflect those that would be expected from an extraction of marijuana. Formic acid was used as the pH modifier. At low pH (ca. pH 2.8, measured in solvent A), the stationary phase was mostly protonated (see Figure 4.1). Accordingly, the column retained the polar/acidic cannabinoid (THCA) better than the neutral ones (CBN, THC, and CBD). In an earlier study of k (retention factor) vs. pK_a on this column, a series of seven acidic herbicides showed an inverse, linear relationship between k and pK_a, i.e., retention increased as the compounds became more acidic.[30]

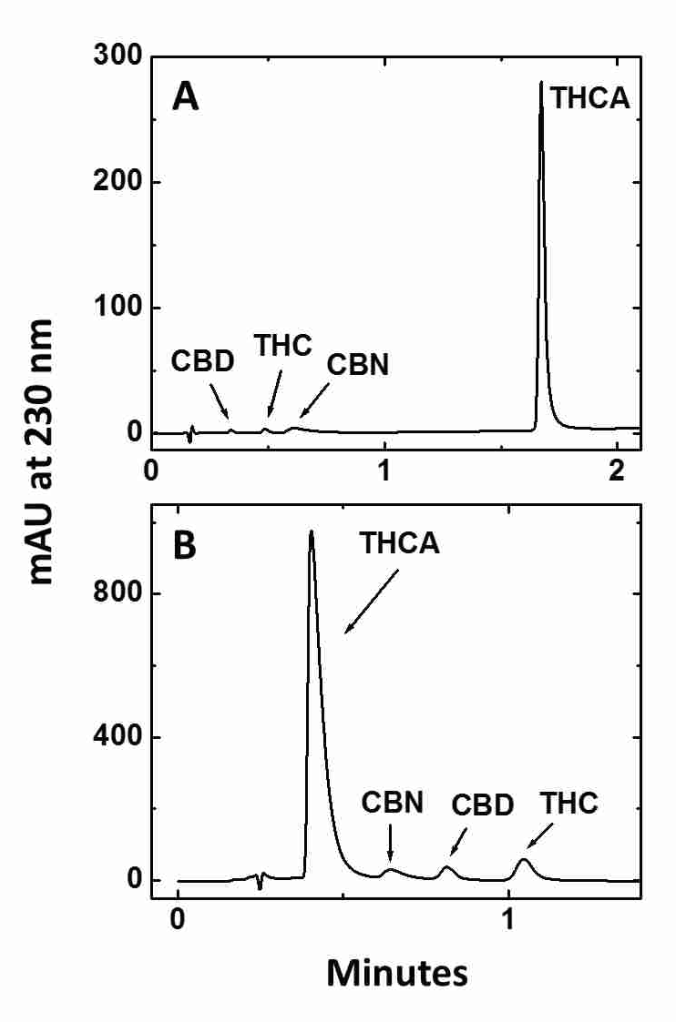

Figure 4.3 (A) Separation of CBD, THC, CBN, and THCA under acidic conditions with a reversed phase (C18) mixed-mode column (4.6 x 33 mm) at 65 °C with mobile phase: A: 40/60 (H_2O/MeOH) and B: 60/40 (MeOH/methyl tert-butyl ether). Two percent formic acid was added into solvents A and B. Gradient elution conditions: 0 min 90 % A, 1.5 min 10 % A, 1.51 min 90 % A and 4.5 min end. The flow rate was 1.5 mL/min and the injection volume was 1 µL. The peak capacity (gradient time divided by the average peak width) for this separation was 26. (B) Separation of THCA, CBN, CBD, and THC under basic conditions using a reversed phase (C18) mixed-mode column (4.6 x 33 mm) at 45 °C with solvents A: 95/5 (H_2O/ACN) and B: MeOH with 0.4 % $N(CH_3)_4^+OH^-$ (25 % in MeOH). The isocratic elution condition was 40/60 (A/B), the flow rate was 1.0 mL/min, and the injection volume was 1 µL. Retention factors, k, and efficiencies, N/m, for THCA, CBN, CBD, and THC in this separation are 1.50 and 13,600, 1.64 and 16,800, 2.33 and 41,500, and 3.27 and 48,950, respectively.

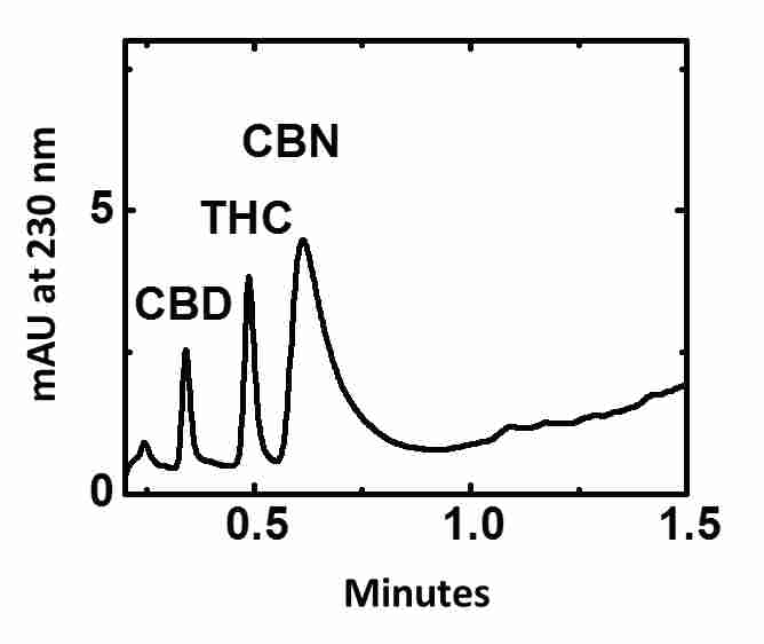

Figure 4.4 The chromatogram showed the details for the separation of CBD, THC, and CBN in Figure 4.3A.

4.4.2. Separation under Basic Conditions of Reversed Phase (C18) Mixed-Mode Column

The same analytes were further tested using the same column, but under basic conditions, where tetramethylammonium hydroxide was used as the pH modifier. A fast separation was again obtained. The pH of the mobile phase (ca. pH 11.4 for the A/B (40/60) mixture, see caption to Figure 4.3B) is above the pK_a for a protonated amine, i.e., the pK_as for the protonated forms of methyl amine, dimethyl amine, and trimethyl amine are 10.62, 10.64, and 9.76, respectively,[32] so we expect the column to exist in a substantially deprotonated (neutral) state at this pH (see Figure 4.1). Clearly one would expect the retention of an anionic species to decrease with increasing mobile phase pH on this column, i.e., with increasing pH there will be fewer protonated amines in the stationary phase. Figure 4.3B shows the isocratic separation of THCA, CBN, CBD, and THC at pH ca. 11.4 (see Figure 4.5 for zoomed in views of CBN, CBD, and THC in Figure 4.3B). As expected, the order of elution (selectivity) is substantially changed compared to the separation at low pH in Figure 4.3A. The more polar, acidic THCA, which will certainly be deprotonated, is retained less and elutes early. The neutral species that were less retained (CBN, CBD, and THC) at low pH now elute after THCA.

All of the cannabinoids considered in this study are phenolic in nature. The pK_a of phenol in water is 9.98.[33-34] Accordingly, one would expect (i) phenol in water to be substantially deprotonated at pH 11.4, and (ii) that in its deprotonated state, it would behave similarly to a deprotonated carboxyl group on the C18, mixed-mode column. However, the pK_as of anionic analytes in water are substantially different from the corresponding pK_as of the same analytes in water-organic mixtures. For example, Sarmini and Kenndler showed that the pKa of benzoic acid

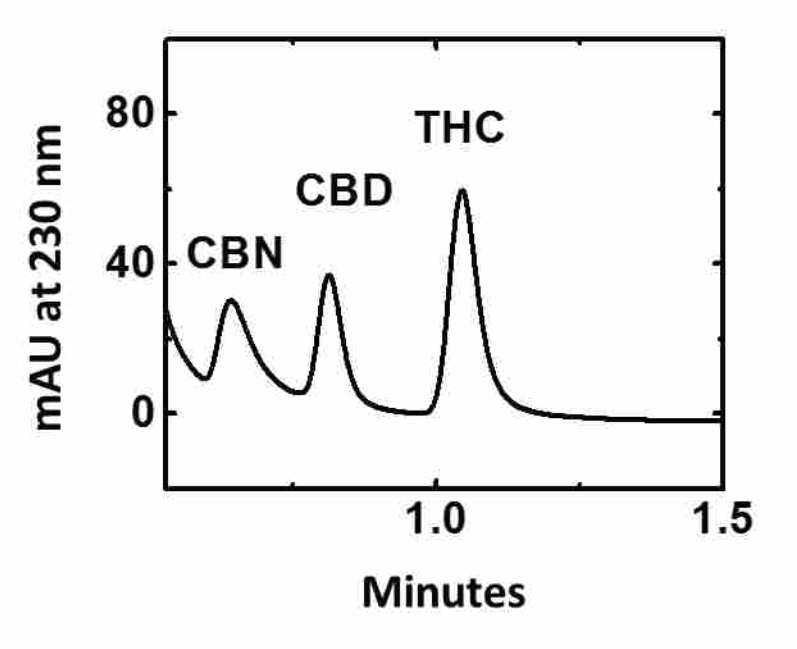

Figure 4.5 The chromatogram showed the details for the separation of CBN, CBD, and THC in Figure 4.3B.

changes by ca. two units with a change in solvent from 100:0 water/ethanol to 40/60 water/ethanol.[35] However, even a change of this magnitude would not alter the fact that THCA is deprotonated under the conditions corresponding to the separation in Figure 4.3B. Sarmini and Kenndler also showed that $\Delta G_a°$ (kJ/mol) for ionization of acetic acid, benzoic acid, and phenol in water and methanol change from 27.1 to 54.2, 24.0 to 53.0, and 56.9 to 82.0, respectively.[35] These results suggest that the pK_a values of the phenolic –OH groups in our analytes similarly increase in a substantial way as they are surrounded by a progressively more organic medium, and that a significant fraction of the phenolic –OH groups are protonated under the conditions of our elevated pH separation. Thus, the greater retention of CBN, CBD, and THC at pH ca. 11.4 is not unexpected. Finally, Sarmini and Kenndler showed that the pK_as of protonated amines in methanol are very similar to their values in water. Accordingly, it is expected that the pK_as of the amine groups in the stationary phase remain nearly unchanged in a water-organic mixture compared to water.[35] Thus, at ca. pH 11.4, the amines in the stationary phase should be in a mostly neutral (deprotonated) state, able to retain cannabinoids through hydrophobic interactions.[28-29]

4.4.3. Separation under Polar Organic Mobile Phase (POMP) of Reversed Phase (C18+) Mixed-Mode Column

The mixed-mode phases under discussion here contain (i) amines that can interact with anionic compounds through anion exchange, and (ii) C18 groups that can interact with analytes through hydrophobic (reversed phase) interactions. In addition, in the synthesis of the particles, the ring opening of epoxides yields hydroxyl groups (see Figure 4.1). Along with the amine groups in the column, these hydroxyl groups can hydrogen bond to the cannabinoids. These interactions can be enhanced by use of a polar organic mobile phase (POMP), which contains no aqueous

component. POMPs have previously been used for the enantiomeric separations of pharmaceuticals, where they have provided different selectivities for these separations.[36-38] In one example, a chiral stationary phase (CSPs) contained both hydrophobic and hydrogen bonding sites,[38] which is analogous to the functionality on the mixed-mode columns explored in this study. Acetonitrile is an effective POMP solvent, i.e., it is a polar aprotic organic solvent that promotes hydrogen bonding between a stationary phase and analytes. These interactions can be moderated by the addition of methanol to the mobile phase, which competes with analytes for hydrogen bonding sites on the stationary phase. POMPs often contain small amounts of acidic or basic modifiers.[36-38]

The cannabinoid mixture was tested with a POMP that contained a small amount of a basic modifier. For this separation, a reversed-phase (C18+) mixed-mode HPLC column was employed. This phase has permanently positively charged (quaternary) amines, so unlike the C18 mixed-mode column that has a protonation state that is affected by mobile phase pH, this column provides a uniform charge state that is unaffected by mobile phase pH or composition. THCA was retained longer than the other analytes in this separation, presumably because of ion pairing interactions between deprotonated THCA molecules and permanent positive charges on the column (see Figure 4.6A). The elution order of the cannabinoids in Figure 4.6A is similar to the order obtained under acidic conditions with the reversed phase (C18) mixed-mode phase (see Figure 4.3A). As a final note, one might expect CBD to also be rather well retained because of its two –OH groups. However, the presence of the single bond between the two rings in the molecule will allow the hexene ring in CBD to rotate with respect to the benzene ring in the molecule, which may sterically limit the interactions of the stationary phase with the –OH groups.

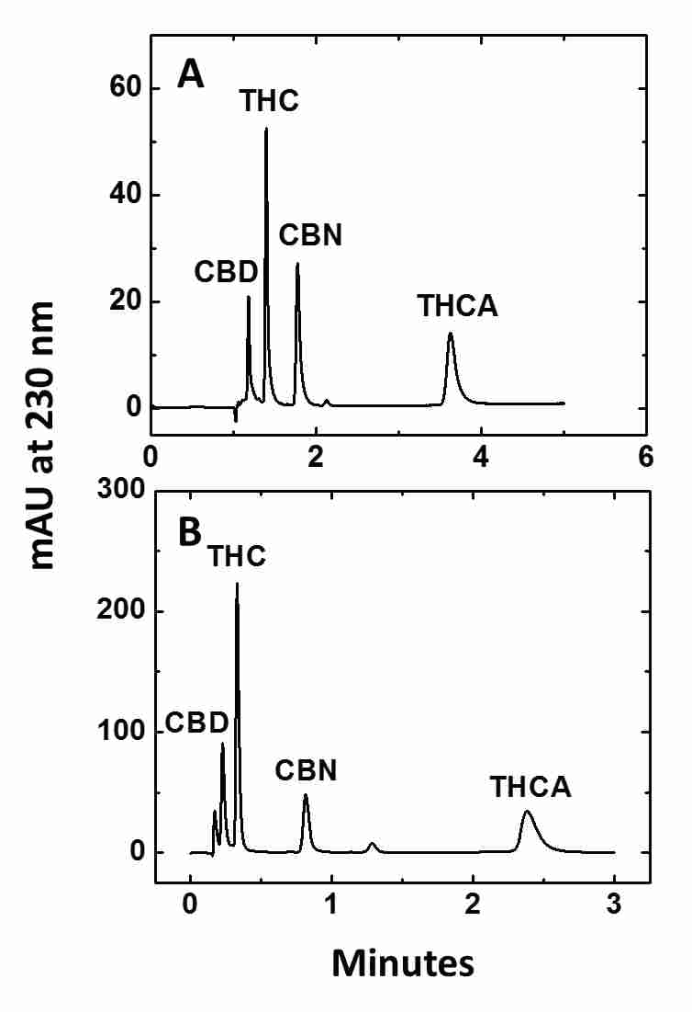

Figure 4.6 (A) Separation of CBD, THC, CBN, and THCA using a reversed phase (C18+) mixed-mode column (4.6 x 33 mm) at 35 °C with a polar organic mobile phase: 20/80 (ACN/MeOH) with 0.4 % $N(CH_3)_4^+OH^-$ (conc. 25 % in MeOH). Flow rate was 1.0 mL/min and injection volume was 1 µL. Retention factors, k, and efficiencies, N/m, for CBD, THC, CBN, and THCA in this separation are 0.16 and 16,700, 0.37 and 22,600, 0.74 and 24,000, and 2.55 and 25,000, respectively. (B) Separation of CBD, THC, CBN, and THCA using a HILIC mixed-mode column (4.6 x 150 mm) at 35 °C with solvent A: 10/90 (H_2O/ACN) with 0.5 % ammonium hydroxide (28-30%, pH 10.4) and B: ACN. Isocratic condition was 40/60 (A/B). Flow rate was 1.5 mL/min and injection volume was 1 µL. Retention factors, k, and efficiencies, N/m, for CBD, THC, CBN, and THCA in this separation are 0.31 and 8,200, 0.94 and 54,300, 3.72 and 25,800, and 12.75 and 48,000, respectively.

4.4.4. Separation under Basic Conditions of Hydrophilic-Interaction Chromatography (HILIC) Mixed-Mode Column

The analyte mixture was also tested using a hydrophilic-interaction chromatography (HILIC) mixed-mode column. This column was prepared by crosslinking the amine-containing polymer in the particles with a diepoxide (1,2,7,8-diepoxyoctane) and then endcapping it with a small molecule that imparted diols to the surface. No hydrophobic ligand, per se, was introduced onto the particles. Thus, this stationary phase has amines and hydroxyl groups that can retain polar analytes through hydrogen bonding, anion exchange, dipole-dipole interactions, etc. Ammonium hydroxide was used as the pH modifier. Figure 4.6B shows the HILIC separation of the cannabinoid test mixture under basic conditions. It is reasonable that the THCA would show the greatest retention. It is the most polar species in the test mixture and will certainly be deprotonated at the mobile phase pH. CBD again shows low retention, which, as noted above, may be related to steric hindrance from the cyclohexene ring blocking interactions between the stationary phase and the molecule's –OH groups.

4.4.5. Comparison of Shorter (4.6 x 33 mm) and Longer (4.6 x 100 mm) Reversed Phase (C18) Mixed-Mode Columns under Basic Conditions

An additional cannabinoid, cannabidiolic acid (CBDA), was added to the test mixture and a gradient elution was performed to separate the molecules at high pH (ca. pH 11.6, measured in

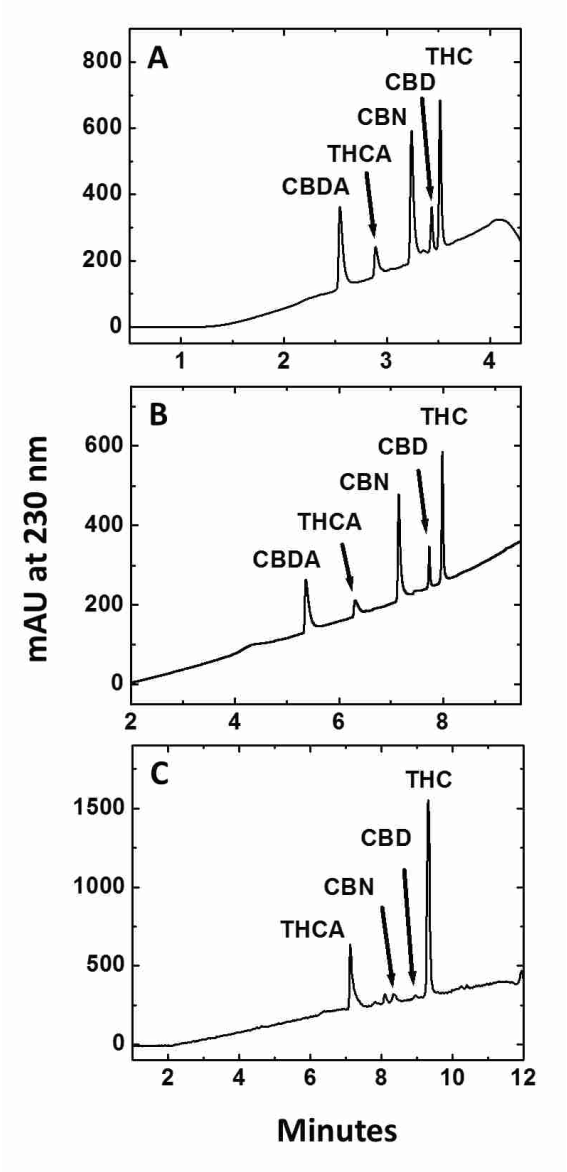

Figure 4.7 (A) Separation of CBDA, THCA, CBN, CBD and THC under basic condition using a reversed phase (C18) mixed-mode column (4.6 x 33 mm) at 30°C with solvents A: 95/2.5/2.5 (H_2O/MeOH/ACN) and B: 10/20/70 (H_2O/MeOH/ACN). 0.2 % $N(CH_3)_4^+OH^-$ (conc. 25 % in MeOH) was added to solvents A and B. Gradient elution conditions: 0 min 100 % A, 3 min 0 % A, 3.01 min 100 % A, and 8 min end. The flow rate was 1.0 mL/min, and the injection volume was 1 µL. The peak capacity (gradient time divided by the average peak width) for this separation was 55. (B) Separation of CBDA, THCA, CBN, CBD and THC under basic conditions using a longer reversed phase (C18) mixed-mode column (4.6 x 100 mm) at 35 °C with solvents A: 95/2.5/2.5 (H_2O/MeOH/ACN), and B: 10/20/70 (H_2O/MeOH/ACN). 0.2 % $N(CH_3)_4^+OH^-$ (conc. 25 % in MeOH) was added to solvent A and B. Gradient elution conditions: 0 min 100% A, 8min 0 % A, 8.01 min 100 % A, and 14 min end. The flow rate was 1.0 mL/min, and the injection volume was 1 µL. The peak capacity (gradient time divided by the average peak width) for this separation was 44. (C) Separation of bubble hash extract under basic conditions using a reversed phase (C18) mixed-mode column (4.6 x 50 mm) at 30 °C with solvents A: 95/2.5/2.5 (H_2O/MeOH/ACN) and B: 10/20/70 (H_2O/MeOH/ACN). 0.2 % $N(CH_3)_4^+OH^-$ (conc. 25 % in MeOH) was added to solvents A and B. Gradient elution conditions: 0 min 100 % A, 10 min 0 % A, 10.01 min 100 % A, and 16 min end. The flow rate was 1.0 mL/min, and the injection volume was 2 µL. The DAD detector was set at 230 nm. The peak capacity (gradient time divided by the average peak width) for this separation was 56.

solvent A) with a reversed phase (C18) mixed-mode column (4.6 x 33 mm). We note here that THC and THCA are the addition products of CBD and CBDA, respectively, with themselves, i.e., through the addition of an –OH group on the aromatic ring across the carbon-carbon double bond in the molecule. Figure 4.7A shows the baseline separation of this test mixture. The two acids, CBDA and THCA, which will be deprotonated, show the least retention. Interestingly, the intramolecular reactions that (at least in theory) could produce THCA from CBDA and THC from CBD result in more planar molecules that exhibit greater retention. In the previous reversed phase separation discussed herein (see Figure 4.3B), THC similarly showed greater retention than CBD. A longer reversed phase (C18) mixed-mode column (4.6 x 100 mm) was also evaluated. Under similar elution conditions, this longer column showed a better baseline separation of CBD and THC (see Figure 4.7B). An impurity peak between the CBN and CBD signals was also better resolved.

4.4.6. Separation of a Real World (Bubble Hash) Extract

A bubble hash extract was separated on a reversed phase (C18) mixed-mode column (4.6 x 50 mm) under gradient condition (see Figure 4.7C). The chromatogram showed peaks due to THCA, CBN, CBD, and THC, respectively, where the amounts of THCA and THC were higher compared to CBN and CBD. This separation demonstrated the analysis of a real cannabinoid sample using a mixed-mode HPLC column packed with superficially porous carbon/nanodiamond/amine-polymer particles.

4.5. Conclusions

Two cannabinoid test mixtures that contained THCA, CBN, CBD, THC, and in some cases CBDA were separated using various mixed-mode HPLC columns packed with carbon/nanodiamond/amine-polymer-based superficially porous particles. As expected, different selectivities were achieved by varying the mobile and stationary phase conditions. The reversed phase (C18) mixed-mode column showed strong retention of THCA under acidic conditions. However, under basic conditions on this column, THCA was weakly retained. Under basic, POMP conditions on the reversed phase (C18+) mixed-mode column, the THCA was also very strongly retained. HILIC again showed strong retention of the polar THCA compared to the (more) neutral cannabinoids under basic conditions. A longer reversed phase (C18) mixed-mode column (4.6 x 100 mm) showed better resolution for analytes and a contaminant than a shorter column. Separations on these mixed-mode columns are fast – generally under five minutes and sometimes under two minutes. A bubble hash extract was analyzed by gradient elution.

Acknowledgements

We acknowledge funding by Diamond Analytics, a US Synthetic Company, Orem, UT, USA. We also acknowledge the Department of Chemistry and Biochemistry at Brigham Young University for their support of this work.

Part of the column technology described herein has been licensed by Brigham Young University to Diamond Analytics. According to the licensing agreement, authors of this paper may receive royalties from sales of products that employ this technology.

4.6. References

1. Backer, B. D.; Debrus, B.; Lebrun, P.; Theunis, L.; Dubois, N.; Decock, L.; Verstraete, A.; Hubert, P.; Charlier, C., *J. Chromatogr. B* **2009,** *877*, 4115-4124.

2. Fernandez, M. d. M. R.; Boeck, G. D.; Wood, M.; Lopez-Rivadulla, M.; Samyn, N., *J. Chromatogr. B* **2008,** *875*, 465-470.

3. Sharma, P.; Murthy, P.; Bharath, M. M. S., *Iran. J. Psychiatry* **2012,** *7* (4), 149-156.

4. llias, Y.; Rudaz, S.; Mathieu, P.; Christen, P.; Veuthey, J.-L., *J. Sep. Sci.* **2005,** *28*, 2293-2300.

5. Romano, L. L.; Hazekamp, A., *Cannabinoids* **2013,** *1* (1), 1-11.

6. Patton, A. L.; Seely, K. A.; Chimalakonda, K. C.; Tran, J. P.; Trass, M.; Miranda, A.; Fantegrossi, W. E.; Kennedy, P. D.; Dobrowolski, P.; Radominska-Pandya, A.; McCain, K. R.; James, L. P.; Endres, G. W.; Moran, J. H., *Anal. Chem.* **2013,** *85*, 9390-9399.

7. Wohlfarth, A.; Scheidweiler, k. B.; Chen, X.; Liu, H.-f.; Huestis, M. A., *Anal. Chem.* **2013,** *85*, 3730-3738.

8. Akamatsu, S.; Mitsuhashi, T., *J. Sep. Sci.* **2014,** *37*, 304-307.

9. Espy, R. D.; Teunissen, S. F.; Manicke, N. E.; Ren, Y.; Ouyang, Z.; van Asten, A.; Cooks, R. G., *Anal. Chem.* **2014,** *86*, 7712-7718.

10. Swell, R. A.; Poling, J.; Sofuoglu, M., *Am. J. Addict.* **2009,** *18* (3), 185-193.

11. Bianchi, V.; Donzelli, G., *J. Chromatogr. B Biomed. Appl.* **1996,** *675*, 162-167.

12. Gustafson, R. A.; Moolchan, E. T.; Barnes, A.; Levine, B.; Huestis, M. A., *J. Chromatogr. B* **2003,** *798*, 145-154.

13. Masoud, A. N.; Wingard, D. W., *J. High. Resolut. Chromatogr.* **1979,** *2* (3), 118-122.

14. Saini, G.; Jensen, D. S.; Wiest, L. A.; Vail, M. A.; Dadson, A.; Lee, M. L.; Shutthanandan, V.; Linford, M. R., *Anal. Chem.* **2010,** *82* (11), 4448-4456.

15. Pedrouzo, M.; borrull, F.; Pocurull, E.; Marcé, R. M., *J. Sep. Sci.* **2011,** *34*, 1901-1101.

16. Masound, A. N.; Wingard, D. W., *J. Sep. Sci.* **1979,** *2* (3), 118-122.

17. de Jager, A. D.; Bailey, N. L., *J. Chromatogr. B* **2011,** *879*, 2642-2652.

18. Guo, H.; Li, X.; Frey, D. D., *J. Chromatogr. A* **2014,** *1323*, 57-65.

19. Hung, C.-H.; Wiest, L. A.; Singh, B.; Diwan, A.; Valentim, M. J. C.; Christensen, J. M.; Davis, R. C.; Miles, A. J.; Jensen, D. S.; Vail, M. A.; Dadson, A. E.; Linford, M. R., *J. Sep. Sci.* **2013,** *36* (24), 3821-3829.

20. Wiest, L. A.; Jensen, D. S.; Hung, C.-H.; Olsen, R. E.; Davis, R. C.; Vail, M. A.; Dadson, A. E.; Nesterenko, P. N.; Linford, M. R., *Anal. Chem.* **2011,** *83* (14), 5488-5501.

21. Saini, G.; Jensen, D. S.; Wiest, L. A.; Vail, M. A.; Dadson, A.; Lee, M. L.; V., S.; Linford, M. R., *Anal. Chem.* **2010,** *82* (11), 4448-4456.

22. Saini, G.; Yang, L.; Lee, M. L.; Dadson, A.; Vail, M. A.; Linford, M. R., *Anal. Chem.* **2008,** *80* (16), 6253-6259.

23. Kirkland, J. J.; Henderson, J. W.; DeStefanoa, J. J.; van Straten, M. A.; Claessens, H. A., *J. Chromatogr. A* **1997,** *762*, 97-112.

24. Peristyy, A. A.; Fedyanina, O. N.; Paull, B.; Nesterenko, P. N., *J. Chromatogr. A* **2014,** *1357*, 68-86.

25. Teutenberg, T.; Hollebekkers, K.; Wiese, S.; Boergers, A., *J. Sep. Sci.* **2009,** *32* (9), 1262-1274.

26. Bobály, B.; Guillarme, D.; Fekete, S., *J. Pharm. Biomed. Anal.* **2015,** *104*, 130-136.

27. Hung, C.-H.; Jensen, D. S.; Miles, A. J.; Zukowski, J.; Dadson, A. E.; Linford, M. R. *FLARE C18 Mixed-Mode Column: Separation of Apo-Transferrin and Bovine Serum Albumin (BSA) by LC-MS*; Application Note: DA1014-A; Diamond Analytics: Orem, Utah.

28. Hung, C.-H.; Davis, T. C.; Jensen, D. S.; Miles, A. J.; Zukowski, J.; Dadson, A. E.; Linford, M. R. *FLARE C18 MIxed-Mode Column: Alkaloids*; Application Note: DA1013-A; Diamond Analytics: Orem, Utah.

29. Hung, C.-H.; Davis, T. C.; Jensen, D. S.; Miles, A. J.; Zukowski, J.; Dadson, A. E.; Linford, M. R. *FLARE C18 Mixed-Mode Column: Tricyclic Antidepressants (TCAs)*; Application Note: DA1001-C; Diamond Analytics: Orem, Utah.

30. Singh, B.; Jensen, D. S.; Miles, A. J.; Dadson, A. E.; Linford, M. R. *Probing the Retention Mechanism of the Flare Mixed-Mode Column at Low pH via Acidic Herbicides with Different pK_a Values*; Application Note: DA1000-C; Diamond Analytics: Orem, Utah.

31. Jansen, M.; Terris, R., *J. Cannabis Ther.* **2002,** *2* (3/4), 133-141.

32. Hall Jr., H. K., *J. Am. Chem. Soc.* **1957,** *79* (20).

33. Liptak, M. D.; Gross, K. C.; Seybold, P. G.; Feldgus, S.; Shields, G. C., *J. Am. Chem. Soc.* **2001,** *124*, 6421-6427.

34. Gross, K. C.; Seybold, P. G., *Int. J. Quantum Chem.* **2001,** *85*, 569-579.

35. Sarmini, K.; Kenndler, E., *J. Biochem. Bioph. Methods* **1999,** *38*, 123-137.

36. Chang, S. C.; Reid III, G. L.; Chen, S.; Chang, C. D.; Armstrong, D. W., *Trends Anal. Chem.* **1993,** *12* (4), 144-153.

37. Zukowski, J., *Chirality* **1998,** *10*, 362-363.

38. Zukowski, J.; Pawlowska, M.; Armstrong, D. W., *J. Chromatogr.* **1992,** *623*, 33-41.

Chapter 5: Conclusions and Future Work

5.1. Conclusions

In my graduate work, I have improved the quality of the carbon cores for carbon/nanodiamond/amine-polymer-based core-shell materials.[1-2] This was done by synthesizing spherical, carbonized poly(divinylbenzene) (PDVB) microspheres.[1] Preliminary results obtained with the PDVB microspheres showed better particle size distributions and porosity than with our previous porous graphitic carbon (PGC) core materials. Even better results were obtained by using commercially available PDVB microspheres. The efficiencies of columns prepared with these particles improved from our previous report of ca. 70,000 plates per meter (N/m) to ca. 110,000 N/m.[1-3] These new columns also have better temperature stability (up to 100 °C) than those described in our previous report (80 °C) and are considered stable up to 120 °C.[1] PDVB particles were thoroughly characterized throughout their synthesis/preparation by applying multiple analytical tools to monitor them after each step in their preparation. It is valuable to use a variety of analytical instruments to obtain a more complete understanding of a material. Results showed that uniform PDVB microspheres remained spherical after each chemical or thermal treatment and that oxygen was introduced onto their surfaces when carbonized PDVB particles underwent acid treatments, which were useful for improving the adhesion of the amine-based polymer employed in the layer-by-layer synthesis of the core-shell particles. The resulting columns have mixed-mode properties and are able to retain acidic and basic analytes at different pHs because of the contributions of the amine-based polymers to the stationary phases. Different types of mixed-mode columns have now been developed to retain analytes under different conditions. For example, a group of cannabinoids were tested on different types of columns and the results showed that the

acidic cannabinoids separated from the neutral groups under various conditions. Some good separations of proteins, alkaloids, tricyclic antidepressants, and ginsenosides were also reported, and a series of application notes was developed around these separations to showcase the capabilities of these columns.[4-8] Recently, our newly-developed carbon/nanodiamond/amine-polymer-based mixed-mode high performance liquid chromatography (HPLC) columns were introduced onto the market by Diamond Analytics, a US Synthetic company. A series of application notes that highlight the capabilities of this column can be found at the company's website.

5.2. Future Work

The carbon/nanodiamond/amine-polymer-based core-shell materials show promise in HPLC to extend the pH and temperature ranges in separations. In addition, the mixed-mode properties of the column provide different selectivities that are different from traditional reversed-phase or mixed-mode HPLC columns. Recently, different types of columns with different column lengths have been developed and the quality of the columns has improved continuously through better manufacturing processes and new chemistries. As future work, there are two areas that need improvement in order to produce better columns.

First, the materials consist of carbon, nanodiamond, and polymer, and the retention mechanism of the columns is complex. The columns show strongly adsorbing sites that in some cases lead to peak tailing. These peak tailing issues are similar to the peak tailing issues of PGC columns that have pi-pi and charge-induced dipole interactions in the stationary phase.[9] They are possibly the result of exposed nanodiamond that has diamond-like (sp^3) and also graphitic (sp^2)

carbon at its surface.[3] Although additives or strong organic solvents (e.g. THF) are helpful for improving the peak shapes of analytes, these bring challenges for method development. One experiment showed the improvement of the peak shapes by the adsorption of pyrene in the stationary phase for preventing secondary interactions. This experiment indicated that as long as the strongly adsorbing sites are covered, the columns would be comparable in performance to the separations of silica-based columns. I would suggest that to improve column performance further, different structures or molecular weights of the amine-based polymers be used. I would also suggest that nanodiamond particles with different surface oxygen contents be studied as a means of improving nanodiamond-polymer adhesion in the particles.

Second, although the efficiency of the columns (ca. 100,000 - 120,000 N/m) is improved, silica-based columns with similar particle size (ca. 3.5 – 4.0 μm) show better efficiencies (ca. 150,000 - 200,000 N/m).[2] Silica-based materials generally have quite high surface areas: ca. 100 - 200 m^2/g. The surface area of the carbon/nanodiamond/amine-polymer-based materials is much lower (ca. 15 - 23 m^2/g). The nanodiamond used to prepare these particles has a rather broad particle size distribution (ca. 1 - 100 nm) compared to the particle size (ca. 8 nm) of the silica beads in the porous shells used to prepare silica-based core-shell materials.[1, 3, 10] Wider size ranges of nanodiamonds will also result in wider pore size distributions in the porous shells. I suggest that a tighter particle size distribution of nanodiamonds be used to improve both the surface area and the pore size distribution of the particles.

The unique selectivities of the new columns described in this work should be beneficial for orthogonal HPLC separations, which are important in the pharmaceutical industries where scientists wish to conclusively demonstrate that they do not have co-eluting peaks. I propose that

more application notes and papers be published to provide the necessary information to users that wish to perform these separations.

5.3. References

1. Hung, C.-H.; Wiest, L. A.; Singh, B.; Diwan, A.; Valentim, M. J. C.; Christensen, J. M.; Davis, R. C.; Miles, A. J.; Jensen, D. S.; Vail, M. A.; Dadson, A. E.; Linford, M. R., *J. Sep. Sci.* **2013,** *36* (24), 3821-3829.

2. Bobály, B.; Guillarme, D.; Fekete, S., *J. Pharm. Biomed. Anal.* **2015,** *104*, 130-136.

3. Wiest, L. A.; Jensen, D. S.; Hung, C.-H.; Olsen, R. E.; Davis, R. C.; Vail, M. A.; Dadson, A. E.; Nesterenko, P. N.; Linford, M. R., *Anal. Chem.* **2011,** *83* (14), 5488-5501.

4. Hung, C.-H.; Davis, T. C.; Jensen, D. S.; Miles, A. J.; Zukowski, J.; Dadson, A. E.; Linford, M. R. *FLARE C18 MIxed-Mode Column: Alkaloids*; Application Note: DA1013-A; Diamond Analytics: Orem, Utah.

5. Hung, C.-H.; Jensen, D. S.; Miles, A. J.; Zukowski, J.; Dadson, A. E.; Linford, M. R. *FLARE C18 Mixed-Mode Column: Separation of Apo-Transferrin and Bovine Serum Albumin (BSA) by LC-MS*; Application Note: DA1014-A; Diamond Analytics: Orem, Utah.

6. Singh, B.; Jensen, D. S.; Miles, A. J.; Dadson, A. E.; Linford, M. R. *Probing the Retention Mechanism of the Flare Mixed-Mode Column at Low pH via Acidic Herbicides with Different pK_a Values*; Application Note: DA1000-C; Diamond Analytics: Orem, Utah.

7. Hung, C.-H.; Zukowski, J.; Jensen, D. S.; Dadson, A. E.; Linford, M. R. *FLARE C18 Mixed-Mode Column: Separation of Ginsenosides Re and Rd by LC-MS*; Application Note: DA1016-A; Diamond Analytics: Orem, Utah.

8. Hung, C.-H.; Davis, T. C.; Jensen, D. S.; Miles, A. J.; Zukowski, J.; Dadson, A. E.; Linford, M. R. *Flare C18 Mixed-Mode Columns: Tricyclic Antidepressants (TCAs)*; Application Note: DA1001-C; Diamond Analytics: Orem, Utah.

9. Jensen, D. S.; Gupta, V.; Olsen, R. E.; Miller, A. T.; Davis, R. C.; Ess, D. H.; Zhu, Z.; Vail, M. A.; Dadson, A. E.; Linford, M. R., *J. Chromatogr. A* **2011,** *1218* (46), 8362-8369.

10. US7846337B2, Chen, W.; Wei, T.-C., 2010, Agilent Technologies, Inc, Superficially Porous Particles and Methods of Making and Using Same

Appendix 1: General Tutorial on Acid-Base Chemistry as a Basis for Understanding the Diamond Analytics Flare Mixed-Mode Column*

In this tutorial we review the basic concepts of the auto-ionization of water, K_w, pH and pOH, the dissociation of acids and bases in water, K_a and K_b, pK_a and pK_b, and the Henderson-Hasselbach equation. A more complete explanation of this information can be found in most general chemistry books. The purpose of this tutorial is to provide a general, conceptual basis to the chromatographer interested in using the Diamond Analytics Flare mixed-mode column. A more specific tutorial on the chemistry of the Flare column and possible analytes that might be separated on it is given in an application note entitled: ”Guidelines for Understanding the Retention Mechanism of the Diamond Analytics Flare Mixed-Mode Column”.

A1.1. Auto-Ionization of Water

In pure water, some of the water molecules will occasionally collide in such a way that a proton is exchanged between them:

$$H_2O + H_2O = H_3O^+ + OH^- \qquad \text{(A1.1)}$$

Note that this proton may also be referred to as a hydrogen ion, a hydronium ion, H^+, or H_3O^+. The process in Equation A1.1 is referred to as the auto-ionization (self-ionization) of water. It can

*This chapter was published by Diamond Analytics as an application note (Chuan-Hsi Hung, A. A. Kazarian, Andrew E. Dadson, Brett Paull, Pavel N. Nesterenko, Matthew R. Linford)

also be represented in the following equivalent, but abbreviated, way:

$$H_2O = H^+ + OH^- \quad \text{(A1.2)}$$

A1.2. K_w

Because of its auto-ionization, water will always have present at least small amounts of the hydrogen ion (H^+) and hydroxide ion (OH^-) and these concentrations: $[H^+]$ and [OH-] (concentrations in chemistry are represented by placing a chemical species in square brackets) will be equal in pure water. At room temperature, $[H^+] = [OH^-] = 1.0 \times 10^{-7}$ M. Most solutions (not pure water) will have hydrogen ion ($[H^+]$) and hydroxide ion ($[OH^-]$) concentrations that are not equal. However, $[H^+]$ and $[OH^-]$ cannot be varied independently of each other, but rather are constrained by the following relationship:

$$K_w = [H^+][OH^-] = 1.0 \times 10^{-14} \quad \text{(A1.3)}$$

where 1.0×10^{-14} is the equilibrium constant for the auto-ionization of water (K_w) at room temperature, and the concentration of water is always omitted from these types of equilibrium expressions. Equation A1.3 follows directly from Equation A1.2. An equivalent form of Equation A1.3, which would follow from Equation A1.1, can also be written:

$$K_w = [H_3O^+][OH^-] = 1.0 \times 10^{-14} \quad \text{(A1.4)}$$

Thus, we see that if either $[H^+]$ or $[OH^-]$ goes down, the other must go up (they are inversely related), e.g., if $[H^+] = 1.0 \times 10^{-9}$ M then $[OH^-] = 1.0 \times 10^{-5}$ M.

A1.3. pH and pOH

The pH and pOH of an aqueous solution are defined as the negative log of the hydrogen ion and hydroxide ion concentrations, respectively:

$$pH = -\log[H+] = -\log[H_3O^+] \quad \text{(A1.5)}$$

$$pOH = -\log [OH-] \quad \text{(A1.6)}$$

It follows that if we take the negative log of Equation A1.3 or Equation A1.4 and do a little algebra we obtain:

$$pH + pOH = 14.00 \quad \text{(A1.7)}$$

So for a hydrogen ion concentration of 1.0×10^{-7} M, pH = -log[1.0×10^{-7}] = 7.00. A solution with a pH value of 7.00 is said to be neutral. If the hydrogen ion concentration is greater than 1.0×10^{-7} M, the solution is acidic and its pH is less than 7.00, e.g., if $[H^+] = 1.0 \times 10^{-6}$ M, then pH = 6.00. On the other hand, if $[H^+]$ is less than 1.0×10^{-7} M, the solution is basic and its pH is greater than 7.00, e.g., if $[H^+] = 1.0 \times 10^{-12}$ M, then pH = 12.00. From Equation A1.7, we see that if the pH of a solution is equal to 4.00, then the pOH for that solution is 10.00.

A1.4. Dissociation of Acids and Bases in Water

Strong acids and bases dissociate completely in water – they are strong electrolytes, and weak acids and bases, which we will represent as HA and B, generally only dissociate to a very small extent in water – they are weak electrolytes. The dissociations of a weak acid, HA, (Equations A1.8 and A1.9) and of a weak base, B, (Equation A1.10) in water are given as follows:

$$HA + H_2O = H_3O^+ + A^- \quad \text{(A1.8)}$$

or

$$HA = H^+ + A^- \quad \text{(A1.9)}$$

and

$$B + H_2O = BH^+ + OH^- \quad \text{(A1.10)}$$

Equation A1.8 is more complete than Equation A1.9 in the sense that it shows water acting as a base to accept a proton from the weak acid, HA. However, this process is often represented in the abbreviated form given in Equation A1.9. Equation A1.10 shows a weak base, B, removing a proton from water to form the protonated form of B, BH^+, and also OH^-. In Equations A1.8 and A1.9, A^- is referred to as the conjugate base of the weak acid HA, and in Equation A1.10, BH^+ is referred to as the conjugate acid of the weak base B. For an actual weak acid, benzoic acid (C_6H_5COOH), the dissociation represented in Equation A1.9 is as follows:

$$C_6H_5COOH = C_6H_5COO^- + H^+ \quad \text{(A1.11)}$$

where, C_6H_5COOH and $C_6H_5COO^-$ represent the weak acid, HA, and its conjugate base, A^-, respectively. For an actual weak base, ammonia (NH_3), the dissociation represented in Equation A1.10 is as follows:

$$NH_3 + H_2O = NH_4^+ + OH^- \quad \text{(A1.12)}$$

Obviously, NH_4^+/NH_3 are the conjugate acid/base pair here.

A1.5. K_a and K_b

K_a and K_b are the equilibrium constants for the dissociation of a weak acid and a weak base, respectively. Note that subscripts like ‘w’, ‘a’, or ‘b’ are often added to an equilibrium constant to

designate the type of equilibrium under consideration. For Equations A1.8, A1.9, and A1.11, mathematical expressions for K_a can be written as follows:

$$K_a = \frac{[H_3O^+][A^-]}{[HA]} \quad \text{(A1.13)}$$

$$K_a = \frac{[H^+][A^-]}{[HA]} \quad \text{(A1.14)}$$

and

$$K_a = \frac{[C_6H_5COO^-][H^+]}{[C_6H_5COOH]} \quad \text{(A1.15)}$$

Note: Each acid will have its own unique value of K_a, and that the larger the K_a, the greater the dissociation of HA, i.e., $[H^+]$ and $[A^-]$ will be larger for a larger value of K_a so the solution will be more acidic. The K_a values for many common weak acids are in the range of about 10^{-4} to 10^{-10}. For example, the K_a values for formic acid (HCOOH), acetic acid (CH_3COOH) and phenol (C_6H_5OH) are 1.8×10^{-4}, 1.8×10^{-5} and 1.6×10^{-10}, respectively. K_a values do not have units. Obviously formic acid is the strongest of these three weak acids and phenol is the weakest.

For Equations A1.10, and A1.12, mathematical expression for K_b can be written as follows:

$$K_b = \frac{[BH^+][OH^-]}{[B]} \quad \text{(A1.16)}$$

$$K_b = \frac{[NH_4^+][OH^-]}{[NH_3]} \quad \text{(A1.17)}$$

A1.6. pK_a and pK_b

As we have seen, K_a and K_b values can vary over many orders of magnitude. Accordingly, pK_a and pK_b are often used in place of K_a and K_b values, where the pK_a and pK_b are defined as:

$$pK_a = -\log K_a \quad \text{(A1.18)}$$

$$pK_b = -\log K_b \quad \text{(A1.19)}$$

For example, acetic acid has a K_a value of 1.8×10^{-5}, which gives it a pK_a value of -log (1.8×10^{-5}), which is 4.75. Similarly, the K_a value for phenol is 1.6×10^{-10} so its K_a value is 9.80. Thus we see that the lower the pK_a value of an acid (or a base) the stronger it is.

There is a useful relationship between the K_a and K_b values for a conjugate acid/base pair, which we represent as HA and A^-. If we rewrite Equations A1.10 and A1.16 in terms of A^-, the conjugate base of HA, we get:

$$A^- + H_2O = HA + OH^- \quad \text{(A1.20)}$$

and

$$K_b = \frac{[HA][OH^-]}{[A^-]} \quad \text{(A1.21)}$$

Now if we multiply the expression for K_a for HA (Equation A1.14) by the expression for K_b for A^- (Equation A1.21) we obtain:

$$K_a * K_b = \frac{[H^+][A^-]}{[HA]} * \frac{[HA][OH^-]}{[A^-]} = [H^+][OH^-] = K_w = 1.0x10^{-14} \quad \text{(A1.22)}$$

That is:

$$K_a \times K_b = K_w = 1.0 \times 10^{-14} \quad \text{(A1.23)}$$

For example, because ammonia (NH_3) has a K_b of 1.8×10^{-5}, the K_a for its conjugate acid (NH_4^+) is 5.6×10^{-10} (as derived from Equation A1.23).

If we take the negative log of both sides of Equation A1.23 and do a little algebra we obtain another useful relationship:

$$pK_a + pK_b = pK_w = 14.00 \quad \text{(A1.24)}$$

A1.7. Henderson-Hasselbach Equation

The Henderson-Hasselbach equation is used to describe buffers, which are solutions that contain either a weak acid or a weak base with its conjugate. The Henderson-Hasselbach equation will help us better understand how pH influences the ionization state of analytes and the Flare mixed-mode column itself. This equation is derived in a few short steps from Equation A1.14 – we begin by taking the negative log of both sides of that equation:

$$-\log K_a = -\log\left(\frac{[H^+][A^-]}{[HA]}\right) \quad \text{(A1.25)}$$

Using Equation A1.18 and expanding the right side of Equation A1.25 we obtain the following:

$$pK_a = -\log[H^+] - \log\left(\frac{[A^-]}{[HA]}\right) \quad \text{(A1.26)}$$

We now use Equation A1.5 and do a little algebra to obtain the Henderson-Hasselbach equation:

$$pH = pK_a + \log\left(\frac{[A^-]}{[HA]}\right) \quad \text{(A1.27)}$$

The Henderson-Hasselbach equation teaches us some important things about solutions that contain ionizable analytes. First, it tells us that when the concentration of the weak acid ([HA]) and its conjugate base ($[A^-]$) are the same ($[A^-]/[HA] = 1$), the pH of the solution is equal to the pK_a of the weak acid. In other words, the concentrations of HA and A^- are equal when half of the weak acid, HA, is deprotonated, or if we are starting with the weak base, A^-, when half of it is

protonated. Perhaps for a chromatographer, a better way to look at the Henderson-Hasselbach equation is to recognize that by changing the pH of a solution (mobile phase) one can change the ratio of $[A^-]$ and [HA]. Three cases are particularly important here:

(i) if the pH of a solution equals the pK_a value for the weak acid then $[A^-] = [HA]$

(ii) if the pH of a solution is one pH unit above the pK_a for the weak acid ($pH = pK_a + 1$), then there will be ten times as much A^- in solution as HA, i.e., $[A^-] = 10*[HA]$

(iii) if the pH of a solution is one pH unit below the pK_a for the weak acid ($pH = pK_a - 1$), then there will be ten times as much HA in solution as A^-, i.e., $[HA] = 10*[A^-]$.

Because in many cases chromatographic retention is strongly influenced by the protonation state of an analyte, the pH of the mobile phase can have a significant effect on retention and also selectivity in a separation. We see from the Henderson-Hasselbach equation that the protonation state of an analyte is particularly sensitive to the pH of the mobile phase when it is within plus or minus one pH unit of the pK_a for the analyte, i.e., $pH = pK_a \pm 1$. When the pH of the solution is either above or below this range, the analyte will be either mostly deprotonated or protonated, respectively.

As an example, the pK_a for formic acid is 3.74, which means that in an aqueous solution when:

(i) the pH is 3.74 the concentrations of formic acid (HCOOH) and formate ($HCOO^-$) are equal

(ii) the pH is 4.74, $[HCOO^-] = 10*[HCOOH]$

(iii) the pH is 2.74, $[HCOOH] = 10*[HCOO^-]$

(iv) the pH is greater than 4.74 the formic acid is mostly deprotonated

(v) the pH is less than 2.74 the formic acid is mostly protonated

Appendix 2: Guidelines for Understanding the Retention Mechanism of the Diamond Analytics Flare Mixed-Mode Column*

The Diamond Analytics Flare mixed-mode column is made of diamond, carbon, and polymer to allow anion exchange and/or hydrophobic retention mechanisms to be operative in its separations. As with many mixed-mode columns, it is important to understand both the ionic (charged) state of one's analytes as well as that of the stationary phase to best predict retention. Both of these charged states may depend on the mobile phase pH. While the retention mechanism of a mixed-mode column is generally more complex than that of a C18 phase, this added complexity can allow separations that may not be possible on traditional C18 columns. This application note explains the protonation state of both the Flare mixed-mode column and a series of common analytes/functional groups as a function of pH. These general guidelines should help the user best select conditions for chromatographic separations on the Flare column.

The following tutorial assumes some understanding of acid-base chemistry. If the reader is not familiar with this chemistry, he/she may wish to refer to the Diamond Analytics application note: "General Tutorial on Acid-Base Chemistry as a Basis for Understanding the Diamond Analytics Flare Mixed-Mode Column".

* This chapter was published by Diamond Analytics as an application note (Chuan-Hsi Hung, A. A. Kazarian, Andrew E. Dadson, Brett Paull, Pavel N. Nesterenko, Matthew R. Linford)

A2.1. The Stationary Phase of the Diamond Analytics Flare Column

In essence, the stationary phase of the Diamond Analytics Flare column contains two important functionalities: hydrophobic octadecyl (C_{18}) chains and mixed primary, secondary, and tertiary amine groups.

The C18 chains facilitate at least some degree of hydrophobic interactions with analytes at all mobile phase compositions.

The amine groups allow the protonation state of the column to be varied with pH. The pK_a for a molecular amine is about 10 – when we refer here to the pK_a for an amine we really mean the pK_a for the amine in its protonated form. However, the protonation state for an amine-containing polymer, as a function of pH, is be a little more complicated than the situation for molecular species. For example, as the pH of the mobile phase is lowered from ca. 10 to 9, we will not find a ca. 10:1 ratio of protonated to deprotonated amines in the stationary phase. This is because the charged amine groups on the polymer are in close proximity to each other and will repel each other. In other words, the more the column is protonated the more difficult it is to further protonate it so an increasingly lower pH will be required to protonate it. In practice this means that as we lower the pH over a number of pH units we will increasingly protonate the column, which is unlike the more limited pH range over which molecular amines change their protonation state. The removal of protons should be more straightforward – because we are reducing charge repulsions as we remove protons from the column, we should find that the column is mostly deprotonated at ca. pH 11.

Thus, at higher pH values the column will be more deprotonated (neutral) and will behave in a more reversed phase mode. At lower pH values the column will be increasingly protonated,

which means it will be increasingly hydrophilic (less retentive in its reverse phase mode) and more able to interact strongly with anionic analytes.

In general we recommend that a buffer always be present in the aqueous portion of the mobile phase with the Flare mixed-mode column so that the protonation state of the column will remain fixed.

A2.2. Ionization Behavior of Major Classes of Analytes

The following is a list of functional groups found on many analytes with their approximately pK_a values and/or permanent charge states and a discussion of their expected retention on the Flare mixed-mode column. These functional groups/analytes are placed in one of three categories: a. neutral analytes, b. permanently charged analytes, and c. weak acids and bases with protonation states that depend on pH. By noting the charge states, pK_a values, and hydrophobicities of anlaytes, one can predict their retention on the Flare mixed-mode column. Note: while the following rules of thumb are generally accurate, actual results may vary somewhat for different analytes and mobile phases – of course better predictions will be possible if the user knows the actual pK_a values of his/her analytes. Thus, we recommend that as much information as possible be gathered about new analytes/analyte mixtures and that they be tested with a few different mobile phases at different pHs, where the recommendations below may be considered as a starting point for experimentation.

A2.2.1. Neutral Analytes (No Permanently Charged or Ionizable Moiety)

These analytes, depending on their hydrophobicity, may be retained at any pH on the Flare mixed-mode column. In general, however, retention will increase with increasing mobile phase pH because the stationary phase will be increasingly deprotonated and therefore hydrophobic.

There are a number of functional/structural groups on organic molecules that remain neutral over the entire pH range of the Flare column. These include alcohol (-OH) groups (they are very weak acids – pK_a values of ca. 17 - 19), cyano (-CN) groups, alkyl and aryl halides, aromatic rings, alkyl chains, and perfluorinated alkyl chains. Hydroxyl groups can interact with amine functional groups on the Flare mixed-mode adsorbent by formation of relatively weak hydrogen bonds, but as a rule, this should not be a dominant type of interaction.

A2.2.2. Permanently Charged Analytes

A2.2.2.1. Quaternary Amine Groups (-NR3+)

Quaternary amines have permanent positive charges. Unless they are quite hydrophobic, they will not, in general, be well retained in the Flare column at lower pH values because of cation-cation repulsions between the protonated stationary phase and the charged analyte – best retention will be at elevated pH values where the stationary phase is neutral.

A2.2.2.2. Sulfonates (RSO_3^-) and Sulfates ($ROSO_3^-$)

These analytes will be almost entirely negatively charged over the entire pH range of the Flare column. Thus, their retention will increase with decreasing pH as the stationary phase is increasingly protonated (cationic). In addition, the retention of all charged analytes can be regulated by the concentration of the buffer in the eluent, i.e., retention of ionic species will be less with higher concentrations of buffer.

A2.2.3. Weak Acids and Bases with Protonation States that Depend on pH

A2.2.3.1. Aliphatic Amines, pK_a ca. 10, e.g., Tricyclic Antidepressants

Primary, secondary, and tertiary amines have pKa values of ca. 10. Retention will be greatest on the Flare column when both they and the stationary phase are deprotonated – above ca. pH 11 where the column is in reversed phase mode. Below pH 10 one would expect reduced retention because of cation-cation repulsion between the protonated analyte and the protonated stationary phase.

A2.2.3.2. Carboxylic Acids (RCOOH), pKa ca. 4.0, e.g., Various Acidic Herbicides and Benzoic acid

Carboxylic acids are acids. Above ca. pH 5.0 they will be mostly deprotonated (anionic) and will interact strongly with the protonated Flare stationary phase. At higher pH values where the stationary phase is increasingly deprotonated their retention will decrease. Their retention will

also decrease at low pH values (below ca. pH 3.0) where they will be mostly protonated (neutral) and the column will be protonated. That is, best retention is expected from ca. pH 3.0 – 10.

A2.2.3.3. Phenols, pK_a ca. 10, e.g., Phenol (C_6H_5OH)

Phenols are acids. Below ca. pH 9 they will be mostly protonated. At ca. pH 11 they will be mostly deprotonated. Thus, at lower pH values (at or below ca. 9) one will have a neutral analyte and a cationic Flare column. At higher pH values (at or above ca. 11) one will have an anionic analyte and a neutral column. In both of these cases retention will be less than between ca. pH 9 and 11, where a significant amount of both the analyte and the column will be charged; retention will be greatest when charge-charge interactions are attractive – between ca. pH 9 and 11.

A2.2.3.4. Aromatic Amines/Pyridinic-Type Species, pK_a ca. 5, e.g., Aniline ($C_6H_5NH_2$) and Pyridine (C_5H_5N)

The protonated forms of aniline and pyridine have pK_a values of ca. 5. Accordingly, at pH values below ca. 4 they will be mostly protonated and poorly retained on the Flare column because of cation-cation repulsions between these analytes and the stationary phase. Above pH ca. 6 they will be deprotonated (neutral). Retention will thus increase as the mobile phase pH increases and the stationary phase is increasingly deprotonated.

Note: For all charged analytes retention is dependent on the type and charge of the ions composing the buffer, along with the concentration and pH of the buffer. An increase of pH

increases the eluting ability of the buffer for weak acids and the opposite effect takes place for weak bases.

Appendix 3: Flare C18 Mixed-Mode Column: Tricyclic Antidepressants (TCAs)*

A3.1. Introduction

Tricyclic antidepressants (TCAs) have three rings and an amine in their structures, and are commonly used for the clinical treatment of depression.[1] Because of their basicity, they are better retained and separated in HPLC at elevated pH, which places them in their neutral state.[2-3]

The FLARE C18 Mixed-Mode (MM), core-shell HPLC column from Diamond Analytics is made of carbon, polymer, and nanodiamond, which are stable at high pH and elevated temperature.[4-6] These material attributes of the column facilitate the retention and separation of basic analytes.[2, 4]

The FLARE C18 Mixed-Mode (MM) column contains amines in its stationary phase that are deprotonated (neutral) at elevated pH, which allows basic analytes to be retained through hydrophobic interactions. At lower pH, the stationary phase is protonated (positively charged) and retains anionic compounds.[3] In this application note, TCAs are separated with the FLARE C18 MM column at pH 12.

* This chapter was published by Diamond Analytics as an application note (Hung, C-H., Davis, T. C., Jensen, D. S., Miles, A. J., Zukowski, J., Dadson, A. E., Linford, M. R.)

A3.2. Experimental

HPLC system: Waters HPLC 1525 Binary HPLC pump with dual wavelength UV detector (Model No. 2487)

Column: Diamond Analytics FLARE mixed-ode column, 4.6 x 33 mm (cat # FL36-46033)

Injection volume: 5.0 µL

Elution conditions: Isocratic

Detection: UV at 254 nm

Flow rate: 1.5 mL/min

Temperature: 35 °C

Mobile phase: 10 mM phosphate buffer pH 12, ACN (70/30)

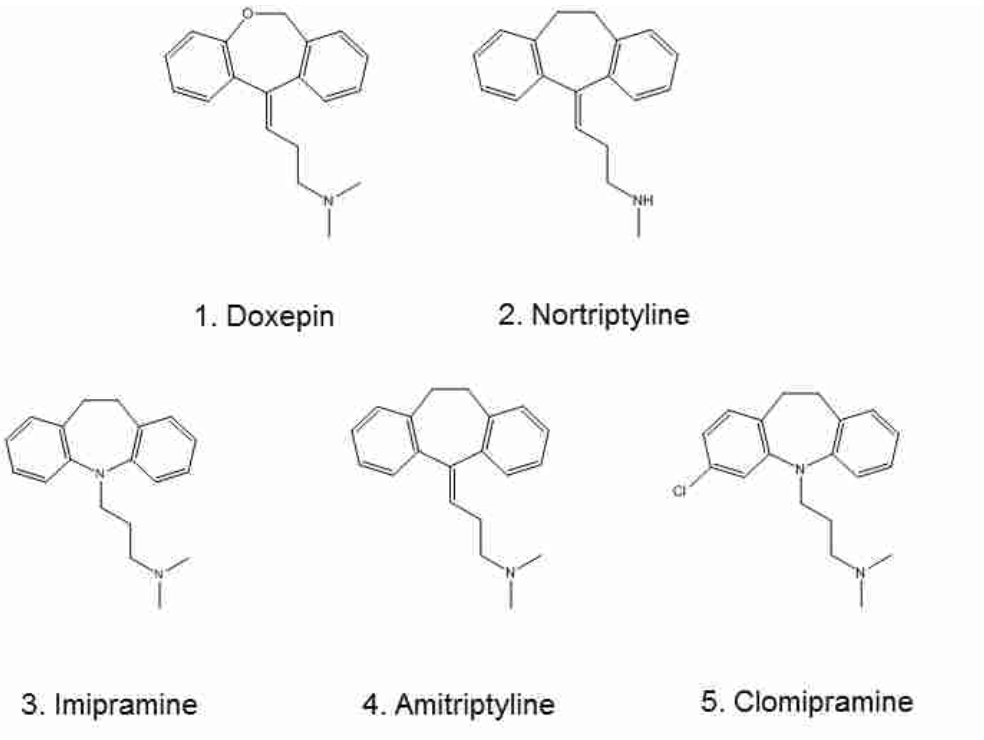

Figure A3.1 Structure of separated tricyclic antidepressants

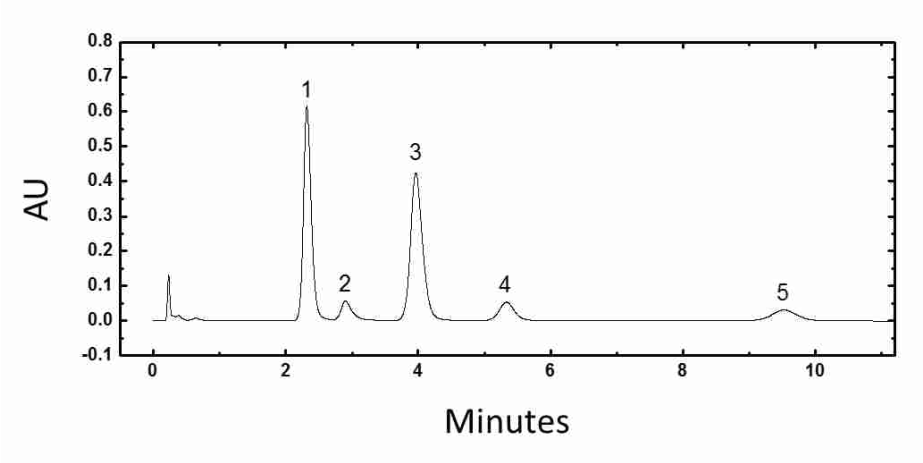

Figure A3.2 Chromatogram of (1) doxepin, (2) nortriptyline, (3) imipramine, (4) amitriptyline, and (5) clomipramine separated at pH 12.

A3.3. References

1. Mercolini, L.; Mandrioli, R.; Finizio, G.; Boncompagni, G.; Raggi, M. A., *J. Sep. Sci.* **2010,** 33, 23-30.

2. Kirkland, J. J.; Henderson, J. W.; Stefano, J. J. D.; Straten, M. A. v.; Claessens, H. A., *J. Chromatogr. A* **1997,** 762, 97-112.

3. Hung, C.-H.; Kazarian, A. A.; Dadson, A. E.; Paull, B.; Nesterenko, P. N.; Linford, M. R., Guidelines for Understanding the Retention Mechanism of Diamond Analytics Flare Mixed-Mode Column. Diamond Analytics.

4. Hung, C.-H.; Wiest, L. A.; Singh, B.; Diwan, A.; Valentim, M. J. C.; Christensen, J. M.; Davis, R. C.; Miles, A. J.; Jensen, D. S.; Vail, M. A.; Dadson, A. E.; Linford, M. R., *J. Sep. Sci.* **2013,** 36 (24), 3821-3829.

5. Saini, G.; Jensen, D. S.; Wiest, L. A.; Vail, M. A.; Dadson, A.; Lee, M. L.; V., S.; Linford, M. R., *Anal. Chem.* **2010,** 82 (11), 4448-4456.

6. Wiest, L. A.; Jensen, D. S.; Hung, C.-H.; Olsen, R. E.; Davis, R. C.; Vail, M. A.; Dadson, A. E.; Nesterenko, P. N.; Linford, M. R., *Anal. Chem.* **2011,** 83 (14), 5488-5501.

Appendix 4: Flare C18 Mixed-Mode Column: Alkaloids*

A4.1. Introduction

The alkaloids are a class of basic, naturally occurring, amine-containing compounds.[1] They are commonly used as local anesthetics and stimulants in clinical practice. For basic analyte analysis using a reversed phase HPLC column, higher pH conditions are desirable because the analytes will be neutral and therefore better retained and separated.[2]

The FLARE C18 mixed-mode (MM) column is a non-silica HPLC column made from carbon, polymer and nanodiamond.[3] These materials are well known for their stability under elevated pH and temperature conditions.[3-4] In addition to its stability, the FLARE column also has mixed-mode properties.[5] With this column, lower pH values often favor the separation of acidic analytes, and higher pH values the separation of basic analytes. This is because the column contains amines in its stationary phase. At lower pH, the stationary phase is positively charged, which allows interactions with acidic analytes through ionic interactions. At higher pH, both basic analytes and the stationary phase are in their neutral forms and interact with each other through hydrophobic interactions.

In this application note, three alkaloids (prilocain, lidocaine, and bupivacaine) are separated at pH 12 using the FLARE C18 Mixied-Mode (MM) column.

* This chapter was published by Diamond Analytics as an application note (Hung, C-H., Davis, T. C., Jensen, D. S., Miles, A. J., Zukowski, J., Dadson, A. E., Linford, M. R.)

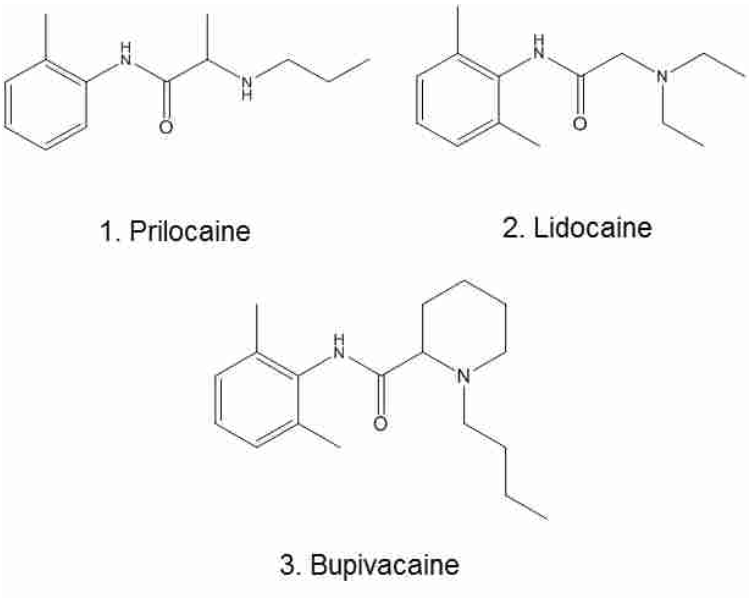

Figure A4.1 Structure of separated alkaloids

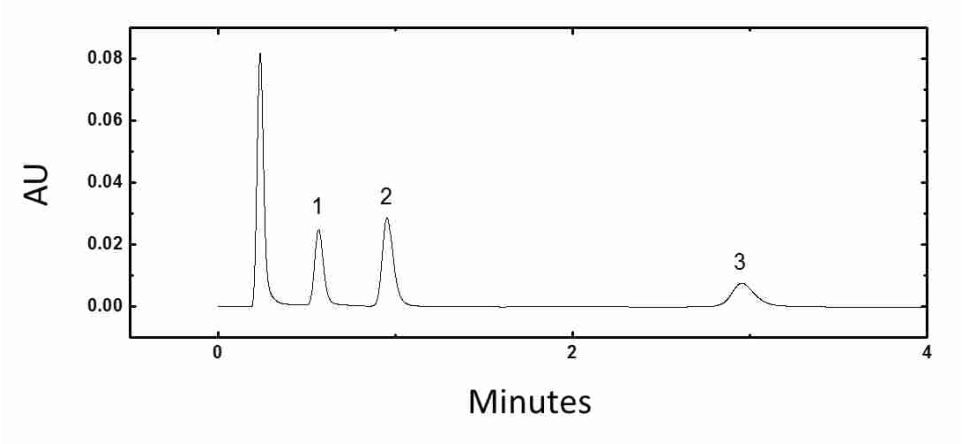

Figure A4.2 Chromatogram of (1) prilocaine, (2) lidocaine, and (3) bupivacaine separated at pH 12.

A4.2. Experimental

HPLC system: Waters HPLC 1525 binary pump with dual wavelength UV detector (Model No. 2487)

Column: FLARE C18MM 4.6 x 33 mm (cat # FL36-46033)

Injection volume: 5.0 µL

Flow rate: 1.5 mL/min

Elution conditions: Isocratic

Detection: UV at 254 nm

Temperature: 35 °C

Mobile phases: 10 mM phosphate buffer at pH 12, ACN (75/25)

A4.3. References

1. Storms, M. L.; Stewart, J. T., *J. Pharm. Biomed. Anal.* **2002,** 30, 49-58.

2. Kirkland, J. J.; henderson, J. W.; DeStefano, J. J.; Straten, M. A. v.; Claessens, H. A., *J. Chromatogr.* **1997,** 762, 97-112.

3. Hung, C.-H.; Wiest, L. A.; Singh, B.; Diwan, A.; Valentim, M. J. C.; Christensen, J. M.; Davis, R. C.; Miles, A. J.; Jensen, D. S.; Vail, M. A.; Dadson, A. E.; Linford, M. R., *J. Sep. Sci.* **2013,** 36 (24), 3821-3829.

4. Wyndham, K. D.; O'Gara, J. E.; Walter, T. H.; Glose, K. H.; Lawrence, N. L.; Alden, B. A.; Izzo, G. S.; Hudalla, C. J.; Iraneta, P. C., *Anal. Chem.* **2003,** 75 (24), 6781-6788.

5. Hung, C.-H.; Kazarian, A. A.; Dadson, A. E.; Paull, B.; Nesterenko, P.; Linford, M. R. Guidelines for Understanding the Retention Mechanism of the Diamond Analytics Flare Mixed-Mode Column; Diamond Analytics.

Appendix 5: Regeneration of the Diamond Analytics Flare Mixed-Mode Column after Exposure to TFA*

A5.1. Introduction

The Flare mixed-mode, core-shell HPLC column from Diamond Analytics is stable at extremes of pH and at elevated temperature.[1-3] In addition, the column has mixed-mode properties, showing both weak anion exchange and hydrophobic retention mechanisms.[4] Because it contains an amine-based polymer, its stationary phase is protonated (charged) or deprotonated (neutral) over different ranges of pH. This amine-containing polymer is not expected to behave like a molecular amine because the charges on the polymer interact as the column is protonated.[4] Thus, it becomes increasingly difficult to protonate the column as it is more and more charged. Accordingly, one would expect a difference in the column at pH 2 and 7, while no such difference would be expected for a molecular amine.

Changes in the protonation state of the Flare column change its retention mechanism. Thus, mobile phase pH is a useful 'knob' to turn to control the column selectivity. At lower pH (pH 1-5), the Flare column retains acidic analytes through ionic interactions. At higher pH (pH > 10), it retains basic analytes through hydrophobic interactions. Neutral analytes are retained over a wide pH range, although this retention is also affected by the protonation state of the column – whether it is more protonated (more hydrophilic) or more deprotonated (more hydrophobic).

A common problem with amine-containing stationary phases is their retention of acidic

* This chapter was published by Diamond Analytics as an application note (Chuan-Hsi Hung, David S. Jensen, Andrew E. Dadson, Matthew R. Linford)

additives like trifluoroacetic acid (TFA). Given the acid-base properties of TFA and the amines in the Flare stationary phase, one would expect that trifluoroacetate could be removed from the column at elevated pH. This type of approach would not be an option for silica-based columns because of their lack of stability under these conditions.

A separation was performed on the Flare column at neutral pH (phosphate buffer at pH 7). The same separation was then performed at pH 2 using a TFA-containing mobile phase. With this change in pH the retention of the neutral analytes dropped. Nevertheless, the column could be regenerated at pH 11, and this regeneration was repeatable. Thus, TFA, a common additive, can be used with the Flare column.

A5.2. Experimental

Analytes: Alkylbenzene mixture (ethyl, butyl, and hexylbenzene)

HPLC system: Waters 1525 Binary HPLC pump with a UV detector

Column: Diamond Analytics Flare mixed-mode column (4.6 x 33 mm, 4 μm)

Injection volume: 5.0 μL

Elution conditions: Isocratic

Detection: UV at 254 nm

Flow rate: 0.7 mL/min

Temperature: 35 °C

Mobile phases: H_2O/ACN (50/50) with

10 mM TFA (pH 2.0), 10 mM phosphate

(pH 7.0), or 0.2 % TEA (v/v), pH then adjusted to 11.0 (pH 11).

A5.3. Results and Discussion

Figure A5.1 shows the retention times of hexyl- and butylbenzene at different mobile phase pH values. Initially, the column was tested at pH 7. The same separation was then attempted at pH 2, and, as expected, the retention times of the analytes decreased. A separation was next performed at pH 11. This step regenerated the column. The following run at pH 7 was then very close to its previous pH 7 value. This process was repeated four times. Interestingly, after the second cycle, the retention times of the analytes at pH 11 and pH 7 were very similar.

Figure A5.2 shows the chromatograms of the alkylbenzene test mixture in the fourth cycle. The pH 2 chromatogram shows substantially less retention than the pH 7 chromatogram. However, the subsequent pH 11 and pH 7 chromatograms are almost identical to the original pH 7 chromatogram. Thus, deprotonation at pH 11 can remove the effects of TFA from the Flare column.

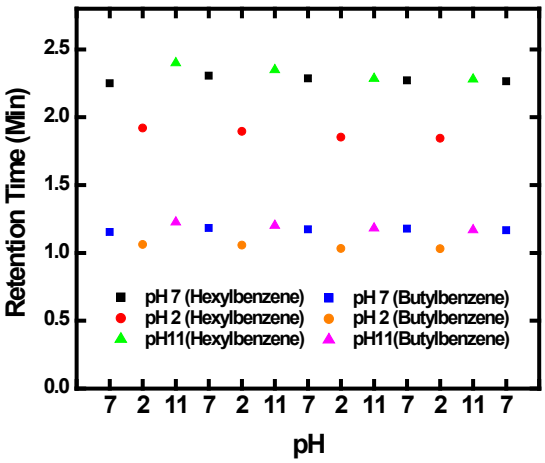

Figure A5.1 Retention times of hexylbenzene (top points) and butylbenzene (lower points) at different mobile phase pHs.

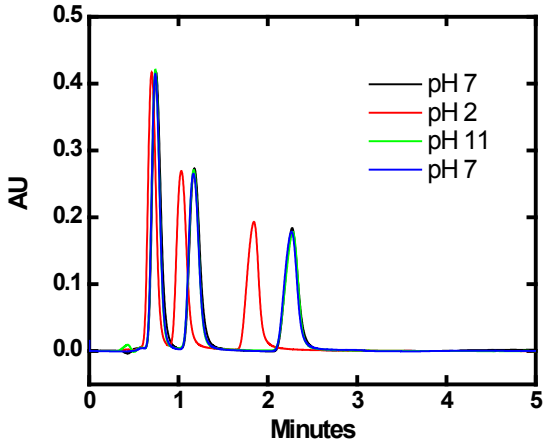

Figure A5.2 Chromatograms of ethyl-, butyl-, and hexylbenzene at pH 7, 2, 11, and then 7.

A5.4. References

1. Saini, G.; Jensen, D. S.; Wiest, L. A.; Vail, M. A.; Dadson, A.; Lee, M. L.; V., S.; Linford, M. R., *Anal. Chem.* **2010,** 82 (11), 4448-4456.

2. Hung, C.-H.; Wiest, L. A.; Singh, B.; Diwan, A.; Valentim, M. J. C.; Christensen, J. M.; Davis, R. C.; Miles, A. J.; Jensen, D. S.; Vail, M. A.; Dadson, A. E.; Linford, M. R., *J. Sep. Sci.* **2013,** 36 (24), 3821-3829.

3. Wiest, L. A.; Jensen, D. S.; Hung, C.-H.; Olsen, R. E.; Davis, R. C.; Vail, M. A.; Dadson, A. E.; Nesterenko, P. N.; Linford, M. R., *Anal. Chem.* **2011,** 83 (14), 5488-5501.

4. Hung, C.-H.; Kazarian, A. A.; Dadson, A. E.; Paull, B.; Nesterenko, P. N.; Linford, M. R., Guidelines for Understanding the Retention Mechanism of Diamond Analytics Flare Mixed-Mode Column. Diamond Analytics.

Appendix 6: Flare C18 Mixed-Mode Column: Separation of Apo-Transferrin and Bovine Serum Albumin (BSA) by LC-MS*

A6.1. Introduction

Proteins are polymeric species composed of amino acid residues that fold into complex three-dimensional structures. The ca. 20 amino acids nature uses in proteins have a variety of side chains that influence protein structure, e.g., smaller or larger, acidic or basic, nonpolar or polar, etc.[1] Many proteins have been extensively analyzed to understand their roles in organisms. In this application note, bovine serum albumin (BSA) and apo-transferrin were separated by LC-MS using the FLARE mixed-mode column from Diamond Analytics.

The FLARE C18 mixed-mode (MM), core-shell column from Diamond Analytics is made of carbon, nanodiamond, and polymer, and is suitable for operation under high temperature and elevated pH conditions.[2-4] Because the amine-based polymer in its stationary phase is positively charged at low pH and neutral at high pH, the column has mixed-mode properties, which allow it to retain acidic analytes at low pH and basic analytes at high pH.[5]

* This chapter was published by Diamond Analytics as an application note (Hung, C-H., Jensen, D. S., Miles, A. J., Zukowski, J., Dadson, A. E., Linford, M. R.)

1. Apo-transferrin

http://en.wikipedia.org/wiki/Transferrin

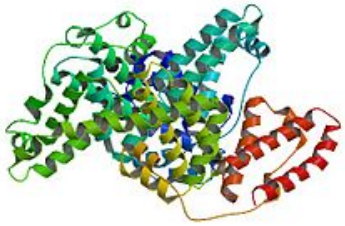

2. BSA

http://en.wikipedia.org/wiki/Bovine_serum_albumin

Figure A6.1 Structure of separated BSA and apo-transferrin

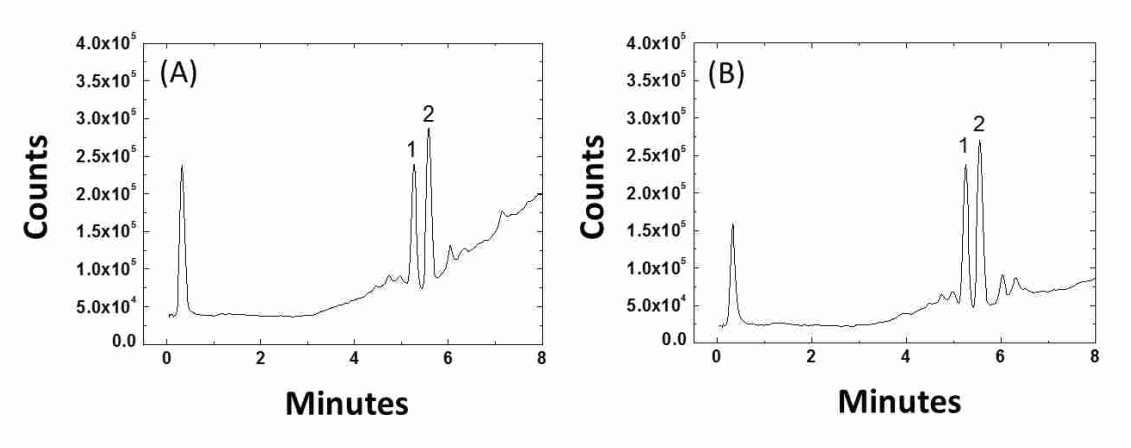

Figure A6.2 Separations of apo-transferrin (1) and BSA (2). (A) 0.1% TFA in buffers A and B, and (B) 0.1% TFA in buffer A and 0.0875% TFA in buffer B.

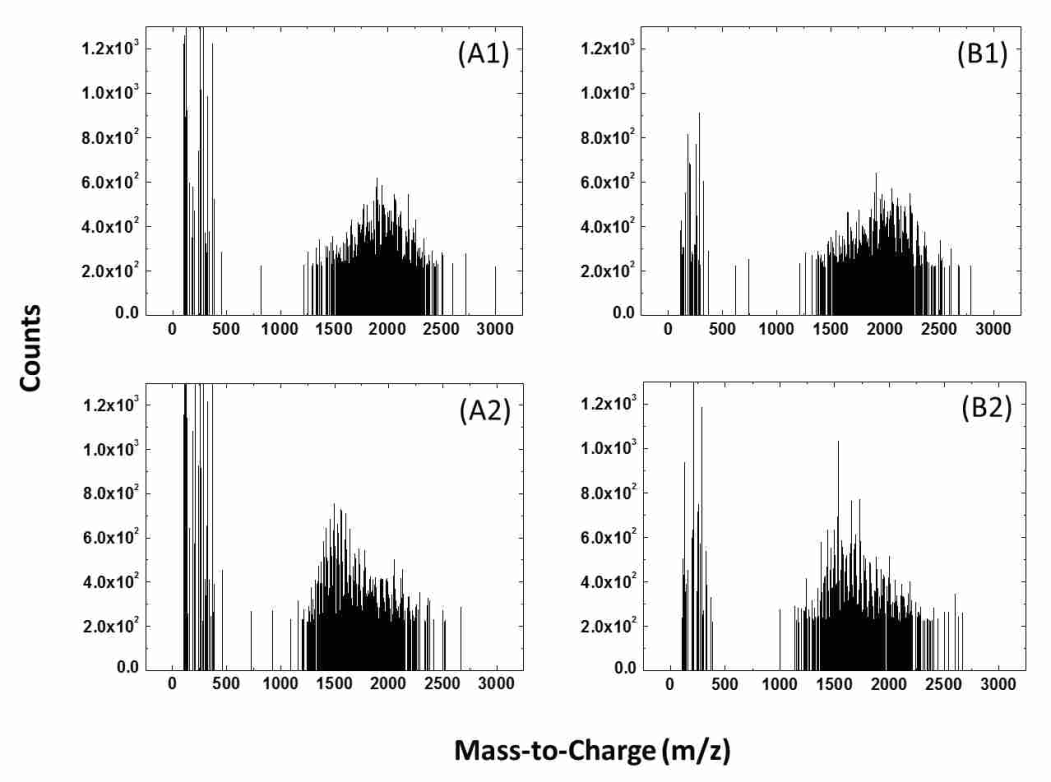

Figure A6.3 Mass spectra of apo-transferrin (A1 and B1) and BSA (A2 and B2) from the corresponding peaks in the chromatograms in Figure 1 (A) and (B).

A6.2. Experimental

HPLC system: Agilent 1260 Infinity coupled with an Agilent 6230 TOF LC-MS in positive ion mode

Analytes: Apo-transferrin and BSA (ca. 0.5 mg/mL in ACN)

LC Conditions:

Column dimensions: 2.1 x 50 mm (id: TM0001 08/14/14 TB)

Injection volume: 10.0 μL

Flow rate: 0.4 mL/min

Temperature: 30 °C

A: 1000 mL H_2O + 1 mL TFA

B: 1000 mL ACN + 1 mL or 0.875 mL TFA

Gradient:

0 min 100% A 0% B

8 min 0% A 100% B

8.1 min 100% A 0% B

20 min End

MS conditions:

Gas temperature: 300 °C

Drying gas: 5 L/min

Nebuilizer: 35 psig

Capillary voltage: 3500 V

Fragmentor: 150 V

Skimmer: 65 V

OCT 1Rf Vpp: 750 V

A6.3. Conclusions

BSA and apo-transferrin have been separated by LC-MS using the Diamond Analytics FLARE C18 mixed-mode column by gradient elution and with commonly used reagents: water, ACN, and TFA. The concentration of the TFA additive affects the baseline.

A6.4. References

1. Kussell, E.; Shimada, J.; Shakhnovich, E. I., *Proteins-Struct. Funct. Gen.* **2003,** 52 (1), 303-321.

2. Hung, C.-H.; Wiest, L. A.; Singh, B.; Diwan, A.; Valentim, M. J. C.; Christensen, J. M.; Davis, R. C.; Miles, A. J.; Jensen, D. S.; Vail, M. A.; Dadson, A. E.; Linford, M. R., *J. Sep. Sci.* **2013,** 36 (24), 3821-3829.

3. Saini, G.; Jensen, D. S.; Wiest, L. A.; Vail, M. A.; Dadson, A.; Lee, M. L.; V., S.; Linford, M. R., *Anal. Chem.* **2010,** 82 (11), 4448-4456.

4. Wiest, L. A.; Jensen, D. S.; Hung, C.-H.; Olsen, R. E.; Davis, R. C.; Vail, M. A.; Dadson, A. E.; Nesterenko, P. N.; Linford, M. R., *Anal. Chem.* **2011,** 83 (14), 5488-5501.

5. Hung, C.-H.; Kazarian, A. A.; Dadson, A. E.; Paull, B.; Nesterenko, P.; Linford, M. R., Guidelines for Understanding the Retention Mechanism of the Diamond Analytics Flare Mixed-Mode Column. Diamond Analytics.

Appendix 7: Flare C18 Mixed-Mode Column: Separation of Gingsenosides Re and Rd by LC-MS*

A7.1. Introduction

Ginseng is a commonly used herb in Asia. In 2010, approximate 80,000 tons of it were produced in Asia (China and South Korea) and North America (Canada and the United States).[1] The worldwide market for ginseng is approximately 2 billion dollars per year. Ginsenosides or panaxosides are the active compounds in ginseng. Liquid chromatography is commonly used to assay the amounts of ginsenosides in ginseng. In this application note, ginsenoside Re and ginsenoside Rd were separated by LC-MS using the FLARE mixed-mode column.

The particles in the FLARE C18 mixed-mode (MM) core-shell column are made of carbon, nanodiamond, and an amine-based polymer, and are stable at elevated temperature and pH.[2-5] The amine-based polymer in the stationary phase provides it with mixed-mode properties, allowing it to retain analytes via anionic and hydrophobic interactions with a retention mechanism that varies with pH.[2] In this application note, a 2.1 x 50 mm mixed-mode FLARE C18 column was used to separate two ginsenosides using TFA as an additive.

* This chapter was published by Diamond Analytics as an application note (Hung, C-H., Zukowski, J., Jensen, D. S., Dadson, A. E., Linford, M. R.)

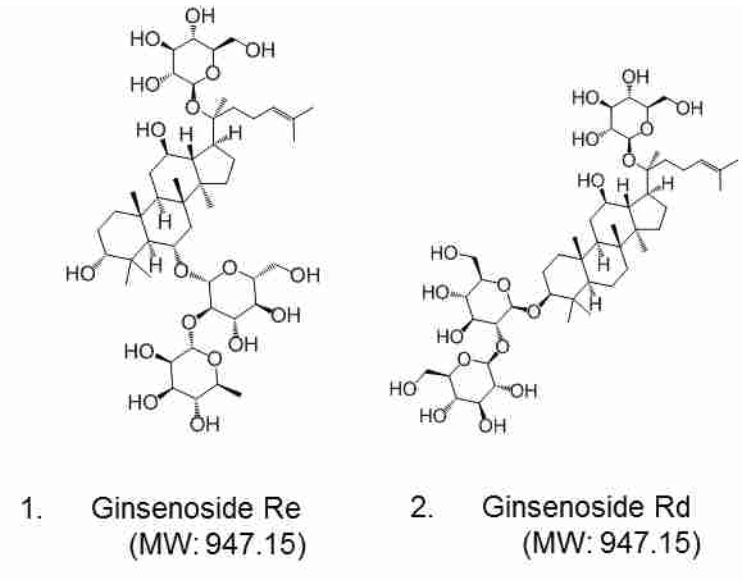

Figure A7.1 Structure of separated ginsenoside Re and Rd.

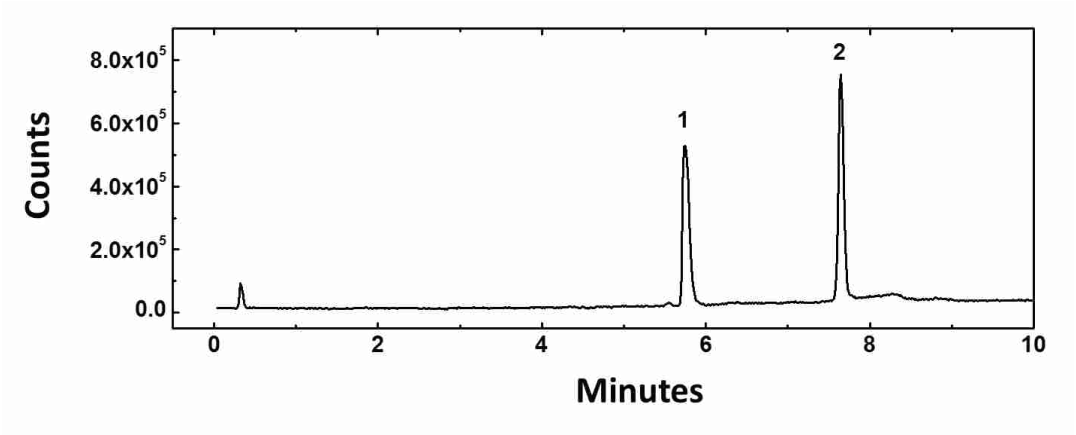

Figure A7.2 Separations of ginsenoside Re (1) and ginsenoside Rd (2).

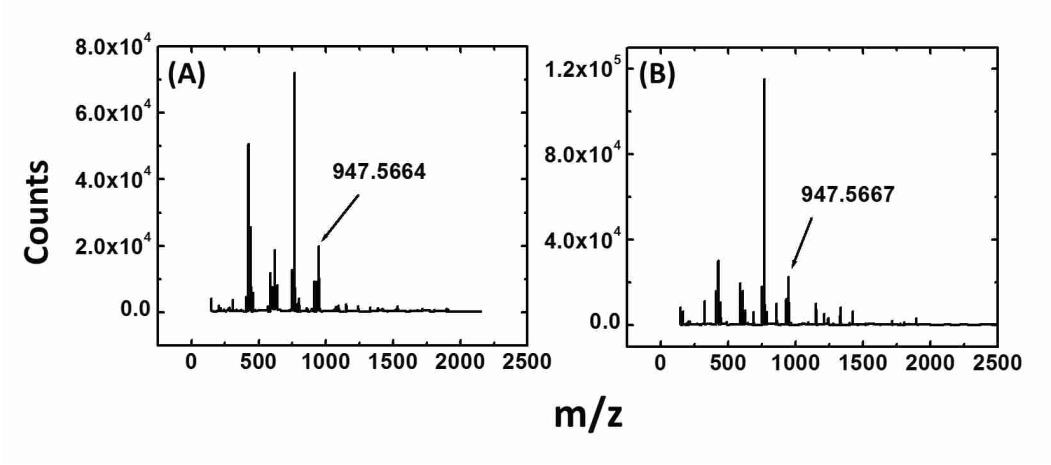

Figure A7.3 Mass spectra of ginsenoside Re (A) and ginsenoside Rd (B) from the corresponding peaks (1 and 2) in the chromatogram in Figure A7.1.

A7.2. Experimental

HPLC system: Agilent 1260 Infinity coupled with an Agilent 6230 TOF LC-MS in positive ion mode

Analytes: Ginsenoside Re and Rd (ca. 0.5 mg/mL in MeOH)

LC Conditions:

Column dimensions: 2.1 x 50 mm (id: 16598.16-3)

Injection volume: 6.0 µL

Flow rate: 0.4 mL/min

Temperature: 35 °C

A: 1000 mL H_2O + 1 mL TFA

B: 1000 mL ACN + 1 mL or 0.875 mL TFA

Gradient:

0 min 100% A 0% B

15 min 0% A 100% B

15.1 min 100% A 0% B

20 min End

MS conditions:

Gas temperature: 300 °C

Drying gas: 5 L/min

Nebuilizer: 35 psig

Capillary voltage: 3500 V

Fragmentor: 170 V

Skimmer: 65 V

OCT 1Rf Vpp: 750 V

A7.3. References

1. Baeg, I.-H.; So, S.-H., *J. Ginseng Res.* **2013,** 37 (1), 1-7.

2. Hung, C.-H.; Kazarian, A. A.; Dadson, A. E.; Paull, B.; Nesterenko, P.; Linford, M. R., Guidelines for Understanding the Retention Mechanism of the Diamond Analytics Flare Mixed-Mode Column. Diamond Analytics.

3. Hung, C.-H.; Wiest, L. A.; Singh, B.; Diwan, A.; Valentim, M. J. C.; Christensen, J. M.; Davis, R. C.; Miles, A. J.; Jensen, D. S.; Vail, M. A.; Dadson, A. E.; Linford, M. R., *J. Sep. Sci.* **2013,** 36 (24), 3821-3829.

4. Saini, G.; Jensen, D. S.; Wiest, L. A.; Vail, M. A.; Dadson, A.; Lee, M. L.; V., S.; Linford, M. R., *Anal. Chem.* **2010,** 82 (11), 4448-4456.

5. Wiest, L. A.; Jensen, D. S.; Hung, C.-H.; Olsen, R. E.; Davis, R. C.; Vail, M. A.; Dadson, A. E.; Nesterenko, P. N.; Linford, M. R., *Anal. Chem.* **2011,** 83 (14), 5488-5501.

Appendix 8: Sonication for Improved Particle Size Distribution of Core-Shell Particles*

A8.1. Abstract

In one or more embodiments, a porous composite particulate material includes a plurality of composite particles including an acid-base-resistant core particle at least partially surrounded by one or more layers of acid-base-resistant shell particles. The shell particles are adhered to the core particle by a polymeric material. The shell particles and/or core particles may be made from an acid-base-resistant material that is stable in harsh chemical conditions. During application of the polymeric material/shell particle bilayer, the core particles are sonicated to homogenize the particle size distribution and minimize agglomeration of particles. Multiple bilayers of polymer/shell particles may be applied. In one embodiment, the core particle comprises generally spherical glassy carbon, while the shell particles may comprise nano-sized diamond particles. Other acid-base-resistant materials may be employed. The porous composite particulate materials may be used in separation technologies, including, but not limited to, chromatography and solid phase extraction.

*This appendix was published as a United States Patent, US Patent number: 8658039, issued February 25, 2014. Details regarding this patent can be found online at https://www.google.com/patents/US20120145623.